(4)

Annual Report

Growth, Characterization and Device Development in Monocrystalline Diamond Films

Supported under Contract #N00014-86-K-0666
for the period June 1, 1987 – May 31, 1988

School of Engineering
North Carolina State University
Raleigh, North Carolina

UNCLASSIFIED
SECURITY CLASSIFICATION OF THIS PAGE

ADA199321

REPORT DOCUMENTATION PAGE

1a. REPORT SECURITY CLASSIFICATION: Unclassified	1b. RESTRICTIVE MARKINGS: N/A
2a. SECURITY CLASSIFICATION AUTHORITY: N/A	3. DISTRIBUTION/AVAILABILITY OF REPORT: Approved for public release; distribution unlimited
2b. DECLASSIFICATION/DOWNGRADING SCHEDULE: N/A	
4. PERFORMING ORGANIZATION REPORT NUMBER(S)	5. MONITORING ORGANIZATION REPORT NUMBER(S)
6a. NAME OF PERFORMING ORGANIZATION: N. C. State University c/o Materials Sic. & Eng.	6b. OFFICE SYMBOL (If applicable)
6c. ADDRESS (City, State, and ZIP Code): Raleigh, NC 27695-7907	7a. NAME OF MONITORING ORGANIZATION: ONR, Code 1114
	7b. ADDRESS (City, State, and ZIP Code): Arlington, VA 22217
8a. NAME OF FUNDING/SPONSORING ORGANIZATION: SDIO	8b. OFFICE SYMBOL (If applicable): IST
	9. PROCUREMENT INSTRUMENT IDENTIFICATION NUMBER: N00014-86-K-0666
8c. ADDRESS (City, State, and ZIP Code): Washington, DC	10. SOURCE OF FUNDING NUMBERS

PROGRAM ELEMENT NO	PROJECT NO	TASK NO	WORK UNIT ACCESSION NO
6322 OC	IST	SRR	003

11. TITLE (Include Security Classification): Growth, Characterization and Device Development in Monocrystalline Diamond Films

12. PERSONAL AUTHOR(S): R. F. Davis, J. T. Glass, G. Lucovsky, K. J. Bachmann and R. J. Nemanich

13a. TYPE OF REPORT	13b. TIME COVERED	14. DATE OF REPORT (Year, Month, Day)	15. PAGE COUNT
Annual	FROM 6/1/87 TO 5/31/88	1988, June 1	

16. SUPPLEMENTARY NOTATION

17. COSATI CODES			18. SUBJECT TERMS (Continue on reverse if necessary and identify by block number)
FIELD	GROUP	SUB-GROUP	

19. ABSTRACT (Continue on reverse if necessary and identify by block number)

Cu single crystals have been grown and prepared for use as a lattice matched substrate. A literature survey of potential substrates which are both lattice and energy matched with diamond to promote two-dimensional growth has also been completed and promising materials are currently being utilized for diamond growth. Two chemical vapor deposition systems have been designed. The first, a hot filament system, has been constructed, characterized and used to deposit diamond on a variety of substrates. A microwave CVD system and an in-situ analysis system are currently under construction. Films have been analyzed by numerous techniques, the most significant being Raman spectroscopy and the first reported high resolution lattice imaging of CVD diamond. Diamond power MESFET devices have been theoretically evaluated and found to be capable of generating rf power output levels greater than other existing or proposed semiconductors, including GaAs. Efficiency for the diamond MESFETs greater than 40% was determined and a more linear response and greater dynamic range than GaAs was found.

20. DISTRIBUTION/AVAILABILITY OF ABSTRACT	21. ABSTRACT SECURITY CLASSIFICATION
☒ UNCLASSIFIED/UNLIMITED ☐ SAME AS RPT ☐ DTIC USERS	
22a. NAME OF RESPONSIBLE INDIVIDUAL	22b. TELEPHONE (Include Area Code) / 22c. OFFICE SYMBOL

DD FORM 1473, 84 MAR — 83 APR edition may be used until exhausted. All other editions are obsolete.

SECURITY CLASSIFICATION OF THIS PAGE
UNCLASSIFIED

154-203

Table of Contents

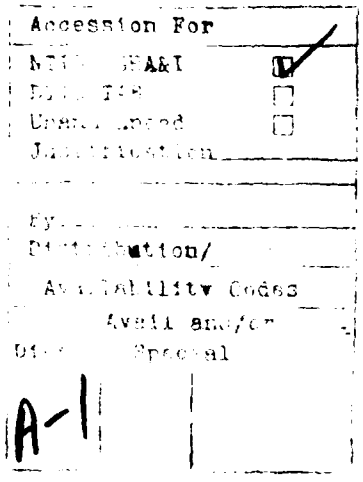

I. Introduction

Diamond is an excellent candidate material for various electronic microwave devices as well as devices for use in high temperature and/or high flux radiation environments and for high current density or high power applications. This very diverse applicability is due to its superior thermal conductivity, saturated drift velocities, resistance to chemical attack and thermal stability. However, to realize this potential of diamond, high quality monocrystalline films must be grown and thoroughly characterized. The latter research is necessary as an iterative procedure for the improvement of the growth process and to guide future device design and fabrication. To achieve these goals, the NCSU diamond program couples investigators from four departments to obtain a unique combination of expertise and experience.

More specifically, the principal objectives of this collaborative research are to (1) grow monocrystalline diamond films on suitable substrates such as Ni and SiC using both past and newly generated knowledge regarding gas species generation, deposition and reaction, and energy and momentum transfer at the growing surface, (2) characterize these films in terms of bonding, structural and electrical character, (3) model and fabricate device structures from these films and (4) work in a collaborative manner with personnel at the Research Triangle Institute in their diamond fabrication research.

This report is comprised of several papers which have been published or submitted for publication during the past year. These manuscripts discuss the most important progress during this period. Copies of viewgraphs/slides from the recent SDIO/IST–ONR Diamond Technology Seminar are also included which give even more recent results from this program. A summary of the most significant results is given below:

Substrates: Cu single crystals have been grown in a newly constructed Bridgemann furnace for use as lattice matched substrates. Spark cutting and polishing have been accomplished to prepare the samples for diamond growth. Such substrates have been supplied to other SDIO sponsored programs as well as NCSU. The furnace has also been prepared for Ni growth. A literature survey of potential substrates which are both energy and lattice matched with diamond has also been recently completed and promising materials are currently being utilized for diamond growth.

Diamond Growth: Two chemical vapor deposition systems have been designed and constructed and one has been characterized by growth parameter variations. Both hot filament and microwave plasma methods are under investigation and a variety of unique capabilities have been incorporated into the systems (ultra high purity, in situ analysis techniques, remote and immersed plasma, etc.). Results using various single crystal substrates (Si, SiC, Cu, CuNi, NbC, SiC/Ni) have been obtained indicating that; (i) surface steps have no affect on the nucleation of diamond, (ii) carbide substrates studied do not help form monocrystalline films, (iii) lattice matching is probably a necessary but not sufficient condition for two dimensional film growth. These results led to the literature survey discussed above.

Diamond Characterization: Analysis of films via SIMS, SEM, TEM, AES, XPS, and EELS has been completed. This includes the first high resolution lattice imaging of CVD diamond in both plan-view and cross section. The major characterization results indicate that (i) films of relatively high purity composed of true diamond can be easily achieved, (ii) very high defect concentrations are present due to the growth, (iii) interface buffer layers are present during slower growth runs and increase adhesion to the substrate and (iv) certain substrate/particle orientational relationships observed are encouraging with regard to achieving epitaxial films in the future.

Device Modeling: Diamond Power MESFET devices have been theoretically evaluated using a complex, large signal device simulator. They were found to be capable of generating RF output power levels greater than existing and proposed semiconductor transistors including GaAs (~1.5 vs. 25 W/unit width for GaAs vs. Diamond, respectively). An efficiency for the diamond in excess of 40% was determined and diamond was found to have a more linear response and greater dynamic range than GaAs in the MESFET structures. These results indicate the exceptional potential for diamond electronic devices using the known properties of natural diamond.

Chemical vapor deposition and characterization of diamond films grown via microwave plasma enhanced CVD

J. T. Glass*, B. E. Williams, and R. F. Davis

North Carolina State University, Department of Materials Science and Engineering, Campus Box 7907, Raleigh, NC 27695-7907

ABSTRACT

Diamond is an excellent candidate material for use in electronic and wear resistant coating applications due to its hardness, strength, thermal conductivity, high electron drift velocity, chemical and thermal stability, radiation hardness and optical transmission. Electronic devices of particular interest include high power/high frequency devices and devices to be utilized in high temperature, chemically harsh and/or high radiation flux environments. The recent development of techniques for growth of crystalline diamond films using low pressure gases has created the potential for growing thin films for such electronic devices or wear resistant coatings. In this research, diamond thin films grown on silicon by microwave plasma enhanced chemical vapor deposition were characterized by a variety of materials analysis techniques including secondary ion mass spectroscopy (SIMS), x-ray photoelectron spectroscopy (XPS), scanning electron microscopy (SEM), transmission electron microscopy (TEM), and infrared spectroscopy (IR). This paper reports the characterization of these polycrystalline diamond films and discusses the impurities, bonding, and structure of the as-grown diamond films.

1. INTRODUCTION

The current emphasis on obtaining electronic-grade diamond films can be understood in terms of the many potential applications which arise from its exceptional electronic, thermal, and mechanical properties. The electron and hole mobilities in diamond are very high (2000 and 1800 $cm^2.V^{-1}.sec^{-1}$, respectively).[1] Diamond also has a much higher thermal conductivity (from 1000 to 10,000 W/m-K)[2] than even copper, which is considered a good thermal conductor. Diamond films may thus be utilized as heat sinks on which to mount various electronic devices fabricated from more conventional semiconductors such as Si or GaAs. Other potential uses in electronics include microwave devices as well as devices to be employed in high power, high current density, high temperature and/or high radiation flux applications. Researchers have deposited polycrystalline diamond films via RF-plasma CVD[3], microwave plasma CVD,[4,5] and electron assisted CVD[6,7] on a variety of substrates such as Si, β-SiC, Mo, and Ni. Thus far, single crystal diamond films have only been obtained on diamond substrates. An understanding of the basic science of diamond growth and application of this knowledge to produce device-quality monocrystalline diamond films must be obtained before new technology utilizing diamond films for devices can be developed. Therefore, the goal of this research is to better understand the properties of these diamond films in order to apply this knowledge toward future research involving the growth of single-crystal diamond films on non-diamond substrates.

2. EXPERIMENTAL

2.1 Microwave Plasma Enhanced CVD System

A schematic of the deposition system used to grow the diamond films in this research is shown in Figure 1. The 2.45 GHz microwave power source used was guided through an isolator and a three stub tuner to the quartz tube reaction chamber which is 44 mm in inner diameter. The substrate was placed in the quartz tube which was in the path of the rectangular wave guide. The substrate temperature depended strongly on the microwave power and gas pressure since microwave induction heating and plasma gas collisions were responsible for substrate heating (no other substrate heating was utilized).

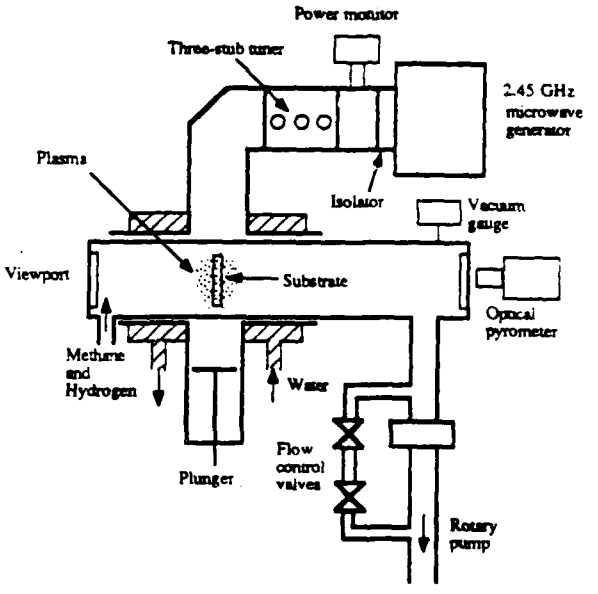

Figure 1. Schematic diagram of the microwave plasma CVD system.

*On assignment from Kobe Development Corporation, Research Triangle Park, NC 27709.

2.2 Growth Conditions

The diamond films analyzed in this research were grown on 2 cm by 1 cm n-Si(111) substrates immersed in a CH_4/H_2 plasma generated by the 2.45 GHz microwave source . The substrate temperature was measured by an optical pyrometer and was maintained at approximately 800 °C by controlling the microwave power (which was typically 300-350 watts). The total pressure in the chamber was maintained at 30 Torr and only the CH_4/H_2 ratio in the feedgas was varied for the films studied in this work.

3. RESULTS

3.1 Secondary Ion Mass Spectrometry (SIMS).

SIMS Analysis was conducted on diamond films (grown with 1.0% CH_4 in H_2) utilizing a Cameca IMS-3f direct imaging microprobe in order to determine the impurity elements present. Scans of ion counts/sec vs. atomic weight (usually referred to as bar graphs), depth profiles, and chemical maps were conducted on two samples using an O^- primary ion beam. Unfortunately, accurate quantification of SIMS data (i.e., atomic concentrations) is not possible unless implanted standards are utilized. This requires that each impurity whose concentration is desired be implanted into "standard" films at known ion doses and be used for comparison with the unknown concentration of that impurity in the films of interest. This is well suited for the analysis of specific dopant level concentrations but is not feasible for a large number of impurities as is needed in an overview analysis due to the time and expense of implanting and analyzing the standards. Nonetheless, if utilized properly, SIMS can discern various important facts about impurities in a material as discussed below for these diamond films.

3.1.1 Bar Graphs

Ionic counts per second were recorded for molecular weights from 1 to 200. During this sweep, molecular filtering was utilized to avoid interference from molecular (as opposed to elemental) species generated during the analysis. However, interference is still possible, thus relative isotope abundance patterns were utilized to identify elements. As discussed previously, quantification is not possible due to the absence of standards for diamond SIMS analysis. However, a very rough order of magnitude approximation of impurity concentrations can be obtained if matrix effects are ignored and published relative ion yield data[8] is utilized to determine concentrations relative to C ion yield. The results of such an analysis are shown in Table 1 for two samples. The identification of the elements present is believed to be accurate but caution should be exercised in the use of the concentration values.

Table 1. SIMS compositional analysis (~a/o).

	Film #1	Film #2
Hydrogen	0.2	0.2
Oxygen	0.7	0.9
Aluminum	0.03	0.05
Silicon	0.03	0.003
Nitrogen	0.1	

Trace Impurities (<1000 ppm): Mg, Ca, Na, Cl, K, Fe, Cu, Ti, Zn, Cr

Besides the lack of standards, inaccuracies arise due to impurity segregation which causes much higher local concentrations since the image field for these bar graphs (~150 μms) is larger than segregated regions as discussed below. When different scans yielded different concentrations due to this segregation, the maximum concentration observed is given. Furthermore, a high hydrogen background and the use of O^- as the primary beam imply that data for these elements are approximations of the upper bounds on the concentrations and in actuality they may be much lower. Nonetheless, the film has been determined to be mostly carbon, the impurity elements have been identified, and rough approximations of upper bounds of their concentrations have been determined.

Since the Cameca instrument is a direct imaging probe, chemical mapping of impurities was also accomplished with a spatial resolution of ~5 to 10 μm and an image field of 400 μm. Although this data could not be quantified, it indicated that the silicon, aluminum, oxygen, and hydrogen were segregated in regions ranging from 5 to 20 μm in diameter. Furthermore, in certain areas these elements appeared to come from the same regions of segregation, whereas in others the segregated regions of different elements were unrelated.

3.1.2 Depth Profiles

Depth profiles of C, Si, O and H were also obtained and are shown in Figure 2. The hydrogen ion yield is similar in both the film and the substrate indicating that it is possibly due to the background level. Although the oxygen concentration appears to be greater in the substrate than in the film, this is probably due to the change in matrix (i.e., diamond to silicon) interacting with the primary O^- ion beam. Thus, no conclusions should be drawn about the oxygen concentrations except the rough approximation of the upper limits as discussed in section 3.1.1. One of the most interesting features of the depth profiles of Kobe films are the very smooth concentration changes across the interface. This is contrary to observations of some diamondlike films examined with the Cameca instrument which show a peak in the C ion yield at the interface. The absence of this peak may be indicative of the absence of a buffer layer or its thin nature (≤500Å) in this Kobe sample.

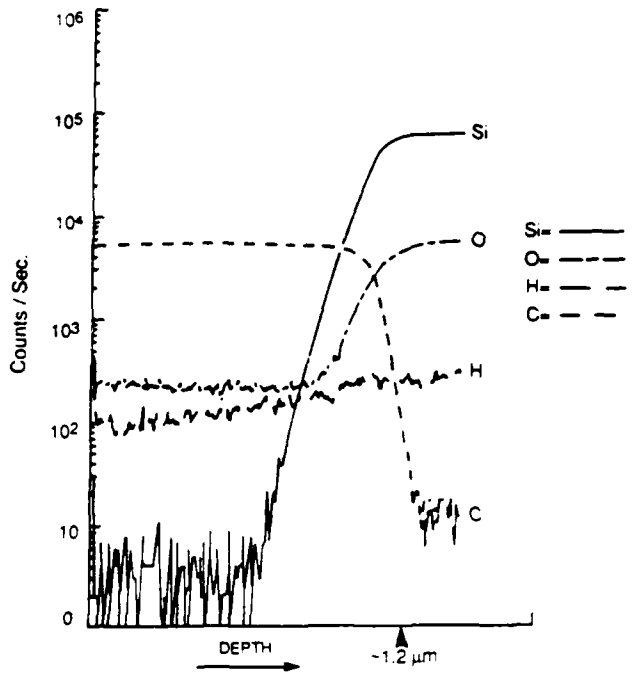

Figure 2. Depth profile of diamond film.

From the depth profiles it also appears that the change in carbon concentration across the interface is more rapid than the change in silicon. This may indicate more silicon diffusion into the film than carbon diffusion into the silicon, possibly due to the numerous grain boundaries in the film. However, this is a very tentative conclusion and has not been verified by repeated depth profiling.

3.1. X-ray photoelectron spectroscopy (XPS)

XPS was conducted at the Research Triangle Institute utilizing a Leybold-Heraeus hemispherical electron energy analyzer and twin anode x-ray source. Mg radiation at 300 W and an analyzed area of 2x10 mm^2 was utilized. Figure 3 is a wide energy range scan of a diamond film grown at 1% methane in hydrogen. The scan contains x-ray excited KLL Auger and 1s peaks for carbon and oxygen as well as silicon 2s and 2p peaks. The relatively high concentrations of silicon and oxygen may be due to x-ray excitation of exposed areas of the silicon substrate where diamond was not deposited as well as silicon and oxygen surface contamination. In the XPS system employed, no method of localizing the x-ray source was possible. This broad energy scan indicates elements which are present but does not yield any information concerning the bonding of the carbon.

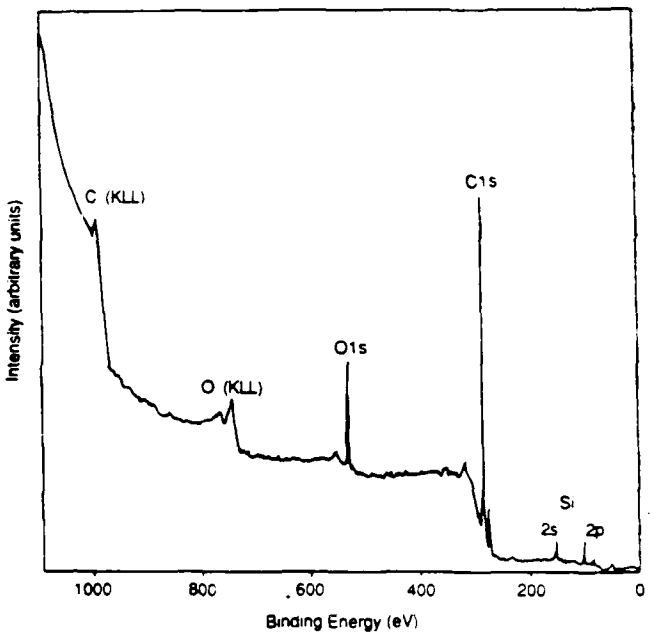

Figure 3. Wide energy range XPS scan of a diamond film grown at 1% CH_4 in H_2.

The more significant data is obtained by analyzing the carbon 1s peak using a small energy window as shown in Figure 4. This curve indicates that the carbon is in an sp^3 (or σ) bonding configuration (characteristic of diamond). If sp^2 (or π) graphitic bonds were present, a secondary peak would be observed as shown in Figure 5. This is confirmed when the intensity axis of this data is expanded such that the electron energy loss fine structure to the left (i.e. lower energy) of the carbon 1s peak can be examined as shown in Figure 6. This energy loss structure is seen to be very similar to that of natural diamond where the peaks labelled P_1, P_2, and P_3 have energy differences from the C1s peak of 11.3, 25.4, and 34.1 eV, respectively.[9] Graphite has been seen to yield a significantly different energy loss spectrum from the C1s peak. (P_1, P_2, and P_3 positions are 6.3, 28.1 and 33.3 eV, respectively).[9]

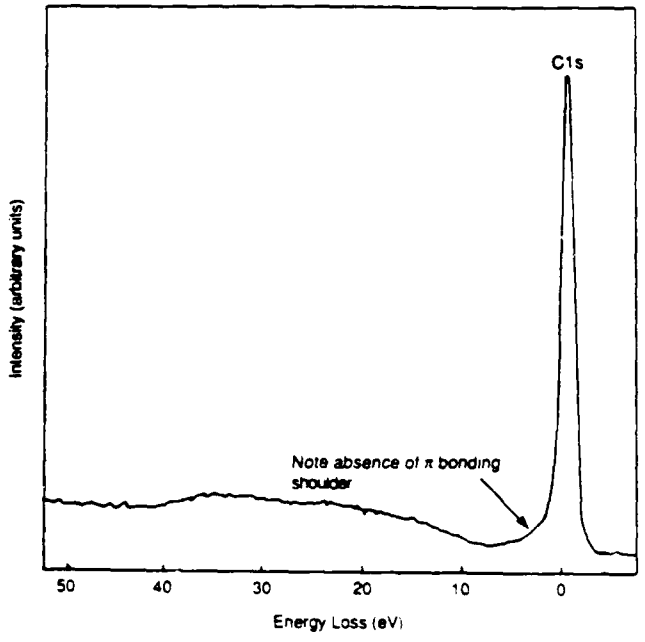

Figure 4. XPS scan about the C1s peak energy.

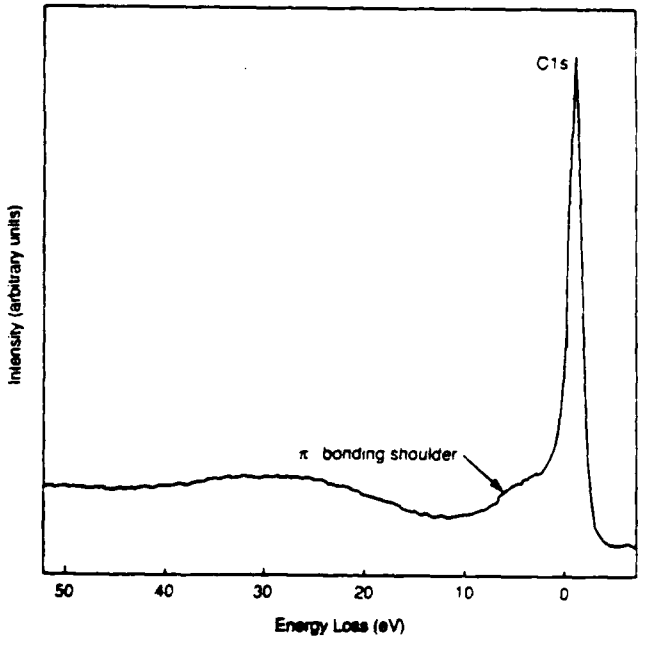

Figure 5. XPS spectrum from pyrolitic graphite about the C1s peak energy.

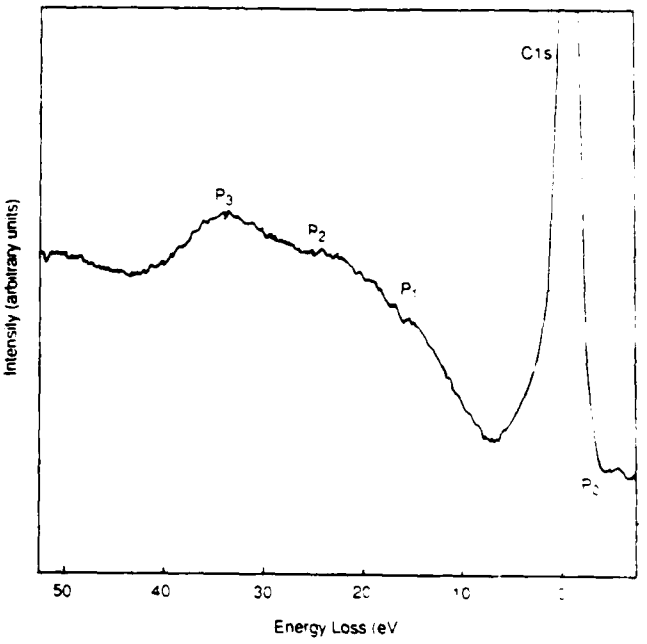

Figure 6. XPS spectrum about the C1s peak energy expanded such that the electron energy loss fine structure is evident.

In summary, this XPS data indicated that true diamond bonding is present at the surface of the diamond films without any evidence of a graphitic component. It should be noted that the sample was not pretreated prior to this analysis. Thus, the surface consists of diamond bonding even after long exposure to the atmosphere. This is significant since it is known that certain pretreatments such as ion bombardment can graphitize the diamond surface.

3.2 Scanning Electron Microscopy (SEM)

In order to examine the surface morphology of the diamond films, an Hitachi S530 scanning electron microscope (SEM) was used. All of the diamond films examined thus far consist of multi-faceted diamond grains ranging from less than one micron up to approximately one micron in size (as measured across a single facet). Although the orientation of the individual diamond grains appears random relative to the substrate, numerous facets have symmetry characteristic of crystallographic planes. For example, Figure 7 shows that four-fold symmetry cube faces are present on several of the grains. This symmetry indicates that these faces are (100) planes. Other high symmetry planes such as three-fold (111) facets have also been observed as shown in the micrograph of another sample shown in Figure 8. Growth ledges on the primary grain are also observed, causing the surface of the facet to appear rough. Another interesting feature observed in Figure 8 is the secondary nucleation which occurred on the large facet of the predominant grain. This secondary growth appears to have formed another grain with three-fold symmetry which has a distinct relationship to the primary face. These (111) planes tend to

predominate in samples grown below approximately 0.4% CH_4 in H_2 whereas (100) planes predominate between ~0.5% and 1.2% CH_4/H_2. Above 1.6% CH_4 the diamond particles become microcrystalline with no observable facets.

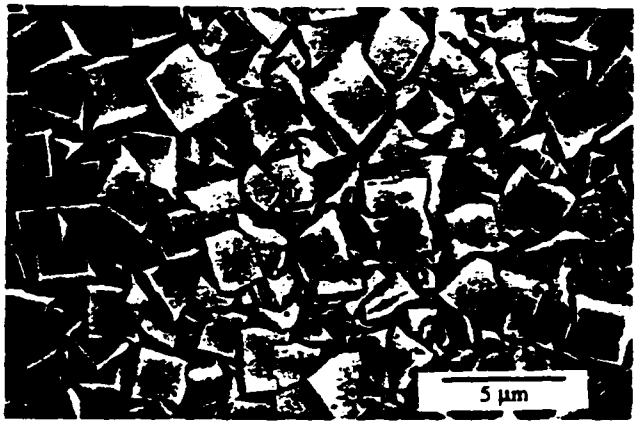

Figure 7. SEM micrograph of diamond film with fourfold faceted grains.

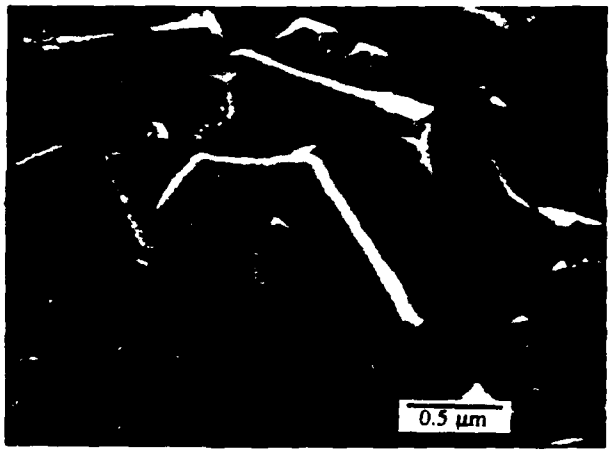

Figure 8. SEM micrograph of threefold faceted diamond grain.

3.4 Transmission Electron Microscopy (TEM)

An Hitachi H-800 STEM at 200 KeV was utilized to observe the diamond films via plan-view transmission electron microscopy (TEM), cross-sectional transmission electron microscopy (XTEM), and selected area diffraction (SAD).

For plan-view TEM, the silicon substrate was first thinned to 65 microns using 600 grit silicon carbide paper and subsequently polished with 0.05 μm Al_2O_3 in water. The substrate was then dimpled to a thickness of ~10 μm using a steel ball coated with 1 micron diamond paste. After mounting the sample on a molybdenum support ring, the sample was ion milled in a Gatan ion mill using a 6 kV beam of Ar^+ ions from the substrate side until perforation was observed. First, in order to confirm that the diamond structure was present, the spacings of different planes in the diamond grain were calculated using a ring pattern from a large area of the sample and the results of these measurements are shown in Table 2. In addition, the ASTM spacings for natural diamond are included in the table for comparison. Excellent agreement between the CVD diamond films and natural diamond is observed.

Table 2. Electron diffraction data for diamond film and reported values for natural diamond.

hkl	Observed d(Å)	Reported (ASTM 6-675) d(Å)
111	2.060	2.060
220	1.265	1.261
311	1.073	1.0754
400	0.896	0.8916
331	0.814	0.8182

Figure 9 is a plan-view TEM of a single diamond grain observed with the electron beam parallel to the [110] direction. Numerous twins are present on the two {111} planes which are in the diffracting condition. An indexed electron diffraction pattern from this grain is also shown in Figure 10. Twinning is found on the $(11\bar{1})$ and $(1\bar{1}1)$ planes, as evidenced by the twin spots which occur between the regular spots and are indicated on the diffraction pattern. These twins have probably occurred in [112] directions which are characteristic of diamond. The streaking in the diffraction pattern is believed to be due to stacking faults or coherent twin boundaries of thickness less than 100 angstroms[10]. Another interesting feature of this bright field examination is that under higher magnification, no particulates or other impurities were observed in the films. Furthermore, the grain boundaries appeared to be very sharp within the resolution limits of the current study. Excellent agreement between natural diamond and the CVD diamond is seen. Furthermore, no graphite or amorphous component was observed during this electron diffraction research.

Figure 9. Plan-view TEM of a single diamond grain observed with the electron beam parallel to the [110] direction.

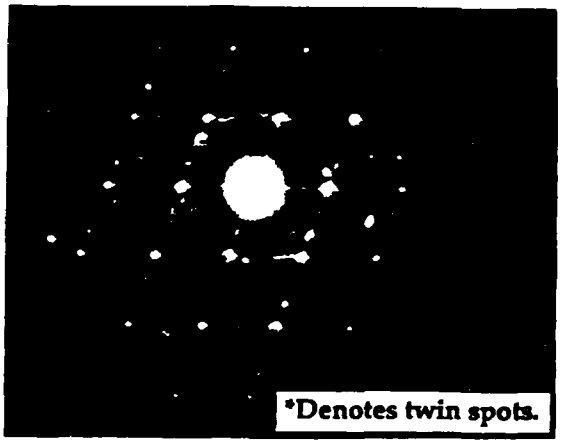

Figure 10. Indexed electron diffraction pattern from the diamond grain in Figure 17.

Cross-sectional TEM (XTEM) is a particularly useful technique because it allows detailed study of the interface between the film and substrate. The procedure for preparing XTEM samples of SiC thin films has been well established at NCSU and was duplicated for the diamond films reported here. It involves using epoxy to glue together a "sandwich" of the film/substrate pieces and silicon support layers to provide rigidity. This "sandwich" is then thinned in much the same manner as the plan-view TEM samples. Figure 11 is a bright field micrograph of a diamond film grown at 0.3% CH_4/H_2 (top) on a Si(111) substrate (bottom). The presence of twins is again observed in the film as well as elastic strain contrast in the lower left area of the film, probably due to poor lattice matching and differences in thermal coefficients of expansion. An interfacial layer approximately 50 angstroms thick was also observed between the diamond and silicon. A selected area electron diffraction (SAD) pattern from this region indicated the presence of a layer of beta silicon carbide. The orientation of at least part of this silicon carbide layer is believed to be close to (111) because the diffraction spots from the SiC layer were aligned with the corresponding diffraction spots from the silicon substrate. It could also be seen from the diffraction pattern that the SiC spots were smeared slightly, indicative of the 20% lattice mismatch between silicon and silicon carbide.

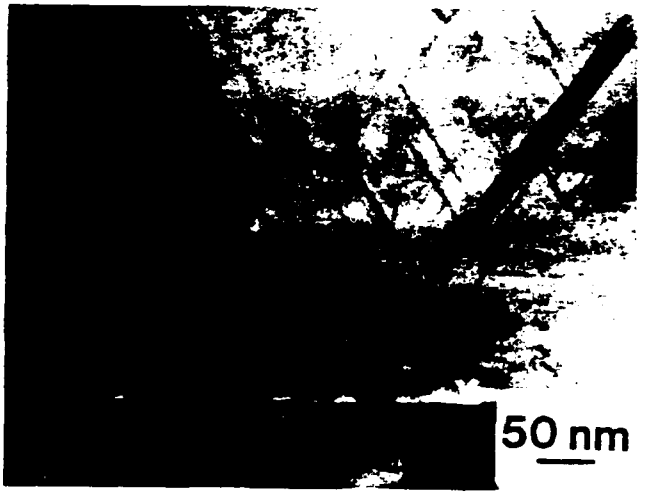

Figure 11. Bright field XTEM micrograph of diamond film grown at 0.3% CH_4/H_2. Top - diamond film, bottom - Si substrate.

Figure 12 is an XTEM micrograph of a sample grown at 2.0% CH_4/H_2. The apparent interface layer present is believed to be an artifact of the ion milling used to thin the sample because no characteristic defect contrast is observed and the layer appears to be only at the surface (i.e., it does not have any depth contrast associated with it). In addition, no other phase was observed in the SAD of this region. Further examination of this layer will be performed to study the reproducibility of this milling artifact. A possible explanation for the lack of a silicon carbide buffer layer in this sample may be the faster growth rate caused by the higher methane concentration which allows less time for the formation of such a layer. Higher defect densities were observed in the films grown at 2.0% CH_4/H_2 than in those grown at lower methane concentrations. In fact, defects could not be identified, as seen in Figure 13, due to this high density. This increased defect density is also attributed to the higher growth rates.

Figure 12. XTEM micrograph of a diamond film grown at 2.0% CH_4/H_2. Top - diamond film, bottom - Si substrate.

3.5 Infrared Spectroscopy (IR).

In Figure 13, IR spectra obtained on a Perkin-Elmer 580 infrared spectrometer are shown for two diamond samples grown with 1.0% CH_4 in H_2. In addition, a spectrum from a sample of CVD-grown β-SiC is also shown. Absorption from the Si substrate has been subtracted from this data. The absorption observed in sample #2 can thus be shown to be a result of the presence of silicon carbide. This observation is consistent with recent TEM results which showed a layer of silicon carbide at the diamond-silicon interface for some samples but more research is necessary to verify this correlation . No absorption minima were observed at C-H, C-O, C=O, C=C, etc. frequencies indicating an absence of such bonding within the resolution limits of this technique. Curiously, sample #1, grown under the same growth conditions, shows no silicon carbide absorption. An investigation as to the cause of this non-reproducibility is ongoing.

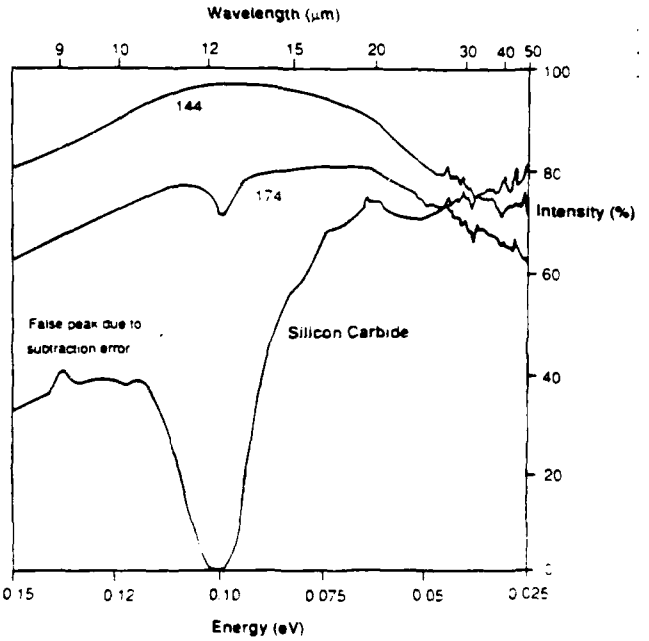

Figure 13. Infrared absorption spectra for two diamond samples and a reference SiC sample.

4. CONCLUSIONS

In summary, diamond and diamondlike films grown by MPECVD have been examined by a variety of analytical techniques. Composition, bonding and structure all verify that a true diamond phase can be grown under appropriate growth conditions. However, diamondlike films have also been deposited under under only slightly different growth conditions. The morphology of the diamond films has also been examined. A polycrystalline grain structure with preferred growth facets dependent on methane concentration during growth was observed on the diamond films. Many defects in the diamond films, including numerous twins and stacking faults as well as dislocations, were identified via TEM and SAD. XTEM observations have shown a SiC buffer layer in certain samples which is epitaxial in local regions.

5. ACKNOWLEDGMENTS

The authors also wish to express their thanks to Mr. Max Yoder of the Office of Naval Research for support and assistance in this research. Kobe Steel, Ltd. (K. Kobashi, K. Nishimura, Y. Kawate, and T. Horiuchi) is gratefully acknowledged for supplying diamond samples, for useful discussions, and for partial support of this research. Dan Vitkavage of the Research Triangle Institute is gratefully acknowledged for assistance in obtaining the XPS data and the assistance of Dieter Griffis, Sean Corcoran, and Peter Richard of NCSU is also gratefully acknowledged.

6. REFERENCES

1. V. K. Bazhenov, I. M. Vikulin, and A. G. Gontar, "Synthetic Diamonds in Electronics (review)," Sov. Phys. Semicond., 19:829-841, (1985).

2. J. E. Field, The Properties of Diamond, Academic Press, New York (1979).

3. S. Matsumoto, "Chemical Vapor Deposition of Diamond in RF Glow Discharge", J. Mat. Sci. Lett., 4:600-602, (1985).

4. Y. Mitsuda, Y. Kojima, T. Yodhida, K. Akashi, "The growth of diamond in microwave plasma under low pressure", J. Mat. Sci., 22:1557-1562, (1987).

5. M. Kamo, Y. Sato, S. Matsumoto, and N. Setaka, "Diamond synthesis from gas phase in microwave plasma", J. Cryst. Growth, 62:642-644, (1983).

6. A. Sawabe and T. Inuzuka, "Growth of diamond thin films by electron-assisted chemical vapor deposition and their characterization", Thin Solid Films, 137:189-199, (1986).

7. A. Sawabe and T. Inuzuka, "Growth of diamond thin films by electron-assisted chemical vapor deposition", Appl. Phys. Lett., 46(2), 146-147 (1985).

8. H. A. Storms, K. F. Brown, and J. D. Stein, "Evaluation of a Cesium Positive Ion Source for Secondary Ion Mass Spectrometry", Anal. Chem., 49(13), 2023-2030 (1977).

9. F. R. McFeely, S. P. Kowalczyk, L. Ley, R. G. Cavell, R. A. Pollak, and D. A. Shirley, "X-ray photoemission studies of diamond, graphite, and glassy carbon valence bands", Phys. Rev. B, 9 (12), 5268-5278 (1974).

10. B. V. Derjaguin, B. V. Spitsyn, A. E. Gorodetsky, A. P. Zakharav, L. I. Bouilov, and A. E. Aleksenko, "Structure of autoepitaxial diamond films", J. Crystal Growth, 31:44-48, (1975).

ELECTRON MICROSCOPY OF DIAMOND FILMS GROWN BY MICROWAVE PECVD

B. E. WILLIAMS*, J. T. GLASS*, R. F. DAVIS*, K. KOBASHI** AND Y. KAWATE**
*Department of Materials Science and Engineering, North Carolina State University, Raleigh, NC 27695-7907.
**Electronics Technology Center, Kobe Steel. Ltd., Kobe, Japan 651.

INTRODUCTION

Thin films of diamond grown by microwave plasma enhanced chemical vapor deposition[1] (MPCVD) have been examined utilizing a variety of electron microscopy techniques including scanning electron microscopy (SEM), transmission electron microscopy (TEM), and high resolution TEM. Film morphology, defect structure, and the nature of the diamond-substrate interface were examined.

RESULTS

Figure 1a is a plan-view TEM micrograph of a diamond film grown with 0.5% CH_4 in H_2. A wide range of grain sizes up to ~ 1 μm is observed and the diamond particles appear randomly oriented. In Figure 1b, a centered dark field (CDF) micrograph of this same film, a crack extends across the field of view (indicated by the arrow on the micrograph).

Under higher magnification, the defect structure within the diamond crystals was observed. Figure 2a is a brightfield micrograph in which a high density of twins is observed on two {111} planes. By using a (111) diffracted spot from one set of the twins, the centered dark field micrograph shown in Figure 2b was obtained. In addition to the high density of twins stacking faults and dislocations were observed. Figures 3a and 3b are bright field XTEM micrographs of diamond films grown at 0.3% and 2.0% CH_4 concentrations, respectively. The diamond film which was grown at 0.3% CH_4 has much lower defect density than the film grown at 2.0% CH_4. In addition, an interfacial layer of β-SiC (confirmed via SAD) was observed in the 0.3% CH_4 film while no such layer was present in the film grown at 2.0% CH_4. Figure 4 is a High Resolution TEM (HRTEM) micrograph of the afore-mentioned film grown at 0.3% CH_4. Note that {111} cross fringes observed in the silicon carbide layer are aligned epitaxially with the fringes observed on the silicon substrate. The thickness of the silicon carbide layer is approximately 50Å. Figure 5 is a HRTEM micrograph of the 2.0% CH_4 diamond film. Note the absence of any apparent layer of SiC. The diamond grain observed in this micrograph is epitaxially twinned relative to the silicon substrate. However, not all the diamond grains showed this twinned relationship as illustrated in Figure 6 where two diamond grains are misoriented relative to the substrate. The widely spaced fringes in the center of the micrograph are Moire fringes caused by the overlap of the two diamond grains. The interface region was damaged by the electron beam during the examination of this sample.

In order to study the nucleation of the diamond crystals, a sample was grown in 1.0% CH_4 for 45 minutes. At this point, a complete film has not formed as shown in Figure 6, a plan-view TEM micrograph of this sample. The silicon substrate was scratched with 0.25 μm diamond paste for one hour prior to deposition and these scratches are visible in this micrograph. Note that some diamond particles have nucleated in scratch-free areas, indicating that a scratch is not necessary for nucleation, although it increases the number of nuclei[1].

Closer examination of these particles reveals that they are multiply twinned. Figure 8a is a bright-field TEM micrograph of a multiply twinned particle (MTP) which exhibits five-fold symmetry. Similar MTP's have been observed in different systems such as evaporated gold particles on silicon[2,3]. Figure 8b is a CDF micrograph obtained by imaging with a (111) spot shared by two quadrants of this particle.

CONCLUSIONS

(1) Diamond crystals contain a high density of defects but the defect concentration is reduced at lower methane concentrations; (2) the defects observed include twins, stacking-faults, and dislocations: no precipitates or second phases were observed; (3) thin (50Å) epitaxial buffer layer of β-SiC was observed when the CH_4 concentration was 0.3%; (4) some diamond grains were found to be in a twinned epitaxial relationship with the Si substrate; (5) preliminary observations indicate that diamond particles can nucleate in scratch-free regions on the silicon substrate.

ACKNOWLEDGEMENTS

The authors gratefully acknowledge the assistance of K. More and J. Bentley of Oak Ridge National Laboratories, J. Posthill of NCSU, Sopa Chevacharoenkul of the MCNC and K. Nishimura of Kobe Steel, Ltd. This research was partially supported by the Division of Material Sciences, U.S. Department of Energy under contract DE-AC05-840R21400 with Martin Marietta Energy Systems, Inc.and the SHaRE program under contract DE-AC05-76-ORO0033 with Oak Ridge Associated Universities, and SDIO/IST through ONR.

REFERENCES

1. K. Kobashi, K. Nishimura, Y. Kawate and T. Horiuchi, submitted to Phys. Rev. B.
2. T. Komoda, Jpn. J. Appl. Phys., 7, 27 (1968).
3. S. Ino and S. Ogawa, J. Phys. Soc. Jpn., 22, 1365 (1967).

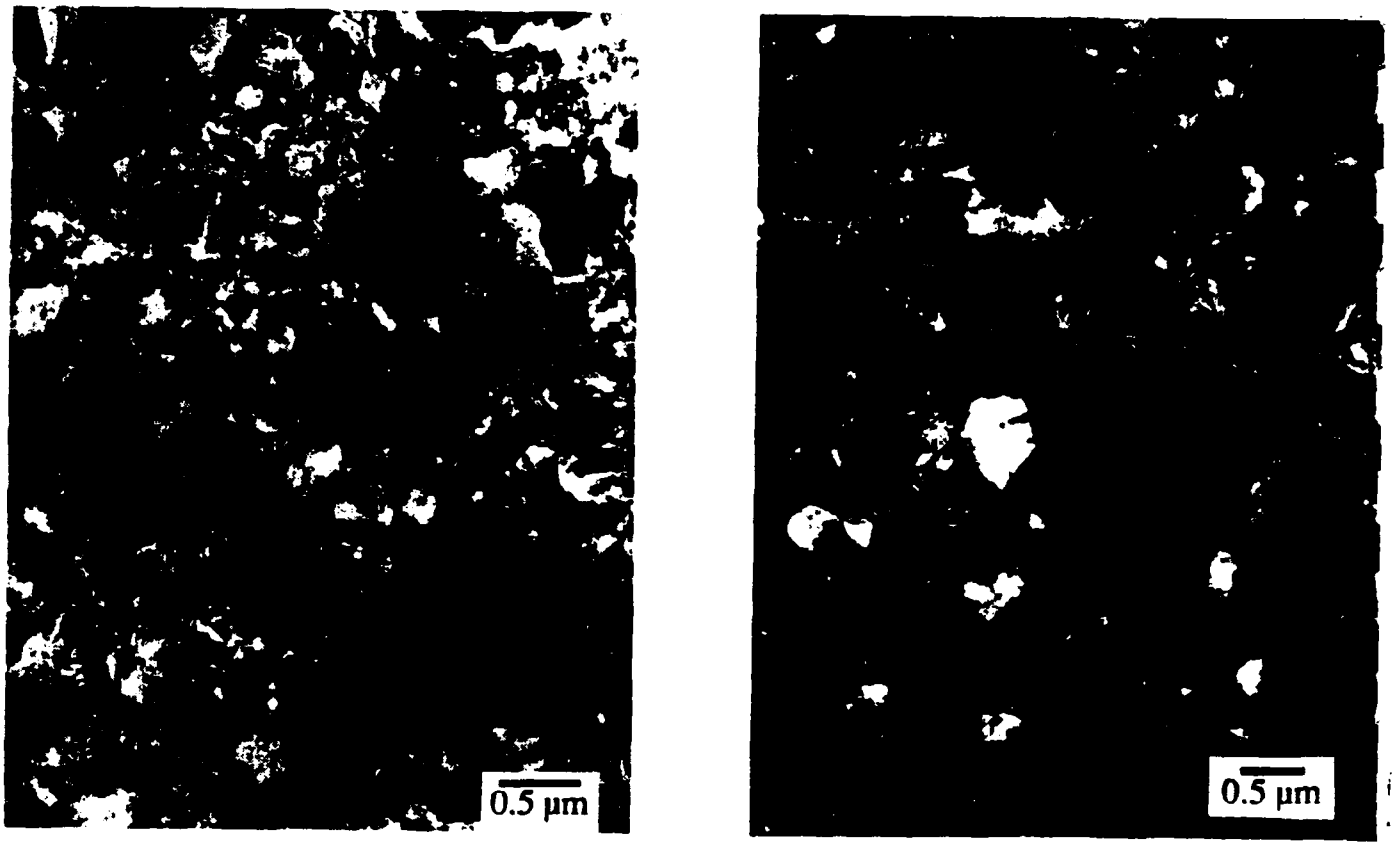

Figure 1

Figure 2a

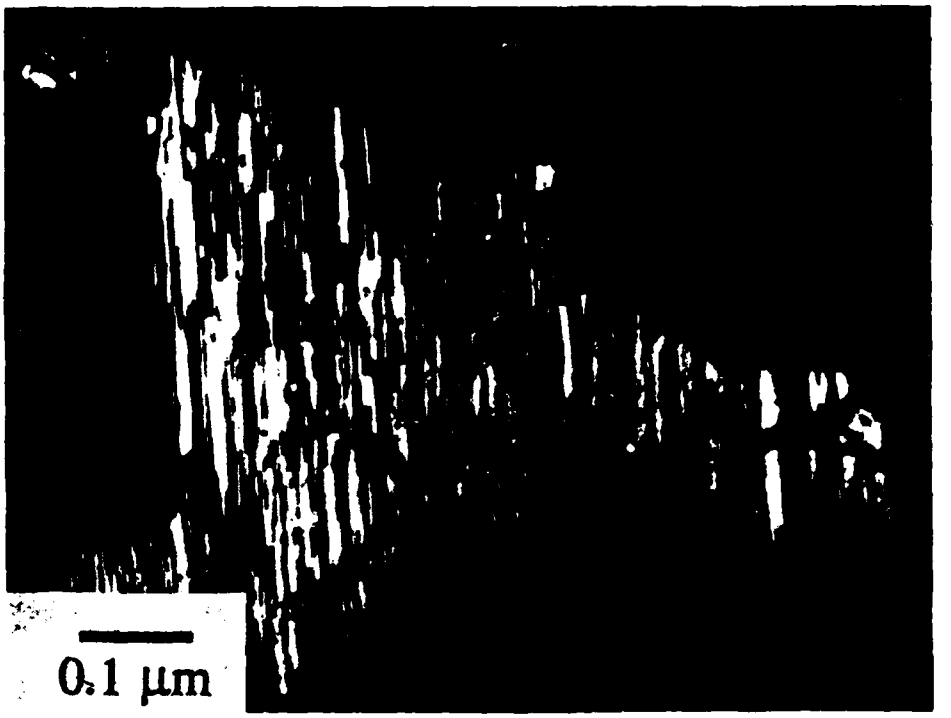

Figure 2b

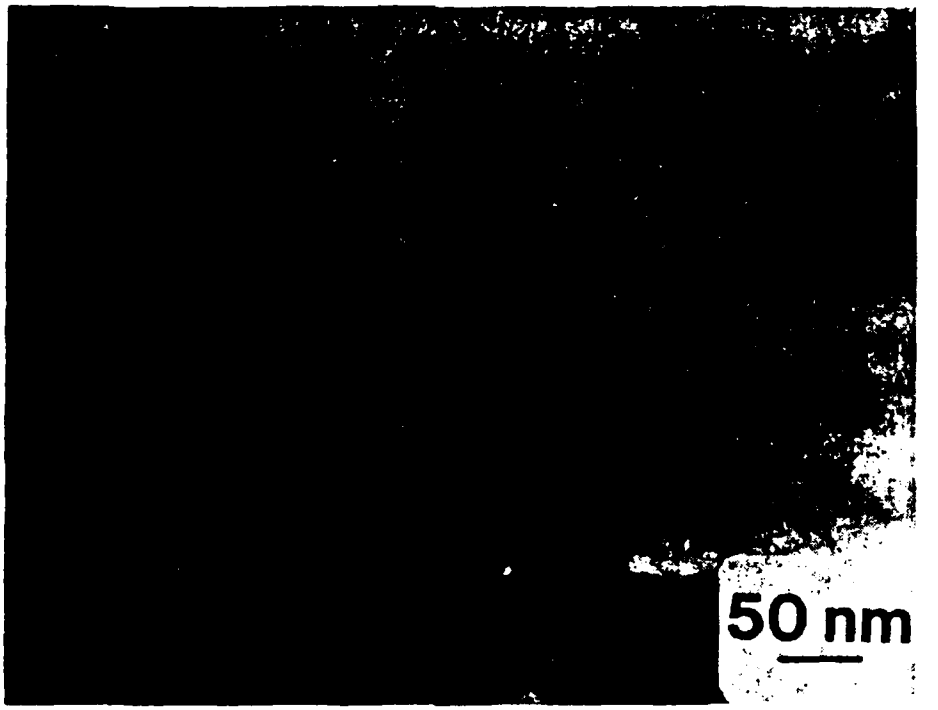

Figure 3a

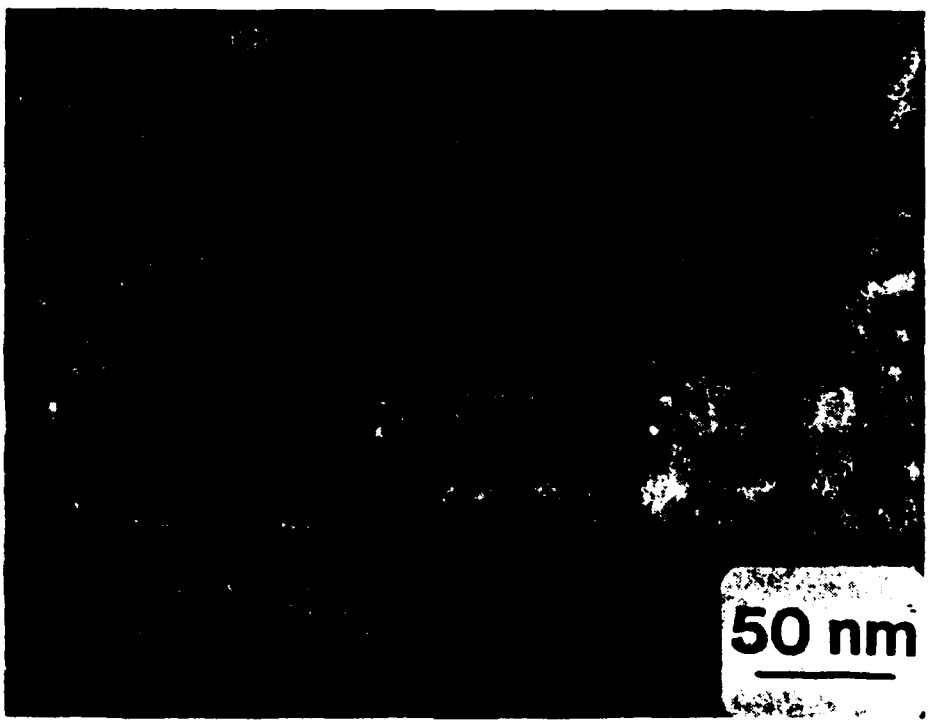

Figure 3b

Figure 4

Figure 5

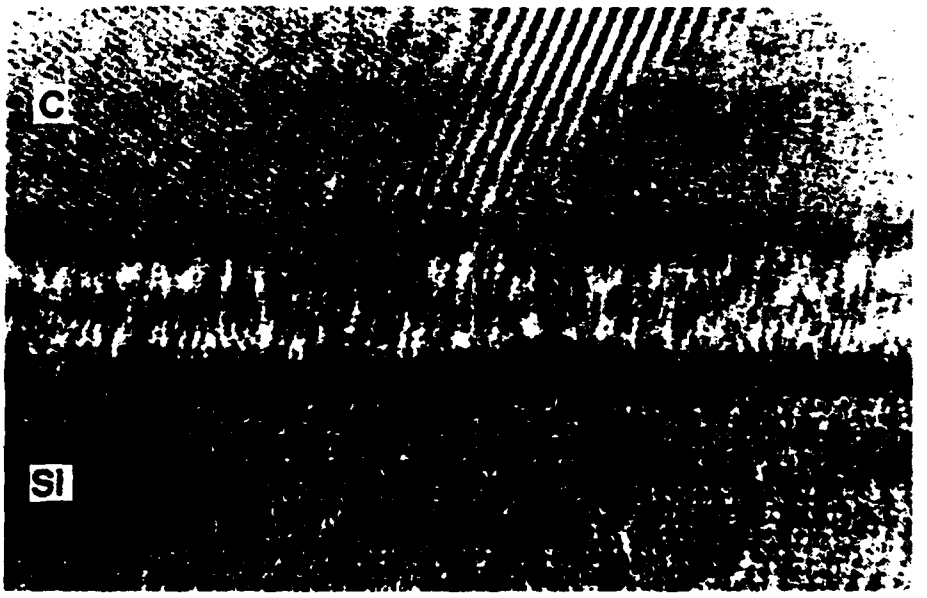

Figure 6

Figure 7

(a) (b)

Figure 8

To appear in the Journal of Vacuum Science and Technology, presented at the 34th National Symposium of the American Vacuum Society, Nov. 1987, Anaheim, CA.

RAMAN SCATTERING CHARACTERIZATION OF CARBON BONDING IN DIAMOND AND DIAMOND-LIKE THIN FILMS

R. J. Nemanich, J. T. Glass, G. Lucovsky, and R. E. Shroder

Departments of Physics and
Materials Science and Engineering
North Carolina State University
Raleigh, NC 27695-8202

ABSTRACT

The atomic bonding configurations of carbon bonding in diamond and diamond-like thin films are explored using Raman scattering. The general aspects of Raman scattering from composites are presented. Effects are discussed due to crystalline or amorphous structures, large vs. microcrystalline domains, and strong optical absorption and transparent regions. The Raman scattering from diamond-like films show several features which are attributed to microcrystalline graphite-like structures which all originate from the same region in the sample. In contrast, the spectra of diamond films show features attributed to different components of a composite film. Components identified are crystalline diamond, and disordered and microcrystalline graphitic structures. The presence of precursor microcrystalline or amorphous diamond structures are also suggested.

I INTRODUCTION

Carbon films produced by plasma enhanced CVD or similar processes are hard, chemically inert and transparent over some wavelength range. The films have been characterized as diamond[1-3] or diamond-like[4-6]. The diamond-like films are very uniform, hard and transparent at wavelengths greater than 2μm.[4-6] These films have already been applied as anti-reflective and/or protective coatings for infrared optics.

The plasma enhanced CVD process has also been used to produce films with optical properties very similar to diamond.[1-3] While these films could also be used for optical coatings, their potential as a high temperature thin film semiconductor is also being explored. One of the major limitations of these films is that they exhibit roughness due to the crystalline grains of the films. To be useful as a semiconductor technology it is necessary to produce smooth films. Heteroepitaxial film growth is one of the goals of the research.

This paper discusses aspects of the characterization of the carbon bonding in diamond and diamond-like thin films.[7] We will emphasize Raman scattering, but related x-ray and electron diffraction measurements will be mentioned. These techniques are often used as structure sensitive probes. Raman scattering displays aspects of the vibrational properties of the material which can then be related to atomic bonding configurations. The films that are produced by the plasma enhanced CVD processes will exhibit varied atomic structures. In fact a particular film will exhibit variations of the structures on several scales and can be considered as a composite. We will focus on the limitations of the techniques to measuring composite films. In addition, the vibrational excitations and the atomic bonding are also dependent on the composite nature of the films and these aspects will be discussed.

The CVD process usually involves methane, hydrogen, and possibly inert gases and oxygen. Films produced by CVD deposition techniques can yield crystalline and amorphous structures. In the case of carbon films an additional question is whether the atomic bonding in the films is three-fold coordinated (sp^2) as in graphite or four-fold coordinated (sp^3) as in diamond. Thus the films have the possibility of four different microstructures - amorphous or crystalline diamond, and amorphous or crystalline graphitic structures. In this terminology, we are suggesting that an amorphous network in which the local atomic configuration of the carbon is approximately tetrahedral would be called amorphous diamond, and if the neasrest neighbor configuration is approximately planar three-fold carbon, then the structure would be termed as amorphous graphitic. Another very interesting possibility is an atomically mixed structure of three- and four-fold coordinated carbon. Hydrogen is also often present in the films and can affect the atomic structure. While the long term goal of the growth studies may be to produce films with a single structure, the films currently being produced are composites of the possible structures

described above. The composite nature extends from the atomic scale with possible co-existing three- and four- fold carbon, up to the micron scale with crystalline and amorphous domains.

While Raman scattering and diffraction measurements are often used to characterize thin films, for the CVD films described here, the results must be interpreted in light of the composite nature of the materials. The techniques may be dominated by particular components of the structure and be insensitive to other components. For instance x-ray scattering from crystalline and amorphous regions will exhibit large differences in intensities, and the light scattering measurements are affected by the differences of the optical absorption of the different components of the film.

II MEASUREMENT CHARACTERISTICS

The Raman scattering process involves inelastic light scattering from vibrational excitations in the sample. For crystalline samples, the spectra are due to vibrations with a wavelength determined by the scattering geometry and k-vector conservation. Because the wavelength of light is long on the scale of phonon wavelengths, these requirements select only wavevectors with k~0 or Brillouin zone center excitations. Thus Raman spectra will display sharp peak(s) representing the zone center mode(s). The wavevector conditions can also be satisfied by two phonons with nearly equal and opposite crystal momentum. This scattering is termed second order scattering. The second order Raman component is continous and often is similar to the vibrational density of states but on twice the frequency scale (since two phonons participate in each scattering event). The first and second order Raman spectra of diamond[8] and graphite[9] are compared in Fig. 1. The sharp features at 1332cm^{-1} and 1580 cm^{-1} are the first order zone center modes of diamond and graphite, respectively. These frequencies are indicative of the different bond strengths of the diamond and graphite bonding. It should be noted that the 1332cm^{-1} mode in diamond is essentially the highest energy vibrational mode of the structure[8] while for graphite, a second order feature is observed at 3240cm^{-1} (or 2 x 1620cm^{-1}) which is due to slightly higher energy phonons[9] than the mode at 1580cm^{-1}. This analysis indicates that modes with energy greater than 1332cm^{-1} cannot be attributed to diamond structures with long range order.

The CVD process often leads to amorphous films, and we consider now the spectrum of amorphous carbon.[7,10] Samples considered to be amorphous graphite have been previously reported and the spectra is overlaid that of graphite in Fig.1. The spectrum of amorphous fims with diamond structure have not to our knowledge been reported. We can approximate what the spectra would look like by comparison with amorphous Si or with the density of vibrational states of crystalline diamond. We have followed the first possibilty by scaling the frequency axis of the Raman spectrum of a-Si by the ratio of the frequencies of the

mode of the crystal (520/1332). This deduced spectra is also shown in Fig. 1 as an overlay to the diamond spectrum.

III COMPOSITE PROPERTIES

Three different composite structures are considered; micron-scale, microcrystalline and atomically disordered. The following discussion outlines some aspects of the structural properties, the vibrational excitations and the interactions with light and x-rays

For micron-scale composites, the structural properties behave as linear combinations of the properties of the constituent materials. The decay length of phonons is in general less than $1\mu m$, therefore boundary scattering will not significantly affect the phonon lifetimes. This means that the vibrational excitations will exhibit the same spectral response as the bulk samples. Raman scattering and x-ray or electron diffraction from micron-scale composites will exhibit properties that are linear combinations of the orientation randomized (ie. powder patterns) bulk spectra. For diamond-graphite mixtures, the diffraction efficiencies will be similar for the two components if they are both crystalline or amorphous. If, however, one component is crystalline and the other is amorphous, the x-ray scattering will be dominated by the crystalline structure. The optical properties of graphite and diamond are, of course, very different, and they will affect the Raman scattering. Because of resonance effects, Raman scattering from absorbing materials is enhanced. The absolute Raman cross-sections of diamond and graphite have been measured,[11] and it is found that the $1580cm^{-1}$ band of graphite is ~50 times stronger than the $1332cm^{-1}$ band of diamond. Thus the Raman scattering will emphasize the graphitic structures.

Microcrystalline samples exhibit crystalline domains that range from 100nm to as small as 2nm. Because the boundary scattering of the phonons is very strong, it can be assumed that the vibrational excitations of the microcrystals will be confined to a single domain. Phonon decay lengths are often larger than these dimensions, thus the boundary scattering causes the vibrational excitations to exhibit lifetime broadened peak widths. In addition, from the Heisenberg uncertainty principle, the wavevector of the excitations is uncertain ($\Delta k \sim 1/d$, where d is the domain size), and the momentum selection rules of the Raman scattering process are relaxed[12]. These effects have been studied in graphite[9], BN[12] and Si[13]. The effects are prononced on microcrystalline graphite[9] shown in Fig. 1. The microcrystalline samples show broader peaks which are shifted toward peaks in the vibrational density of states. Furthermore, a new feature in the first order spectrum is observed at $1355cm^{-1}$ which is attributed to a peak in the vibrational density of states. An additional feature is also observed at 2940 cm^{-1} in the second order spectrum.

A composite on an atomic scale can be called either an alloy or an amorphous network. It is, of course, somewhat incorrect to label these structures as composites. In the case of carbon, an

amorphous network composed of 3- and 4-fold coordinated C could be possible.[7] The vibrational and electronic excitations would not be confined to a single atomic site, and thus would represent an average of the network possibilities. The optical properties would not strongly favor enhancement of the 3-fold (graphitic) over 4-fold sites, and we would expect approximately equal scattering efficiencies. Thus we would anticipate a Raman spectrum with broad features extending from 1100cm^{-1} to 1600cm^{-1}.

IV CVD DIAMOND AND DIAMOND-LIKE FILMS

Consider first the properties of diamond-like thin films produced by plasma enhanced CVD. The Raman spectra of two films produced under differing deposition conditions are shown in Fig. 2. The first thing to note is that the spectra do not compare to any of the spectra discussed as characteristic of amorphous or crystalline diamond or graphite. This implies that the samples are not characteristic of those structures. The two strongest features at 1590cm^{-1} and 1355cm^{-1} are similar to the vibrational features of diamond and graphite. Thus one is tempted to consider this data as indicative of a micron-scale composite of those structures. There are two arguments against this possibility. The first is that the feature at 1355cm^{-1} is at a higher frequency than any of the vibrations of the diamond lattice. While effects such as strain are known to shift frequencies to higher wavelengths, this large shift would indicate a compressive stress of over 10 kbar.

The second argument against the consideration of this peak as due to diamond structures is based on the interpretation of the second order spectrum of graphite and the spectra of microcrystalline graphite samples. The strongest feature in the second order spectrum of graphite is at 2710cm^{-1}. This feature at twice the frequency of 1355cm^{-1} indicates a strong peak in the vibrational density of states of graphite. The peak is also observed in the first order spectrum of microcrystalline graphite, and its presence has been ascribed to the uncertainty of the wavevector of the vibrations due to the finite size of the domains. The next question to be addressed is whether the excitations at 1355cm^{-1} and 1590cm^{-1} represent a composite nature of the film. As noted, there is a feature at 2940cm^{-1} which also appears in the spectrum of microcrystalline graphite. This feature has been ascribed to a two phonon excitation.[9] The energy corresponds to the sum of the 1355 and 1590 cm^{-1}. This indicates that these two modes occur in the same region of the sample. This leads to the conclusion that all of the strong features in the spectra can be accounted for by microcrystalline regions of the sample.

These results do not mean that there are no regions that exhibit diamond structure. In fact electron energy loss experiments show features which can be attributed diamond structures. It is also difficult to account for the optical properties of the diamond like films if they are purely graphitic structures. The Raman scattering from graphite, however, is exceptionally strong

because of the high absorption. Thus it is possible that regions of microcrystalline or amorphous diamond exist in the samples, but are not detected by the Raman scattering.

Under slightly different deposition conditions, diamond thin films can be produced. The substrates are often roughened with diamond powder and then cleaned. The substrate roughness can act as nucleation sites for the growth of diamond films. The Raman spectra of two films prepared at different deposition conditions are shown in Fig. 3. The spectra show a sharp line at 520cm^{-1} which is attributed to the Si substrate. The features due to the Raman scattering ride on top of a strong luminescence background. In Fig. 3a, there is a sharp peak at 1332 cm^{-1}. This is the frequency of diamond crystals. A broad spectral component is observed which is centered at ~1500cm^{-1}. This component is to be distinguished from the features similar to microcrystalline graphite at 1580 and 1355cm^{-1}. The spectrum (b) in Fig.3 shows a very weak spectral feature at 1332cm^{-1} and a strong component at 1500cm^{-1}. This spectrum also shows the double peaks at 1580 and 1355 cm^{-1} which are similar to those associated with microcrystalline graphite. Within the scope of the various possibilities described above it could be concluded that the spectral features indicate a three component composite. The feature at 1332cm^{-1} has the properties that it is very sharp and the intensity does not correlate with that of the other spectral components. This indicates that it is due to micron-scale or large microcrystalline regions of diamond. The other features are broad and can be ascribed to amorphous regions of the sample. These regions may exist between the diamond crystalline domains or they could be inclusions.

The broad spectral features can be separated into two components. The features at 1355 and 1580 cm^{-1} are representative of structures similar to microcrystalline graphite. The broad feature at ~1500cm^{-1} does not have an obvious origin. Two possibilities for this feature are (1) an amorphous network of four- and three-fold coordinated carbon or (2) an impurity-carbon amorphous network. Raman spectra of carbon-rich SiC:H alloys produced by low temperature plasma CVD[14] show a broad Raman spectral feature centered at 1500cm^{-1}. SIMS analysis of some films has indicated the presence of Si, and other studies have reported features attributed to crystalline SiC. Thus we suggest that regions of amorphous carbon rich SiC exist in the diamond films.

The question remains whether there is a diamond-like precursor to the formation of the diamond regions. The only unaccounted strong spectral feature in the Raman spectra is that at ~1140cm^{-1}. This feature is present in films with small amounts of diamond crystalline domains indicating that it could be a precursor structure. This feature occurs in a region that might be expected for amorphous or microcrystalline diamond. The microcrystalline diamond could be traditional or a polytype in the wurtzite structure. The frequencies of wurtzite diamond have not to our knowledge been reported, but by comparison with the frequencies of SiC we would deduce a vibrational frequency of the strongest mode to be ~1175cm^{-1} with an additional weaker feature at

1330cm^{-1}. Thus we suggest that this feature is due to regions of microcrystalline or amorphous diamond.

V CONCLUDING REMARKS

The Raman scattering effects due to composites of carbon components are discussed. The possibilities include crystalline or amorphous diamond or graphite. The strong difference in the optical absorption of the different structures lead to large differences in the Raman sensitivity to different structures. For micron-scale and microcrystalline composites, because of the strong optical absorption, graphite like structures will dominate the Raman spectra while x-ray or electron diffraction will be dominated by crystalline domains. For atomic scale composites or amorphous alloys, it is proposed that the Raman scattering from diamond and graphite like features will exhibit equal scattering strength.

The analysis of the first order spectra of diamond-like films shows no features which can be attributed to crystalline diamond structures. Extending the analysis to the second order spectra shows that the major features of the spectra originate from the same atomic structures. The spectra, therefore, show no evidence of composite nature, but other measurements indicate the presence of diamond structures. It is likely that these are not observed because of the weak signal from the diamond structures with respect to the graphitic structures.

The Raman spectra of diamond films show composite characteristics. Crystalline regions of diamond structure are observed along with microcrystalline or disordered graphitic structures. One feature is observed which can not be accounted for by any of the known structures of graphite or diamond. By comparison with the spectra of amorphous and microcrystalline Si, we ascribe this feature to amorphous or microcrystalline diamond structures.

ACKNOWLEDGEMENT

We gratefully acknowledge R. Markunas, R. Rudder and D. Vitkavage of the Research Triangle Institute and K. Kobashi and T. Horiuchi of Kobe Steel, Ltd. for supplying the samples used in this study. We appreciate the many helpful discussions from the RTI group. This work was supported in part by the Office of Naval Research under contract N00014-86-K-0666.

REFERENCES

1. S. Matsumato, Y. Sato, M. Tsutsumi, N. Setaka, J. Mat. Sci. 17, 3106(1982).

2. A. Sawabe and T. Inuzuka, Thin Solid Films 137, 89(1986).

3. Y. Hirose and Y. Terasawa, Jpn. J. App. Phys 25, L519(1986)

4. C.B. Zarowin, N. Venkataramanan, and R.R. Poole, Appl. Phys. Lett. 48, 759(1986).

5. V. Natarajan, J.D. Lamb, J.A. Woollam, D.C. Liu and D.A. Gulino, J. Vac. Sci. Technol A3, 681(1985).

6. T. Mori and Y. Namba, J. Vac. Sci. Technol. A1, 23(1983).

7. For a review see J. Robertson, Adv. Phys. 35, 317(1986).

8. S.A. Solin and A.K. Ramdas, Phys. Rev. B1, 1687(1970).

9. R.J. Nemanich and S.A. Solin, Phys. Rev. B20, 392(1979).

10. S.A.Solin and R.J. Kobliska, Amorphous and Liquid Semiconductors, ed. by J. Stuke (Taylor and Francis, London, 1974), p.1251.

11. N. Wada and S.A. Solin, Physica 105B, 353(1981).

12. R.J. Nemanich, S.A. Solin and R.M. Martin, Phys. Rev. B23, 6348(1981).

13. P.M. Fauchet and I.H. Campbell, CRC Critical Reviews on Solid State and Materials Science, (in press).

14. A. Morimoto, M. Kumeda, and T. Shimizu, J. Non-Cryst. Solids 59&60, 537(1983).

FIGURE CAPTIONS

FIG. 1 The Raman spectra of diamond, a), graphite, b), and microcrystalline graphite, c). The solid lines in a) and b) represent the first and second order spectra of crystalline diamond and graphite respectively. The broad line labeled α in a) is the spectrum of a-Si scaled to the diamond frequency to represent the spectrum of amorphous diamond, while the broad line labeled α in b) is that due to amorphous graphite (from ref. 10).

FIG. 2 The first and second order Raman spectra of plasma enhanced CVD films produced with different deposition conditions which are characteristic of diamond-like structures. Spectrum (b) shows distinct first order features at 1355 and 1590 cm^{-1} and second order features at 2710 and 2940 cm^{-1}.

FIG. 3. The Raman spectra of CVD films which exhibit the feature at 1332cm^{-1} characteristic of crystalline diamond. The samples were prepared under different conditions using Si substrates, and the sharp feature at 520cm^{-1} is due to the substrate. Both samples show a strong background due to luminescense. Both samples show the feature at ~1330cm^{-1} due to crystalline diamond and broad features due to other components.

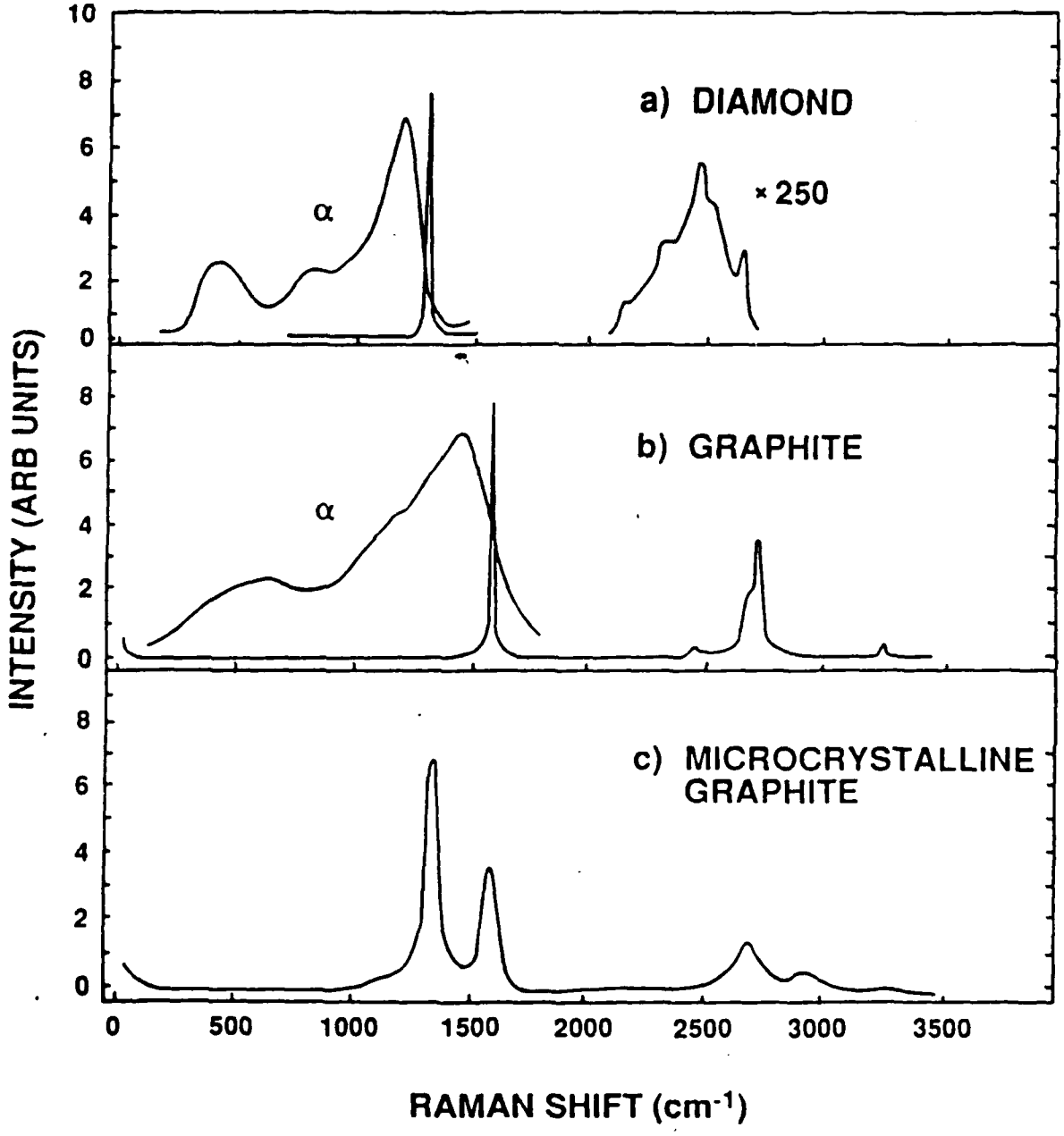
a) DIAMOND
× 250
α
b) GRAPHITE
α
c) MICROCRYSTALLINE GRAPHITE
INTENSITY (ARB UNITS)
RAMAN SHIFT (cm-1)
0
2
4
6
8
10
0
500
1000
1500
2000
2500
3000
3500

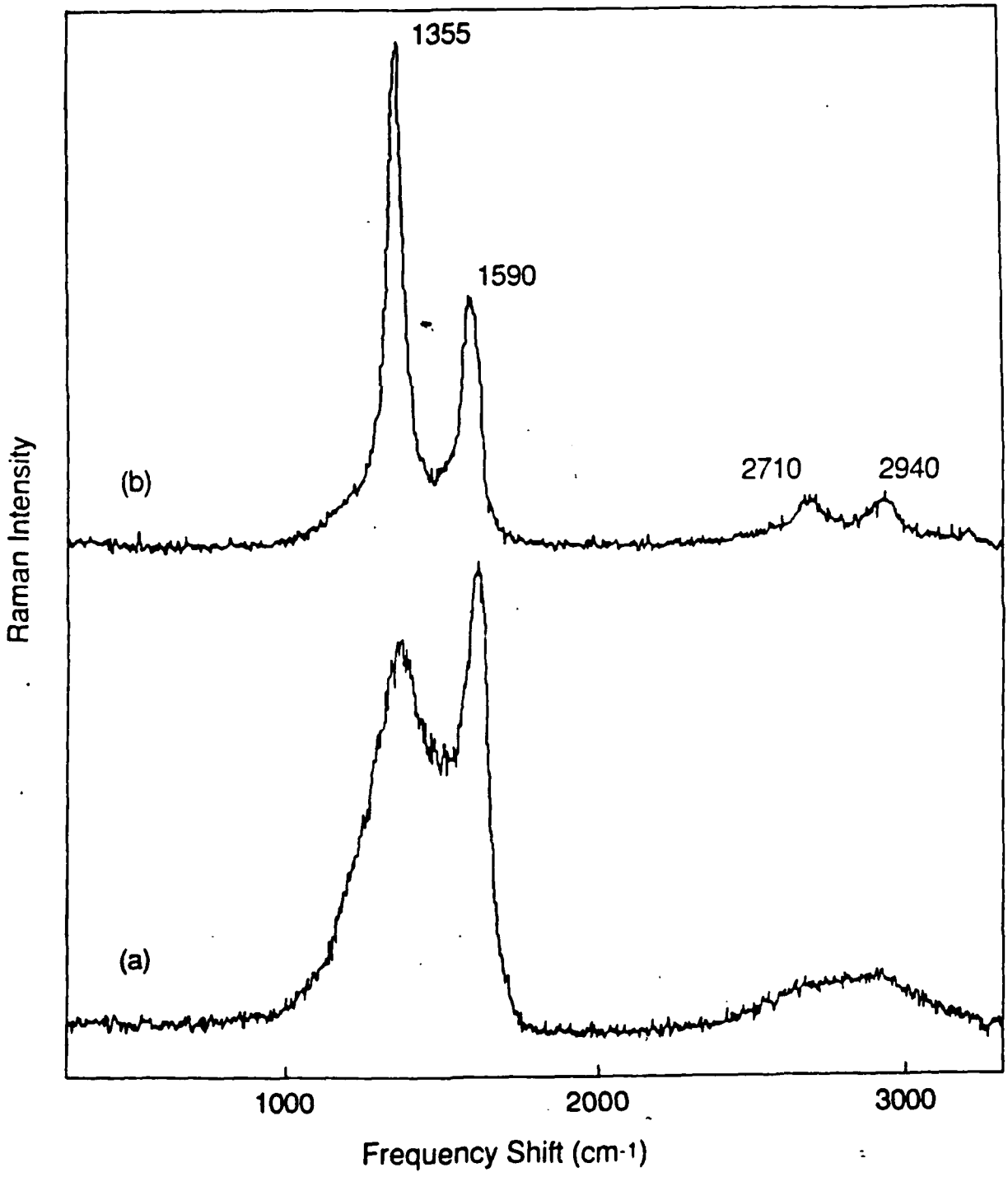
1355
1590
2710
2940
(b)
(a)
Raman Intensity
1000
2000
3000
Frequency Shift (cm-1)

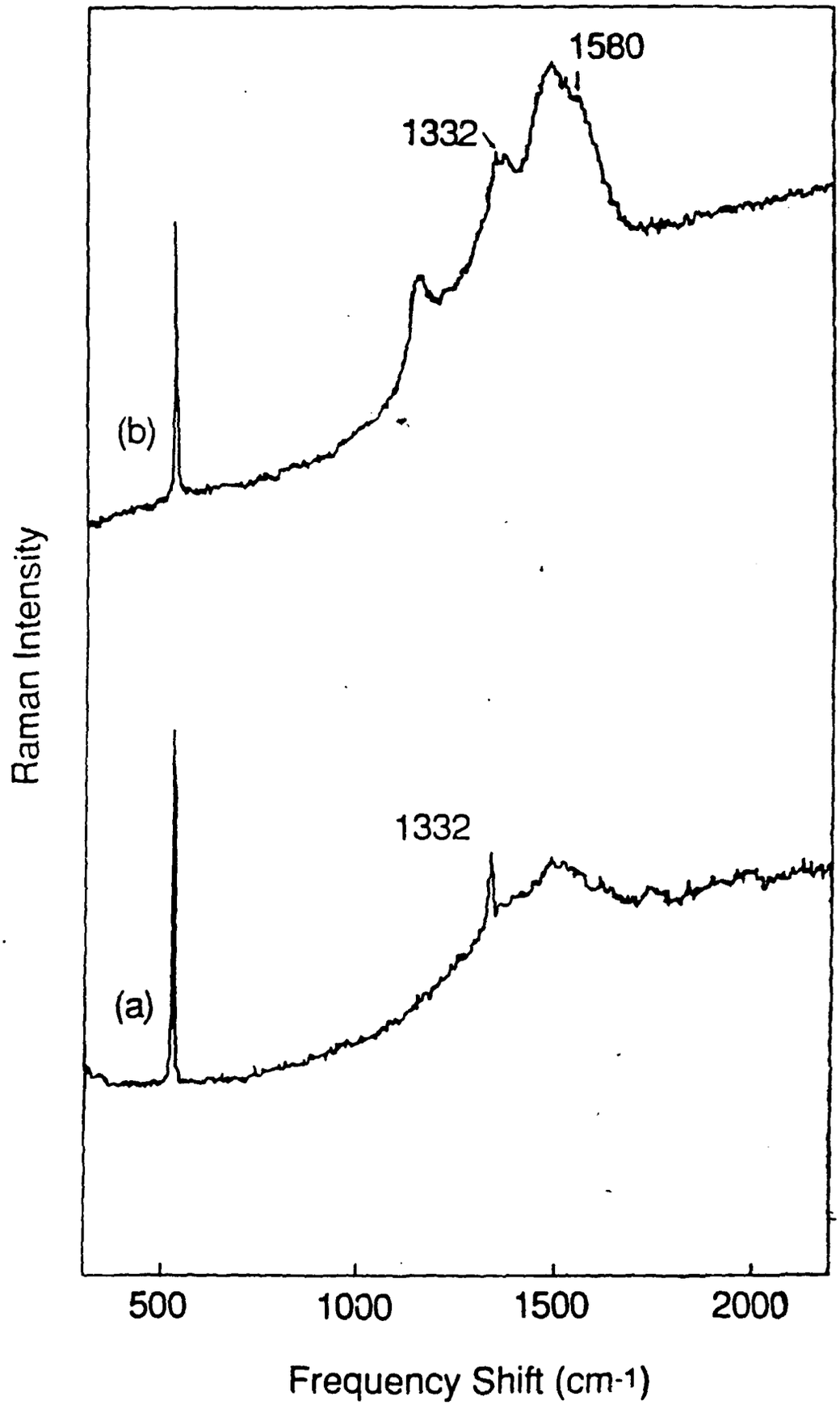
1580
1332
(b)
1332
(a)
Raman Intensity
500
1000
1500
2000
Frequency Shift (cm-1)

SPIE - Optics Conference, San Diego, CA
August, 1983

RAMAN ANALYSIS OF THE COMPOSITE STRUCTURES IN DIAMOND THIN FILMS

R.E. Shroder, R.J. Nemanich, and J.T. Glass

North Carolina State University, Departments of Physics and Materials Science and Engineering, Raleigh, NC 27695-8202

ABSTRACT

Raman spectroscopy has been used to examine diamond thin films produced by various CVD processes. The Raman spectra exhibit features which suggest that the films are composites of diamond (sp^3) and graphite-like (sp^2) bonding. A brief outline of Raman scattering from composites is presented. A first attempt at modeling these types of films using composites of diamond and graphite powders is reported. It is found that the Raman features associated with sp^2 bonding in the films do not correlate well to features exhibited by microcrystalline graphite.

I. INTRODUCTION

In recent years Raman scattering has been used to characterize the carbon films produced by various CVD processes[1-3]. This technique has proved useful for examining the diamond and graphite-like structures in the films. As the goal of the research is to produce single crystal, homoepitaxial diamond on a variety of substrates, Raman spectroscopy could be used to accurately determine the relative concentrations of these structures; thereby, demonstrating the quality of the materials produced in the deposition process. We have examined these possibilities using composites of graphite and diamond powders, and correlated the results to the diamond thin films.

The Raman spectra obtained from the carbon films have generally concentrated on the appearance of the first-order Raman mode of diamond at $1332cm^{-1}$. Diamond is characterized by 4-fold coordinated sp^3-type bonding of F_{2g} symmetry[4]. It possesses a single triply degenerate zone-center optical phonon which corresponds to the highest energy mode in the phonon dispersion curves of diamond, so that features in the spectra with energy higher than $1332cm^{-1}$ cannot be attributed to diamond structures of long range order. Other features do appear in the Raman spectra of carbon films from ~ 1350 - $1600cm^{-1}$, and are normally associated with structures having 3-fold coordinated sp^2-type bonding such as graphite. Films which display a variety of these features can be considered composites of sp^2 and sp^3 bonding (i.e. containing regions of differing atomic structures), and it is these types of films which have been closely examined. Particular attention has been focused on the relative intensities of the peaks associated with each type of bonding, in an effort to determine if the Raman scattering from diamond films can be used to give an estimate of the relative concentrations of sp^3 to sp^2-type bonding in the films.

The Raman spectra of two diamond films produced under differing deposition conditions are shown in Fig. 1. Both spectra contain the diamond peak at $1332cm^{-1}$, but other features are present. Spectum (a) also shows features at $1355cm^{-1}$ and $1580cm^{-1}$ which are similar to those associated with microcrystalline graphite[5], and a feature centered at ~$1500cm^{-1}$ which has been assigned to regions of amorphous carbon.[6] Spectrum (b) shows a broad feature at ~ $1500cm^{-1}$ which is dominated by the diamond peak and has been ascribed to regions of highly disordered graphite[1]. In this study we will show that the size and absorption properties of these sp^2 and sp^3-type domains strongly affect the relative strengths of the Raman features described above. The

details of Raman scattering from different carbon structures has been discussed elsewhere[6], so we provide a brief overview of Raman scattering from composites.

2. COMPOSITE PROPERTIES

The three types of composite structures considered are: micron-scale, microcrystalline, and atomically disordered. For micron-scale constituent materials, the Raman spectrum should appear as a linear combination of the features of the bulk materials. If one of the constituents of the composite is strongly absorbing, then light incident on particles of this type is completely absorbed. The effective absorption depth of the composite should be approximately equal to that of the highly absorbing constituent, modified by the relative concentrations of the absorbing and non-absorbing materials. As the domains decrease to microcrystalline scales, features should begin to appear in the Raman spectrum due to size effects associated with the breakdown of the conservation of wavevector[5]. The small domain size creates an uncertainty in the wavevector ($\Delta k \sim 2\pi/d$ where d is the domain size), and the momentum selection rules for the Raman scattering process are relaxed. The length scale of the crystallites is now on the order of or smaller than the absorption depths of the constituent materials and the decay length of the phonons, so that crystallite diffraction effects create a more uniform illumination of the composite. For an atomically disordered composite, the Raman spectrum becomes the average of the vibrational and electronic properties of the random network, and would appear quite different than the Raman spectra of the bulk materials.

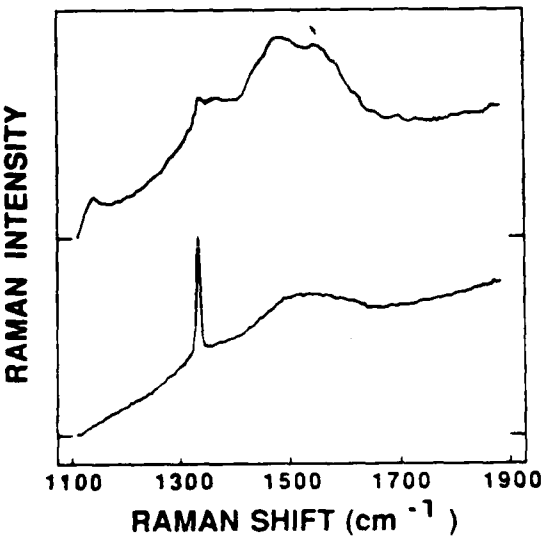

Fig. 1. First-order Raman spectra of diamond thin films. Both of the samples were produced by microwave plasma CVD. The sharp feature at 1322cm^{-1} is indicative of crystalline diamond while features between 1350 and 1600cm^{-1} are attributed to sp^2 bonded carbon.

3. EXPERIMENTAL

In order to model the ratio of sp^2 to sp^3-type bonding in diamond thin films, composites of diamond and graphite powders were examined. These powders were obtained from commercially available sources[7,8]. The diamond powder was slightly gray in appearance and of ~1μm crystallite size. The graphite powder was black and very cohesive and contained crystallites of 30-40μm size. Admittedly, this is large for our purposes, but we wished to examine the effects of the concentration of diamond in the composites. The examination of effects due to crystallite size was left for later. The composites were created as follows; appropriate amounts of diamond and graphite powder were weighed, and the relative concentrations determined. The powders were then mixed using mortar and pestle, and the resulting composites were lightly pressed into

aluminum sample holders. The samples were mounted in the backscattering configuration, and the spectra were taken using the 5145Å line of an Ar^+ laser.

4. RESULTS AND DISCUSSION

A. Raman spectra of diamond and graphite composites

Several of the Raman spectra taken from the composite samples are shown in Fig. 2. The two peaks exhibited are the first-order Raman mode of diamond at $1332cm^{-1}$ and the first-order mode of graphite which has been shown previously to occur at $1580cm^{-1}$ [9]. The relative concentration of diamond in the samples ranges from ~1% up to 60%. The most interesting feature of these spectra is that the ~1% diamond composite displays a 1:1 ratio between the peak intensities of the first-order modes of diamond and graphite. At 50% diamond, it is seen that the peak due to graphite has practically disappeared. Thus, the absorption of graphite has a significant effect on the Raman spectra of the composites, and is shown in the large disparity of the absolute intensity scales of the samples. As is to be expected, the relative intensities of the two peaks change in proportion to the concentration of diamond present in the composite. If the ratio of the peak intensities of diamond and graphite versus concentration of diamond in the samples is plotted, Fig. 3 is obtained. It is again noted that the diamond peak dominates the spectrum even at relatively low concentrations of diamond. The solid curve has been added as a guide to the eye, but the data might be fitted very well using an appropriate model of the Raman scattering from composites of diamond and graphite. This model could then be applied to the diamond films previously discussed and an estimate of the ratio of sp^2 to sp^3-type bonding obtained.

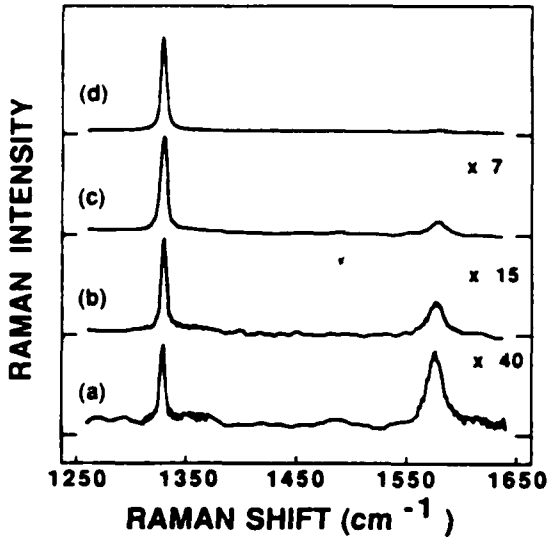

Fig. 2. First-order Raman spectra of the composites of diamond and graphite powders. The relative concentrations of diamond in the samples are: (a) 1.3% (b) 6.6% (c) 21.5% (d) 50.0% The spectra have been multiplied by the indicated value.

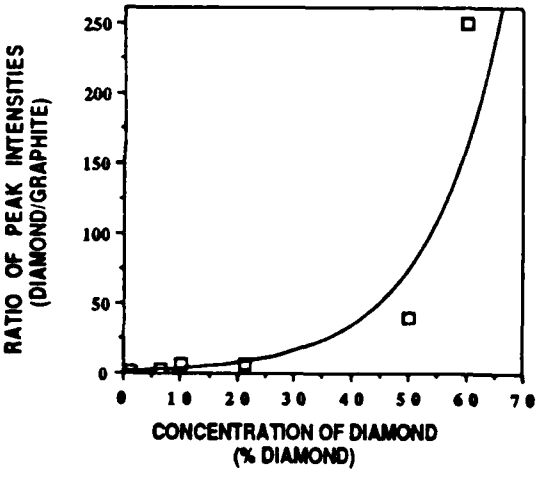

Fig. 3. Ratio of peak intensities (I_D/I_G) vs. relative concentration of diamond in the composite samples. The solid line is not a fit to the data.

B. Theoretical model

In order to model the diamond and graphite composites, we must understand the various parameters which effect the intensity of the Raman signal from these materials. Loudon[10] demonstrated that for a sample mounted in a backscattering geometry, the scattering intensity is given by

$$I = \frac{I_0 S}{S+\alpha_1+\alpha_2}\{\, 1 - \exp[-(S+\alpha_1+\alpha_2)L]\,\} \tag{1}$$

where S is the scattering efficiency, I_0 is the incident intensity, L is the sample thickness in the direction of the incident laser light, and α_1 and α_2 are the absorption coefficients at the respective frequencies of the incident and scattered light. Wada and Solin[11] showed that this equation could be modified to give the ratio of the scattering intensities of two different materials:

$$\frac{I_G}{I_D} = \frac{I_{oG}}{I_{oD}}\left(\frac{A_G}{A_D}\right)\left(\frac{1}{L_D(\alpha_1+\alpha_2)}\right)\left(\frac{\Delta\Omega_G}{\Delta\Omega_D}\right)\left(\frac{(1-R)^2}{(1-R_D)}\right)\left(\frac{(\sum_j [e_2\cdot R_j\cdot e_1]^2)_G}{(\sum_j [e_2\cdot R_j\cdot e_1]^2)_D}\right) \tag{2}$$

where S has been redefined in terms of a scattering efficiency, A, and a summation over the inner product of the Raman tensor, $\mathbf{R}_j$, of the degenerate first-order mode and the polarization unit vectors of the incident and scattered light, e_1 and e_2. I_G and I_D represent the scattered intensity from the graphite and diamond powders, and I_0 represents the incident intensity . $\Delta\Omega$ is the solid angle into which light is scattered, and the term in R corrects for reflection of the scattered light at the sample surface and multiple reflections in the sample as in diamond. Here, α_1 and α_2 are the previously defined absorption coefficients of graphite since it has been assumed that diamond is transparent to the visible laser radiation.

If we now attempt to apply Eq. (2) to the composite samples, several difficulties must be faced. Since the Raman signal is being collected from a region of discreet particles, unique values for L_D and $\Delta\Omega$ no longer exist. Also, even if it assumed that each graphite particle is completely absorbing (i.e. much larger than the absorption depth), reflection losses due to light scattering between the diamond particles must still be accounted for. Finally, note that the last term in Eq. (2) provides unique values for the summations if it is known *a priori* the polarization directions of the incident and scattered light. Since the diamond and graphite composites contain particles of completely random orientation, an angle averaged value of the summations over all possible polarization directions must be taken.

We therefore modeled the diamond and graphite composites as follows; assuming that the collection angle ($\Delta\Omega$) is the same and neglecting reflective losses, the ratio of the scattering intensities of diamond to graphite may be written:

$$\frac{I_D}{I_G} \sim \frac{A'_D N_D V_D}{A'_G N_G V_G} \tag{3}$$

where A' is the angle and polarization averaged scattering efficiency, N is the atomic density of diamond or graphite, and V is the volume of material which is actually sampled by the Raman scattering. In terms of the bond densities of diamond and graphite, the percentage of diamond in the composite may be written as:

$$P_D = \frac{N_D}{\frac{3}{4}N_G + N_D} \quad \text{or re-writing} \quad \frac{N_D}{N_G} = \frac{3}{4}\left(\frac{P_D}{1-P_D}\right) \quad \text{so that Eq. (3) becomes}$$

$$\frac{I_D}{I_G} \sim \frac{3\,A_D\,V_D}{4\,A_G\,V_G}\left(\frac{P_D}{1-P_D}\right) \tag{4}$$

and the factor of 4/3 accounts for the fact that diamond contains 4 nearest neighbor bonds and graphite only 3 nearest neighborbonds per atom. The first-order Raman mode in both diamond and graphite is a bond stretching mode.

It has been reported[11] that the ratio between the scattering efficiencies of diamond and graphite is ~ 50:1, so that the only unknown in Eq. (4) is the ratio of the volumes, V_D/V_G. If we assume an average size for the graphite particles of ~ 30μm diameter, then we can model a unit volume of a 50% composite to be two spheres, each ~ 30μm diameter, one being graphite and the other, a loose collection of diamond particles. As was previously stated, the diamond is essentially transparent to the incident laser light, so that the entire "sphere" would be illuminated. At the 5145Å exciting wavelength, however, graphite has an absorption depth of ~ 300Å[11], although considerable discepancies exist in the literature over the optical constants of graphite. Because the scattered light must also exit the absorbing region, we therefore consider the volume of graphite sampled to be a thin layer, ~150Å thick, across the top half of the graphite "sphere" as shown in Fig. 4. At P_D = 50%, our calculated value for I_D/I_G differs from that shown in Fig. 3 by a factor of two. This is in reasonable agreement considering our approximations.

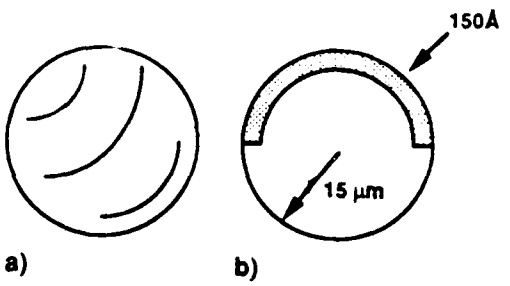

Fig. 4. Model of the unit volumes in the Raman scattering from composites. (a) fully illuminated diamond particles of ~ 30μm size (b) graphite particle of ~ 30μm size, partially illuminated in a 150 Å surface layer.

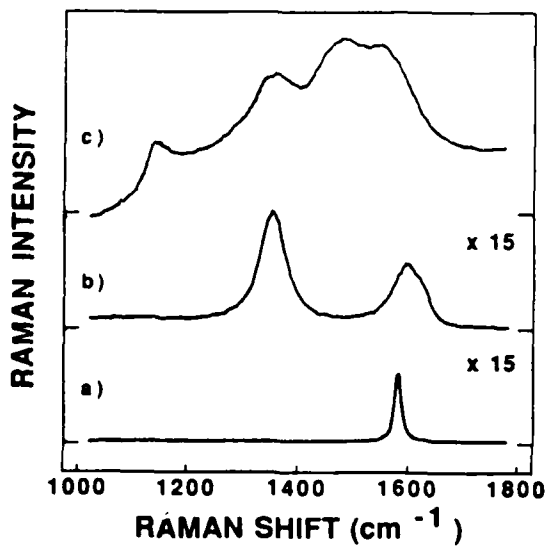

Fig. 5. First-order Raman spectra of (a) highly oriented pyrolytic graphite (b) "glassy" carbon (c) diamond thin film produced by microwave plasma CVD. The spectra have been multiplied by the indicated value.

We wish to emphasize the importance of crystallite size on our results. For smaller values for V_D and V_G, it is expected, from our model, that the peak in the Raman spectrum due to graphite would appear more strongly at higher concentrations of diamond than the results shown in Figs. 2, 3 indicate. This implies that the relative concentration of sp^3-type bonding in the films shown in Fig. 1 is higher than the composite samples suggest.

Upon examining the films in Fig. 1, we become aware of a very important characteristic of the features exhibited in the composite films. In Fig. 5, the Raman spectra of three materials containing sp^2-type bonding are shown. The highly oriented pyrolytic graphite (HOPG) and the "glassy" carbon samples both exhibit peaks at $1580cm^{-1}$ which have approximately the same absolute intensity. However, the composite diamond film shown in Fig. 5(c) has an absolute intensity ~15 times greater than these two. If the sp^2-type features in the diamond films are to be attributed to regions of crystalline or microcrystalline graphite, then this difference in the absolute intensity scales must be accounted for. Upon re-examination of Eq. (1), the two parameters which might significantly affect the intensity are the scattering cross section, A, and the absorption coefficients, α_1 and α_2. We propose that the regions of the diamond films attributed to graphite-like structures are actually regions of sp^2-type bonding, dissimilar to graphite, but distinctly different from a-C such that their respective features may be resolved in the Raman spectrum. The results presented in this paper suggest that the optical constants of these structures must be quite different from those of graphite.

4. Concluding Remarks

The Raman spectra of various diamond thin films have been examined. The features displayed by the films suggest that they are composites of sp^2 and sp^3-type bonding. We have attempted to understand the nature of these films using composites of diamond and graphite powder samples. We have proposed a simple model to the Raman scattering from our composites and found reasonable agreement to our experimental data. Our investigation demonstrates that both concentration and crystallite size have significant effects on the resulting Raman spectra. In diamond films containing regions of true diamond and graphite, we predict that the Raman spectra could be used to estimate the relative concentrations of these regions, but we emphasize that the sizes of the various domains in the films must first be known. We have found that the sp^2-type bonding in the films does not correlate well to graphite-like structures, and we therefore propose that the diamond films are composites of sp^3-type bonding having long-range order and sp^2-type bonding of some as yet unknown configuration.

5. Acknowledgement

Y. Kawate

We gratefully acknowledge K. Kobashi and ~~T. Horiuchi~~ of Kobe Steel, Ltd, for supplying the diamond samples used in this study. We also appreciate the helpful discussions of R. Rudder at the Research Triangle Institute and B. Williams at North Carolina State University, as well as, the help of R. Russell at NCSU in the preparation of the composite powder samples. This work was supported in part by SDIO/IST through the Office of Naval Research under contract N00014-86-K-0666.

6. References

1. S. Matsumato, Y. Sato, M. Tsutsumi, N. Setaka, J. Mat. Sci. 17,3106(1982)
2. A. Sawabe and T. Inuzuka, Thin Solid Films 137, 89(1986)
3. K.Kurihara, K. Sasaki, M. Kawarada, N. Koshino, Appl. Phys. Lett. 52 (6), 437(1988)
4. S.A. Solin and A.K. Ramdas, Phys. Rev. B1, 1687(1970)
5. R.J. Nemanich and S.A. Solin, Phys. Rev. B20, 392(1979)
6. R.J. Nemanich, J.T. Glass, G. Lucovsky, R.E.Shroder, J. Vac. Sci. Tech. A6 (3), 1783(1988)
7. The diamond powder was obtained from AESAR CHEMICALS, Seabrook, NH 03874
8. The graphite powder was obtained from ALFA CHEMICALS, Danvers, MD, 01923
9. F. Tuinsta and J.L. Koenig, J of Chem. Phys. 53, 1126(1970)
10. R. Loudon, Adv. Phys. 13, 423(1964)
11. N. Wada and S.A. Solin, Physica 105B, 353(1981)

VI. SDIO/IST – ONR Diamond Technology Initiative Symposium Presentations

July 12–14, 1988

Crystal City, Virginia

" A QUANTITATIVE ANALYSIS OF CARBON BONDING IN DIAMOND AND DIAMOND-LIKE THIN FILMS USING RAMAN SPECTROSCOPY "

R.E. SHRODER, R.J. NEMANICH, J.T. GLASS
DEPARTMENTS OF PHYSICS AND MATERIALS SCIENCE AND ENGINEERING
NORTH CAROLINA STATE UNIVERSITY
RALEIGH, NC 27695

ACKNOWLEDGEMENTS

DR. R.A. RUDDER OF RESEARCH TRIANGLE INSTITUTE

PARTIALLY SUPPORTED BY SDIO/IST

OUTLINE OF DISCUSSION

- GENERAL FEATURES OF DIAMOND AND DIAMOND-LIKE FILMS
- EXAMINATION OF BORON NITRIDE/ DIAMOND AND GRAPHITE/ DIAMOND POWDER SAMPLES
- CORRELATION OF RESULTS TO DIAMOND AND DIAMOND-LIKE THIN FILMS
- CONCLUSIONS AND AREAS OF FURTHER RESEARCH

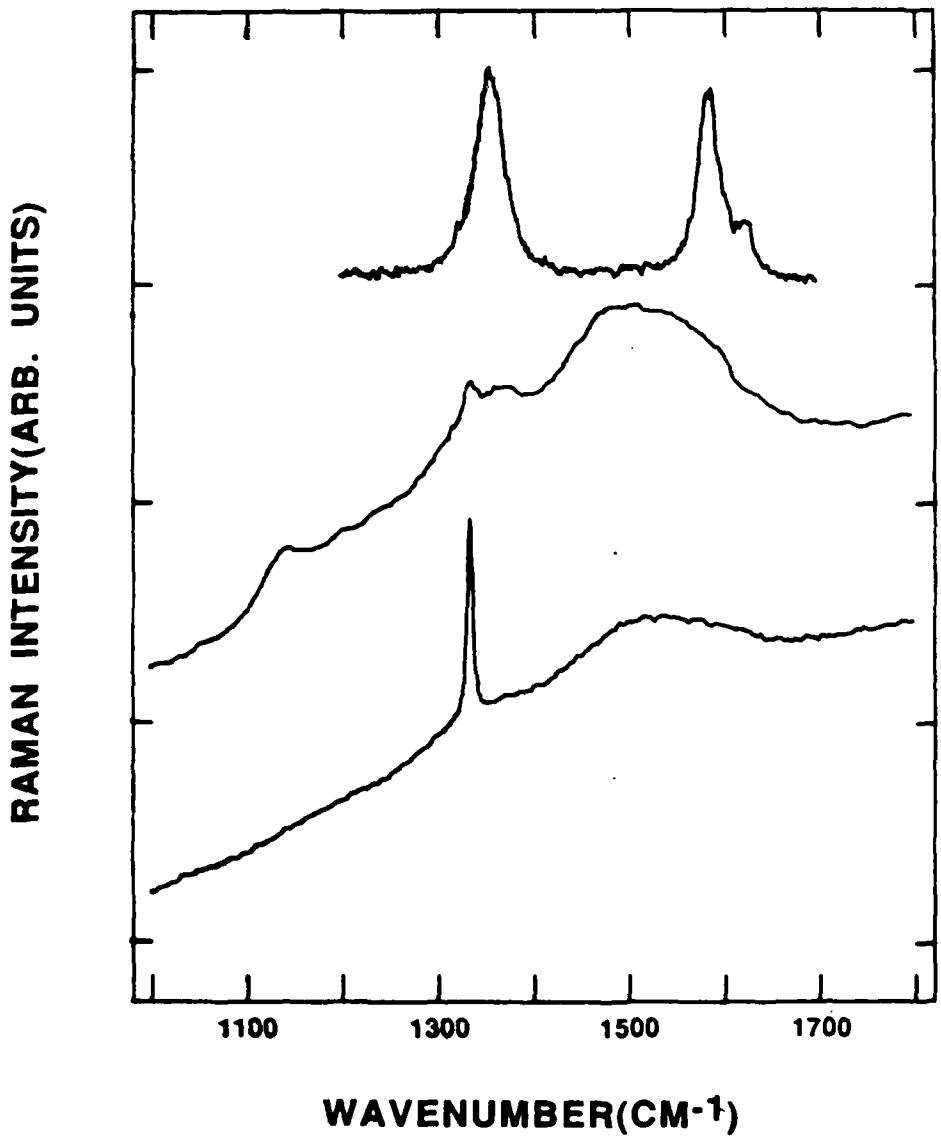
RAMAN INTENSITY(ARB. UNITS)
1100
1300
1500
1700
WAVENUMBER(CM-1)

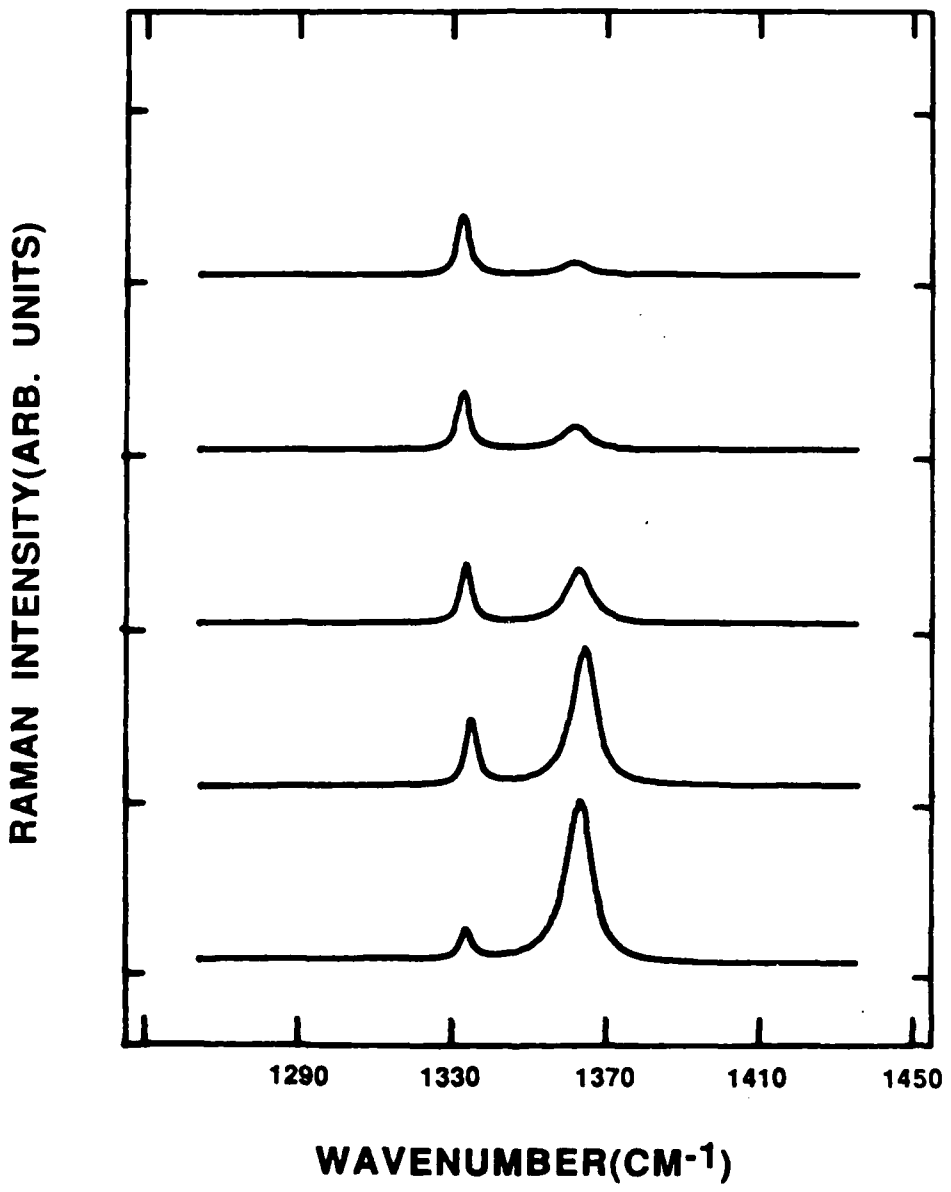
RAMAN INTENSITY(ARB. UNITS)
1290
1330
1370
1410
1450
WAVENUMBER(CM-1)

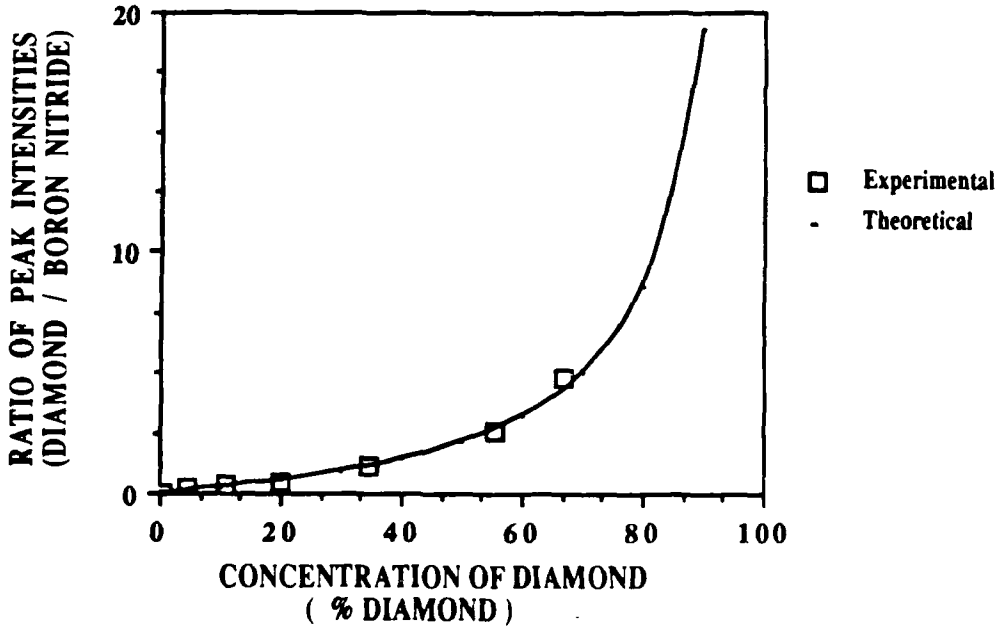

$$I_{\text{BORON NITRIDE}} \sim \alpha_{BN}\, N_{BN}\, V_{BN}$$

$$I_{\text{DIAMOND}} \sim \alpha_{D}\, N_{D}\, V_{D}$$

$$\frac{I_D}{I_{BN}} \sim \frac{\alpha_D\, N_D\, V_D}{\alpha_{BN}\, N_{BN}\, V_{BN}} \qquad V_D \simeq V_{BN}$$

$$\%\ \text{DIAMOND} = P_D = \frac{N_D}{N_{BN} + N_D}$$

$$\frac{I_D}{I_{BN}} \sim \frac{\alpha_D}{\alpha_{BN}} \left\{ \frac{P_D}{1-P_D} \right\}$$

By best curve fitting, $\dfrac{\alpha_D}{\alpha_{BN}} \sim 2.15$

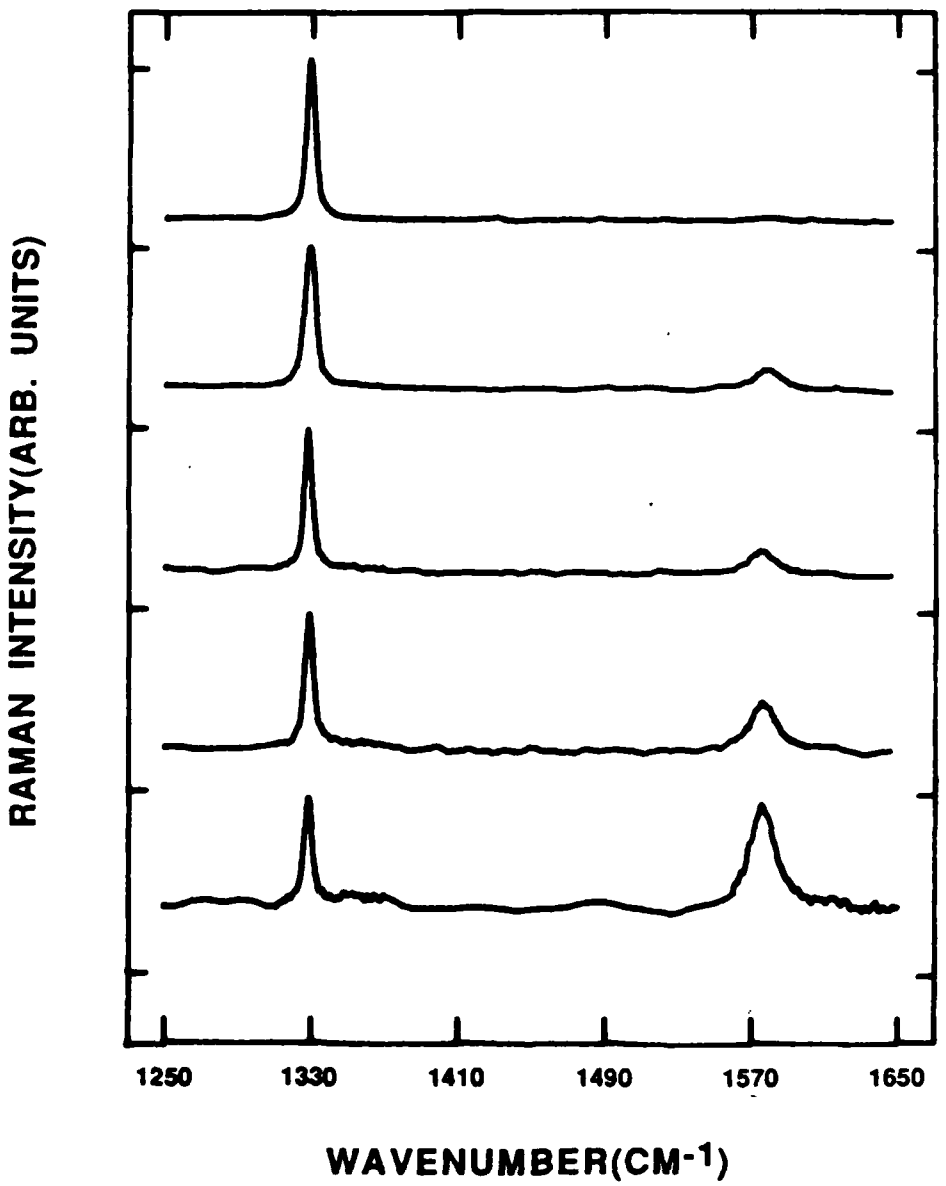
RAMAN INTENSITY(ARB. UNITS)
1250
1330
1410
1490
1570
1650
WAVENUMBER(CM-1)

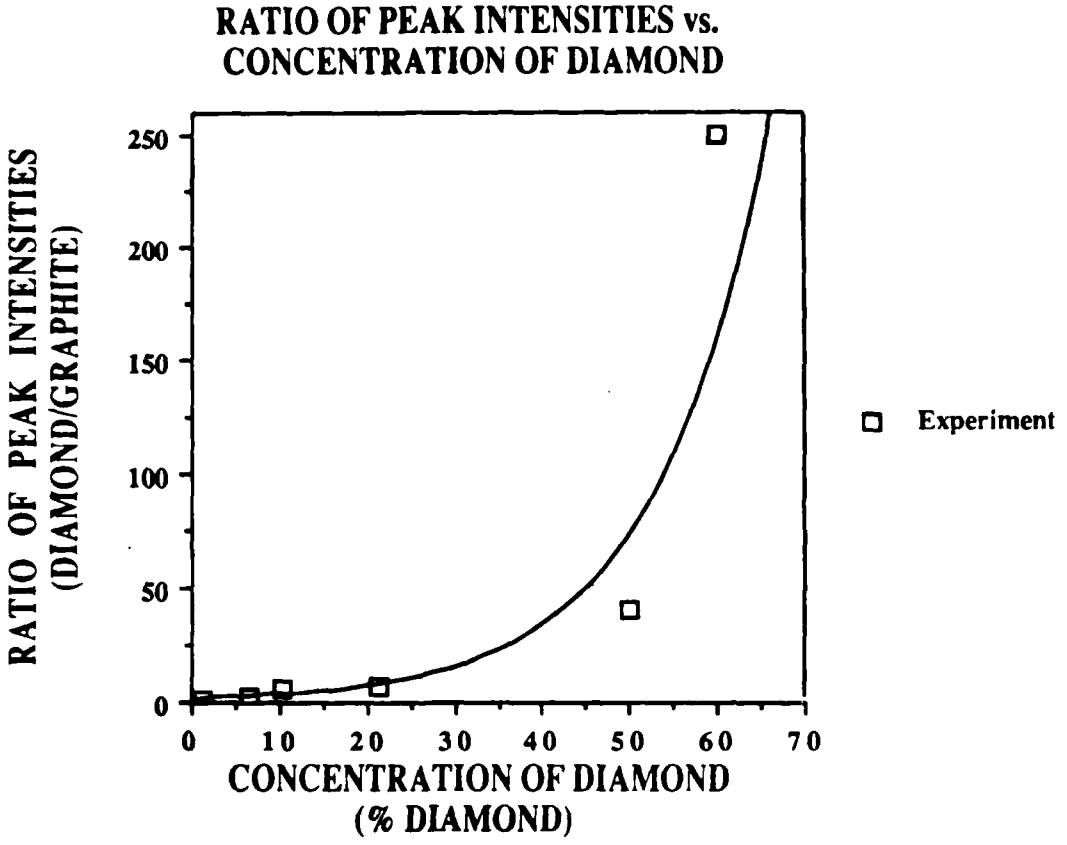
RATIO OF PEAK INTENSITIES vs.
CONCENTRATION OF DIAMOND
RATIO OF PEAK INTENSITIES
(DIAMOND/GRAPHITE)
250
200
150
100
50
0
0
10
20
30
40
50
60
70
CONCENTRATION OF DIAMOND
(% DIAMOND)
Experiment

$$\frac{I_D}{I_G} \sim \frac{\alpha_D N_D V_D}{\alpha_G N_G V_G} \qquad P_D = \frac{N_D}{N_G + N_D}$$

PROBLEMS

1) THE ABSORPTION OF GRAPHITE NOT NEGLIGIBLE

2) MAY NOT ASSUME $V_D = V_G$

$$\frac{I_D}{I_G} \sim \frac{\alpha_D V_D}{\alpha_G V_G} \left\{ \frac{P_D}{1-P_D} \right\} \qquad \alpha_G \sim 50\alpha_D$$

THEN AT $P_D = 50\%$,

$$\frac{I_D}{I_G} \sim \frac{1}{50} \frac{V_D}{V_G} = 35 \qquad \text{OR} \qquad \frac{V_D}{V_G} = 1750$$

MODEL

- INCIDENT LASER LIGHT ABSORBED IN FIRST 400Å
- ASSUME CRYSTALLITE SIZE OF ~ 15μm

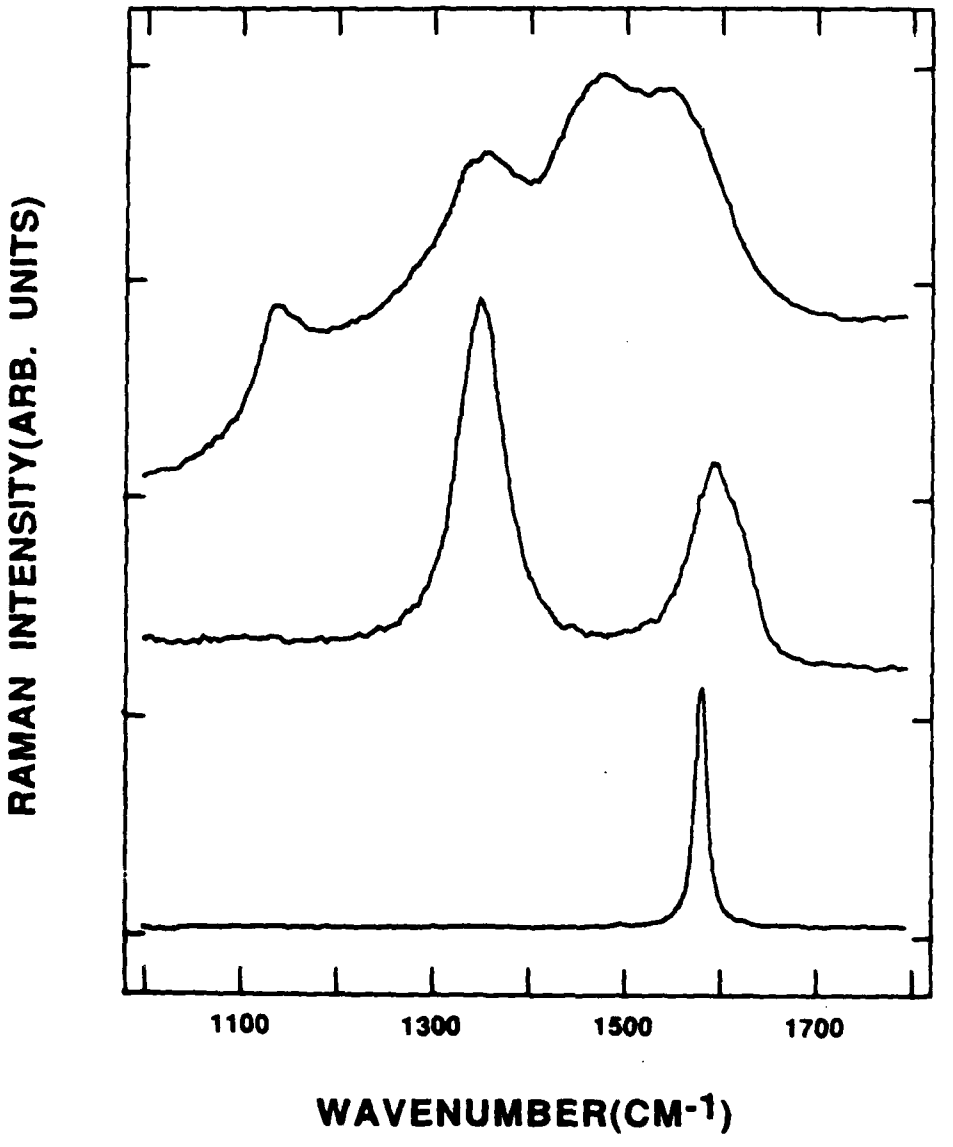
RAMAN INTENSITY(ARB. UNITS)
1100
1300
1500
1700
WAVENUMBER(CM-1)

SUMMARY

- DIAMOND AND DIAMOND-LIKE THIN FILMS ARE COMPOSITES OF SP^2 AND SP^3 STRUCTURES

- SCATTERING CROSS SECTION OF BN GREATER THAN DIAMOND BY A FACTOR OF TWO

- GRAPHITE / DIAMOND COMPOSITES OF 1 % DIAMOND SHOW EQUAL ABSOLUTE PEAK INTENSITIES

- ABSOLUTE PEAK INTENSITIES OF GRAPHITE DO NOT CORRELATE WELL TO STRUCTURES ASSOCIATED WITH SP^2 BONDING IN DIAMOND FILMS

The Analysis of Defect Structures, Substrate/Film Interfaces and Nucleation of Diamond Thin Films

B. E. Williams, J. T. Glass and R. F. Davis
Department of Materials Science and Engineering
North Carolina State University
Raleigh, NC 27695-7907

Thin films of diamond grown by microwave plasma enhanced chemical vapor deposition (MPCVD) have been examined utilizing a variety of electron microscopy techniques including scanning electron microscopy (SEM), transmission electron microscopy (TEM), high resolution TEM (HRTEM), and transmission electron energy loss spectroscopy (EELS). Film morphology, defect structure, the nature of the diamond-substrate interface and the bonding type of relatively local regions will be discussed during the presentation.

The as-grown film surfaces consist of multi-faceted diamond grains up to approximately 1 μm in size. The facets on these diamond grains exhibit symmetry characteristic of certain low index crystallographic planes. In addition, many steps, ledges, and secondary growth sites on the grain facets were observed at high magnification. Plan-view and cross-sectional TEM were utilized to analyze the defects in the diamond films. All of the films examined contained a high density of planar defects that were primarily {111} microtwins and stacking faults. Dislocations in these diamond grains have also been observed. No precipitates or other phases have been observed within the grains or at grain boundaries. However, a thin buffer layer of SiC was observed at the diamond/Si interface. Selected area diffraction and HRTEM indicated it was epitaxial with the Si substrate; however, bright field contrast observed in the layer indicated a high defect density in the layer.

The first lattice imaging of CVD diamond films has also been accomplished and indicates that some diamond grains are in a twinned epitaxial relationship with the Si substrate in local regions, but that other grains are randomly oriented. Finally, a film grown for a relatively short time has been examined to investigate the nucleation stage. No special defects were observed at the scratches and numerous particles were seen to nucleate where no scratches could be seen. Ongoing work includes continued investigation of the initial stages of nucleation and the evaluation of bonding via EELS which has thus far shown no sp^2 component in the film, even in highly defective regions.

Support of SDIO/IST through the Office of Naval Research (M. Yoder, contract monitor) is gratefully acknowledged. Furthermore, partial support of the ORAU-SHaRE program and the efforts of Karren More and James Bentley are very much appreciated. Samples were kindly provided by Dr. K. Kobashi and Y. Kawate of Kobe Steel, Ltd.

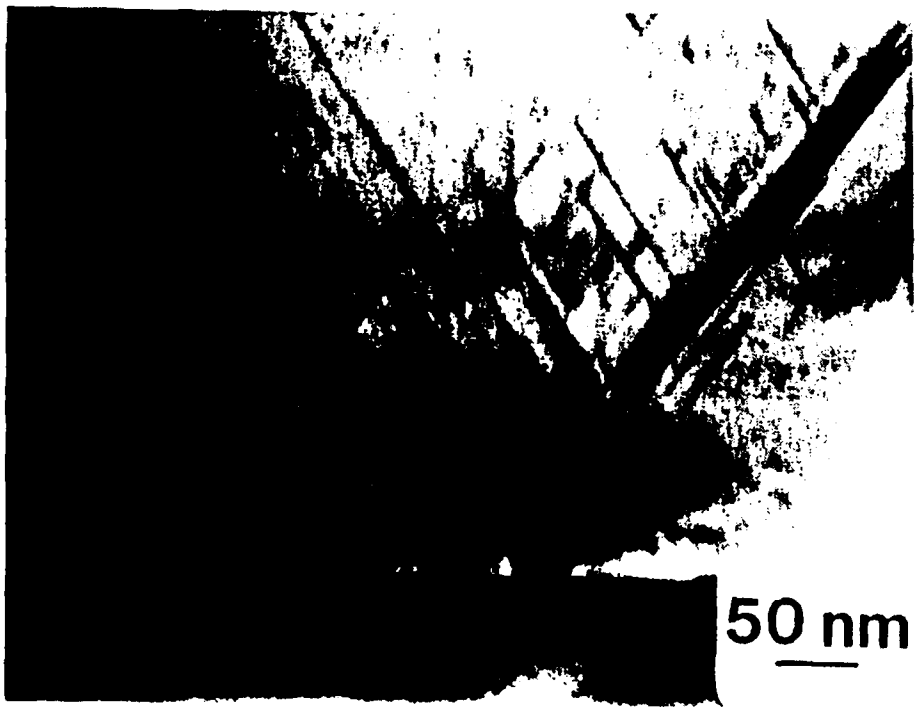
50 nm

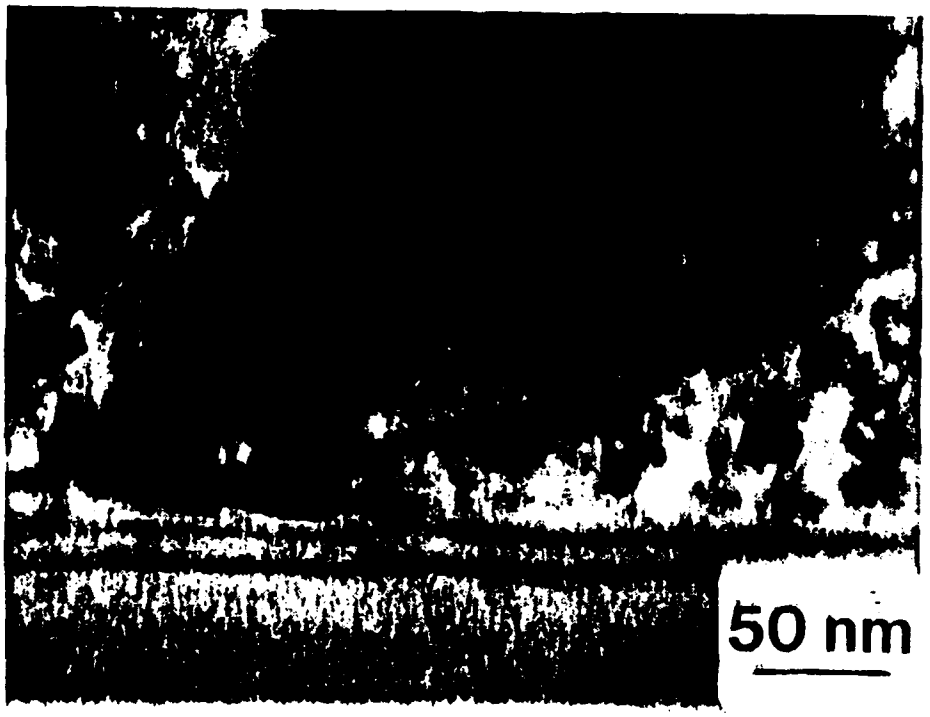
50 nm

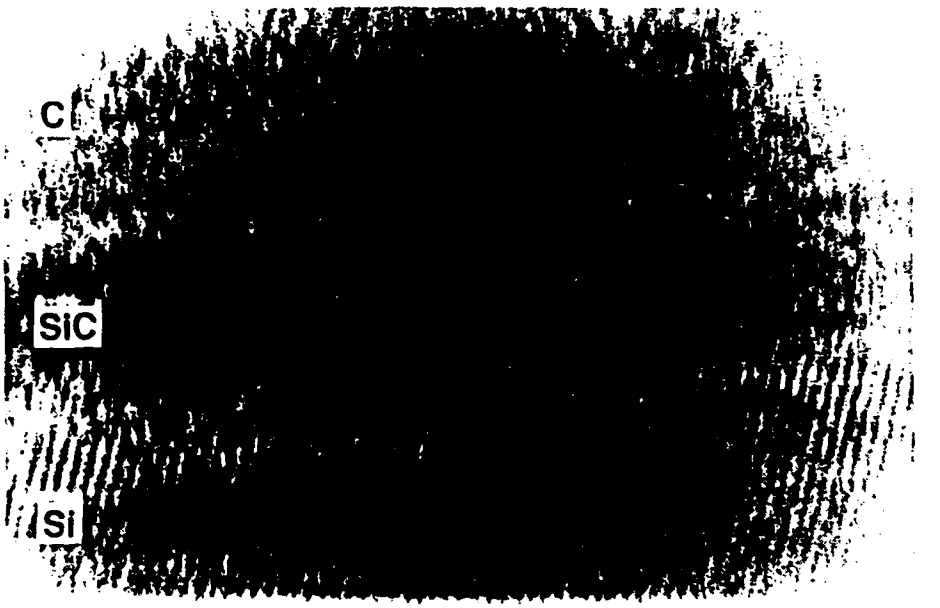
C
SiC
Si

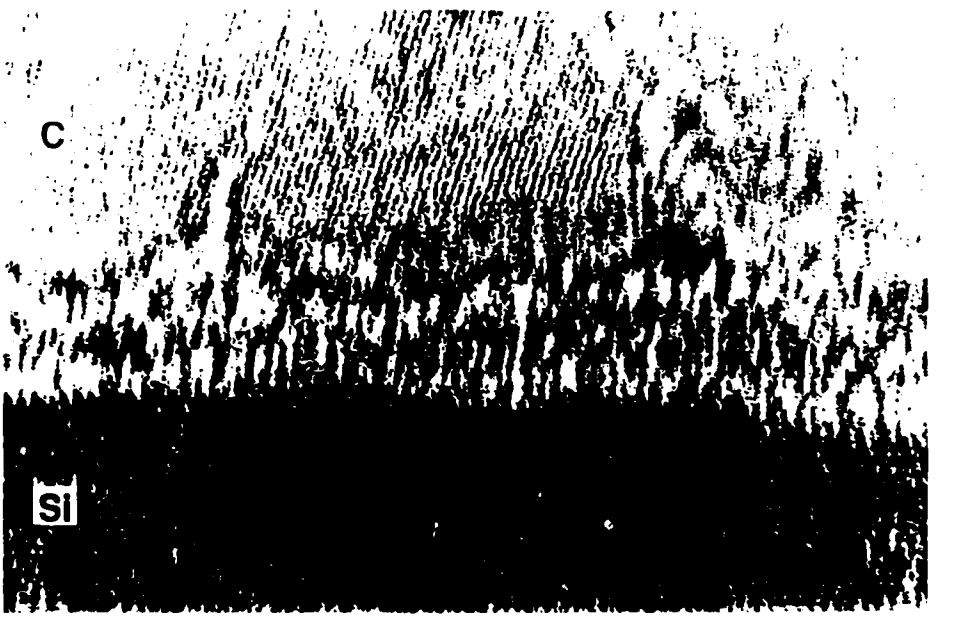
C
Si


0.1 μm

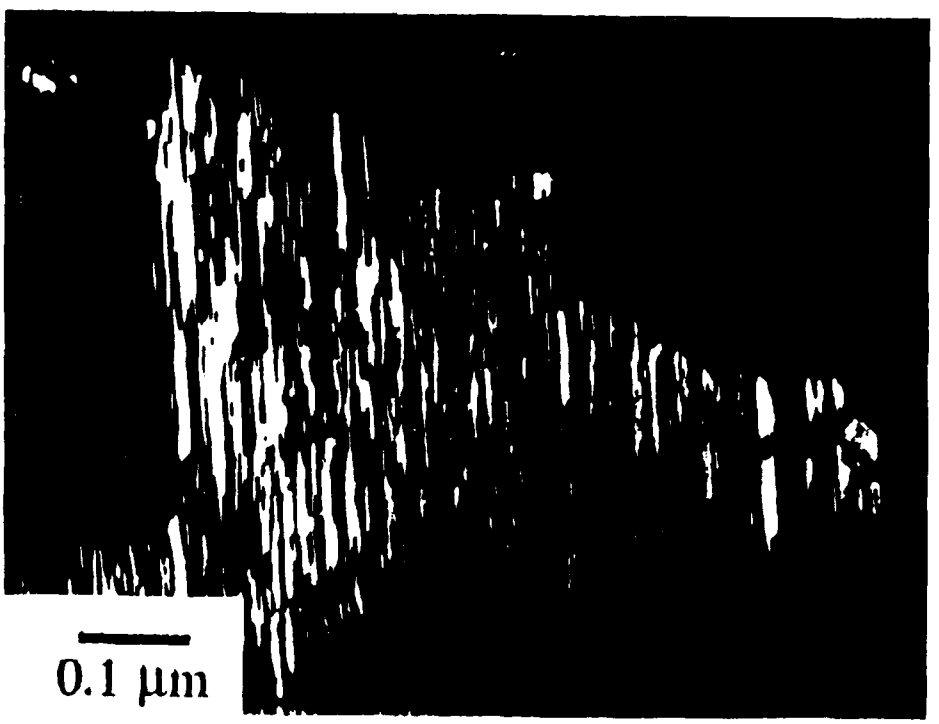
0.1 μm

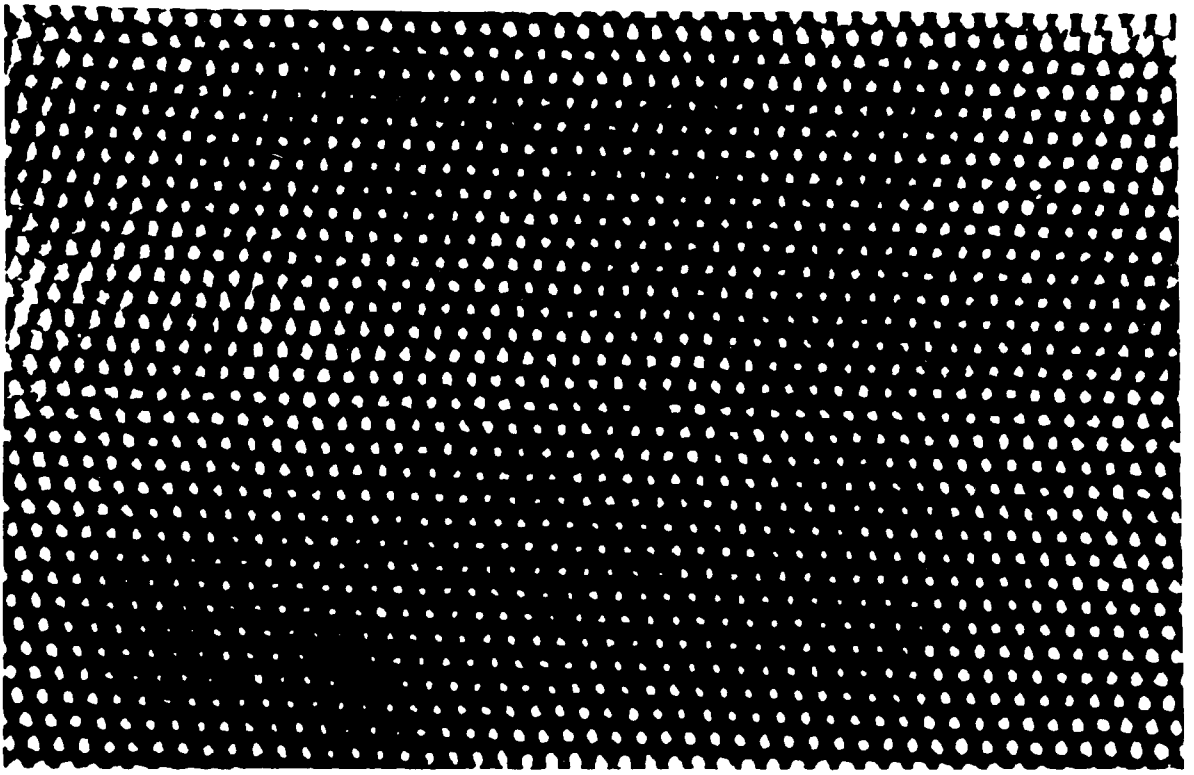

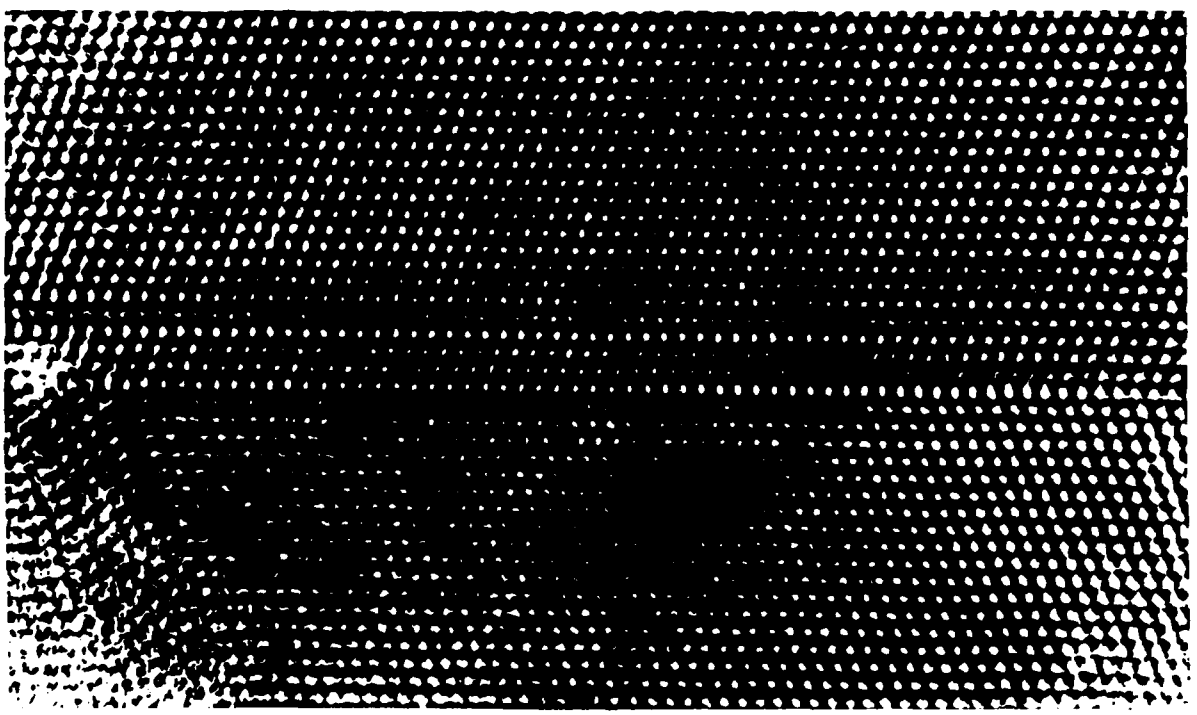

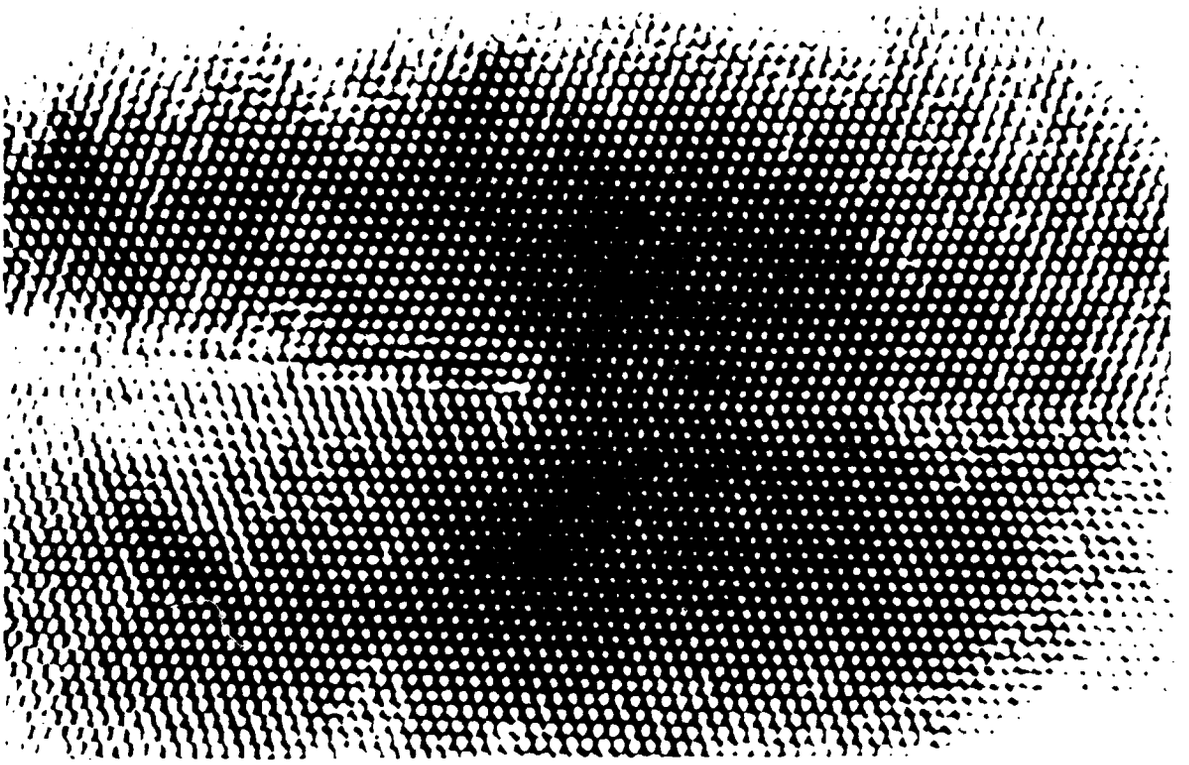

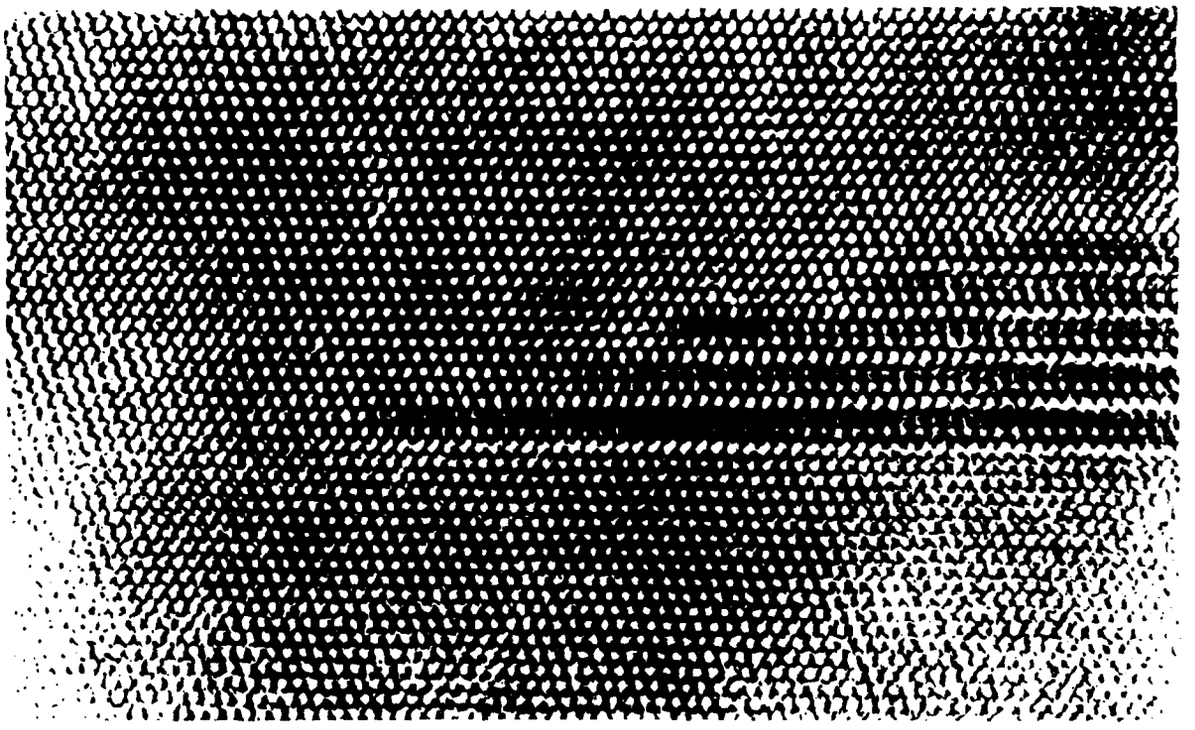


0.1 μm


0.1 μm

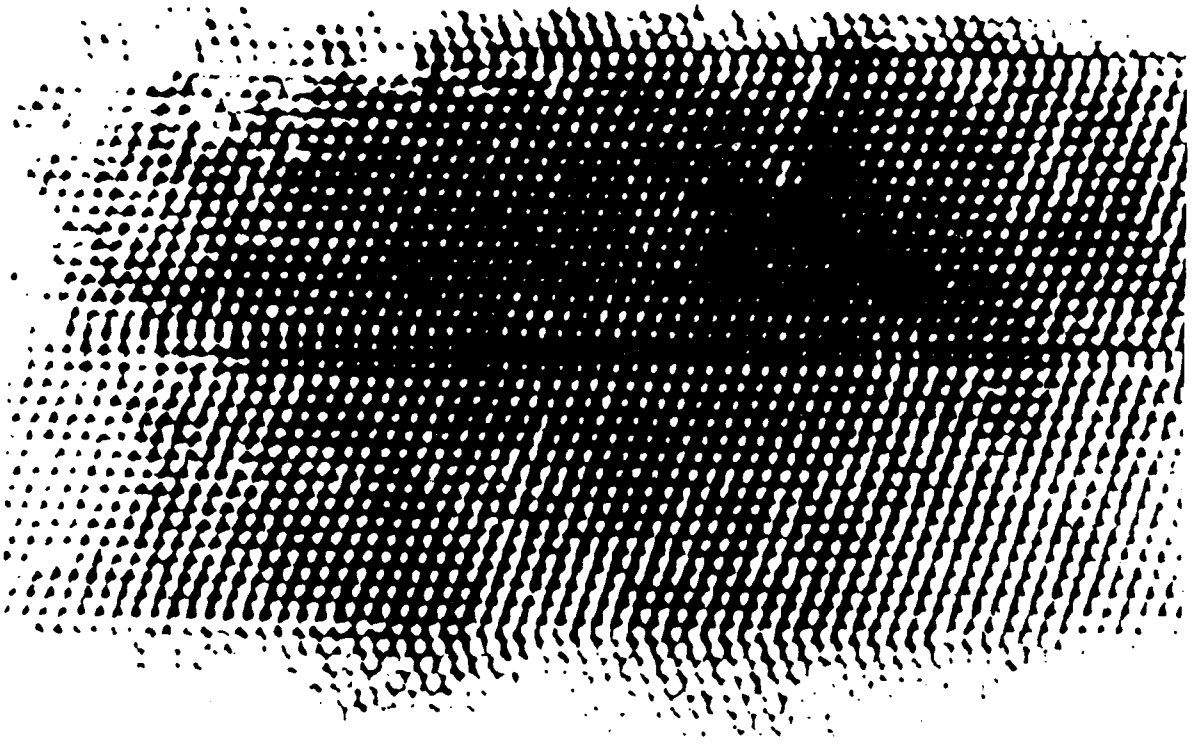


0.1 μm

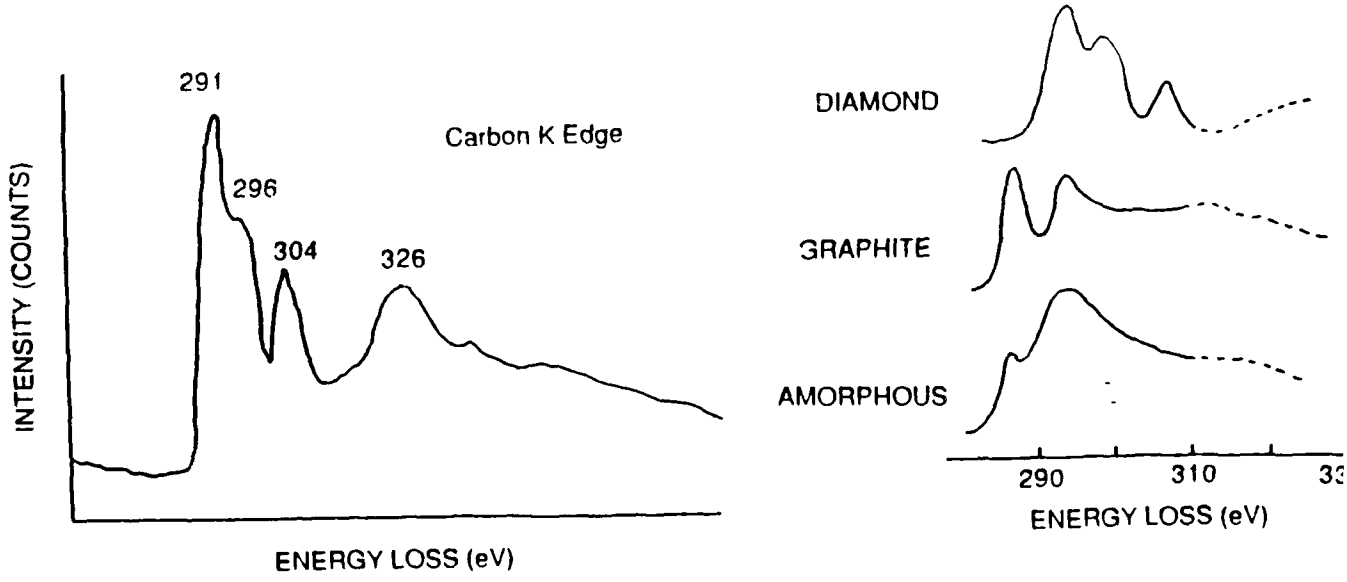
291
296
304
326
Carbon K Edge
INTENSITY (COUNTS)
ENERGY LOSS (eV)
DIAMOND
GRAPHITE
AMORPHOUS
290
310
ENERGY LOSS (eV)


0.1 μm
50 n

Conclusions

- Diamond crystals contain a high density of defects but the defect concentration is reduced at lower methane concentrations
- The defects observed include twins, stacking faults, and dislocations: no precipitates or second phases were observed
- A thin epitaxial buffer layer of β–SiC was observed at the interface when the CH4/H2 was 0.3%
- EELS has been utilized to identify diamond bonding (as opposed to amorphous carbon or graphite)

EVIDENCE FOR PRECURSOR STRUCTURES IN THE DEPOSITION OF DIAMOND FILMS

R.J. NEMANICH, R.E. SHRODER, J.T. GLASS, AND G. LUCOVSKY

DEPARTMENT OF PHYSICS and
DEPARTMENT OF MATERIALS SCIENCE AND ENGINEERING
NORTH CAROLINA STATE UNIVERSITY
RALEIGH, NC 27695-8202

ACKNOWLEDGEMENTS

R.J. MARKUNAS, R.A. RUDDER AND D.J. VITKAVAGE
OF THE RESEARCH TRIANGLE INSTITUTE

K. KOBASHI AND T. HORIUCHI OF KOBE STEEL, LTD

PARTIALLY SUPPORTED BY SDIO/IST

OUTLINE

1) CHARACTERIZE RAMAN FEATURES
2) IDENTIFY COMPOSITE FEATURES
3) PHOTOLUMINESCENCE
4) GROWTH vs TIME

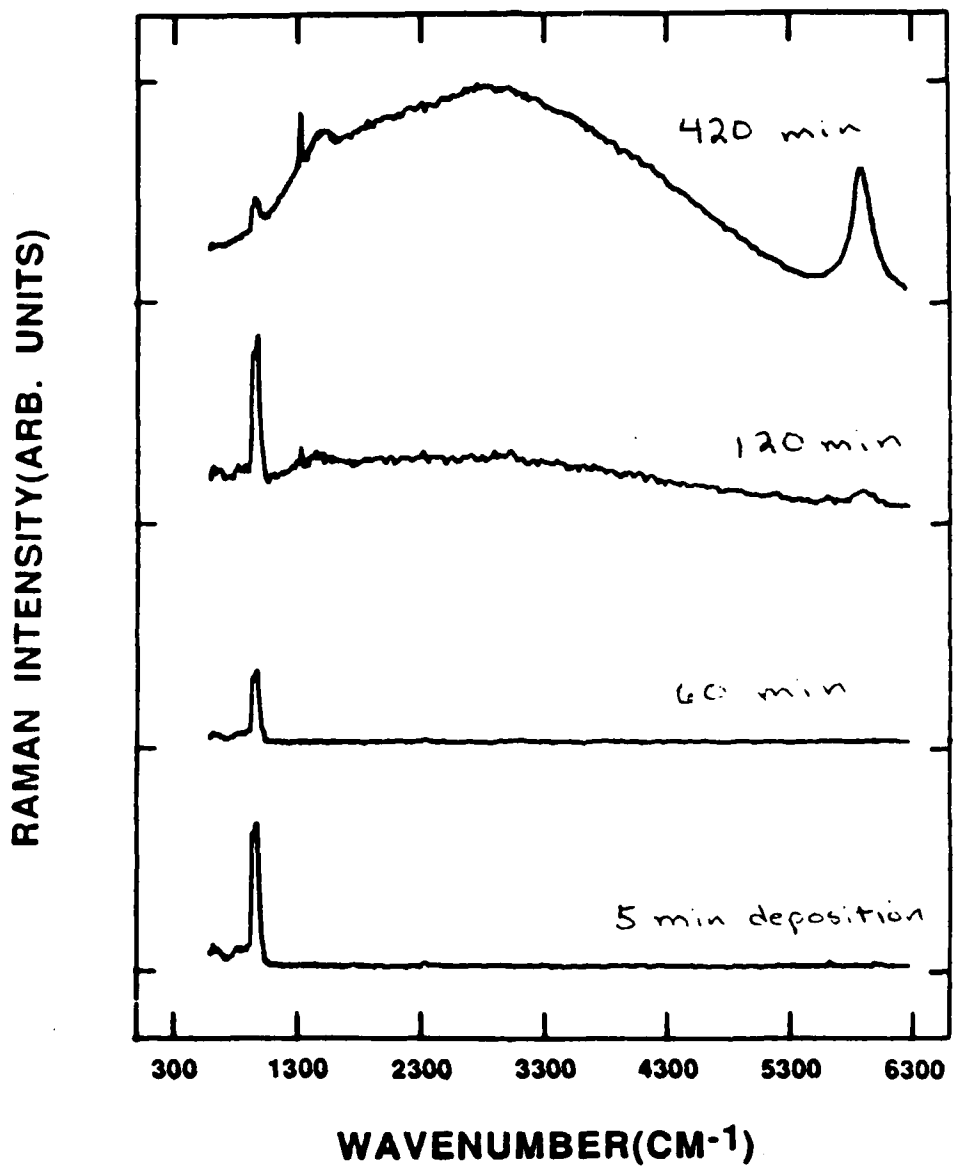
420 min
120 min
60 min
5 min deposition
300
1300
2300
3300
4300
5300
6300
RAMAN INTENSITY(ARB. UNITS)
WAVENUMBER(CM-1)

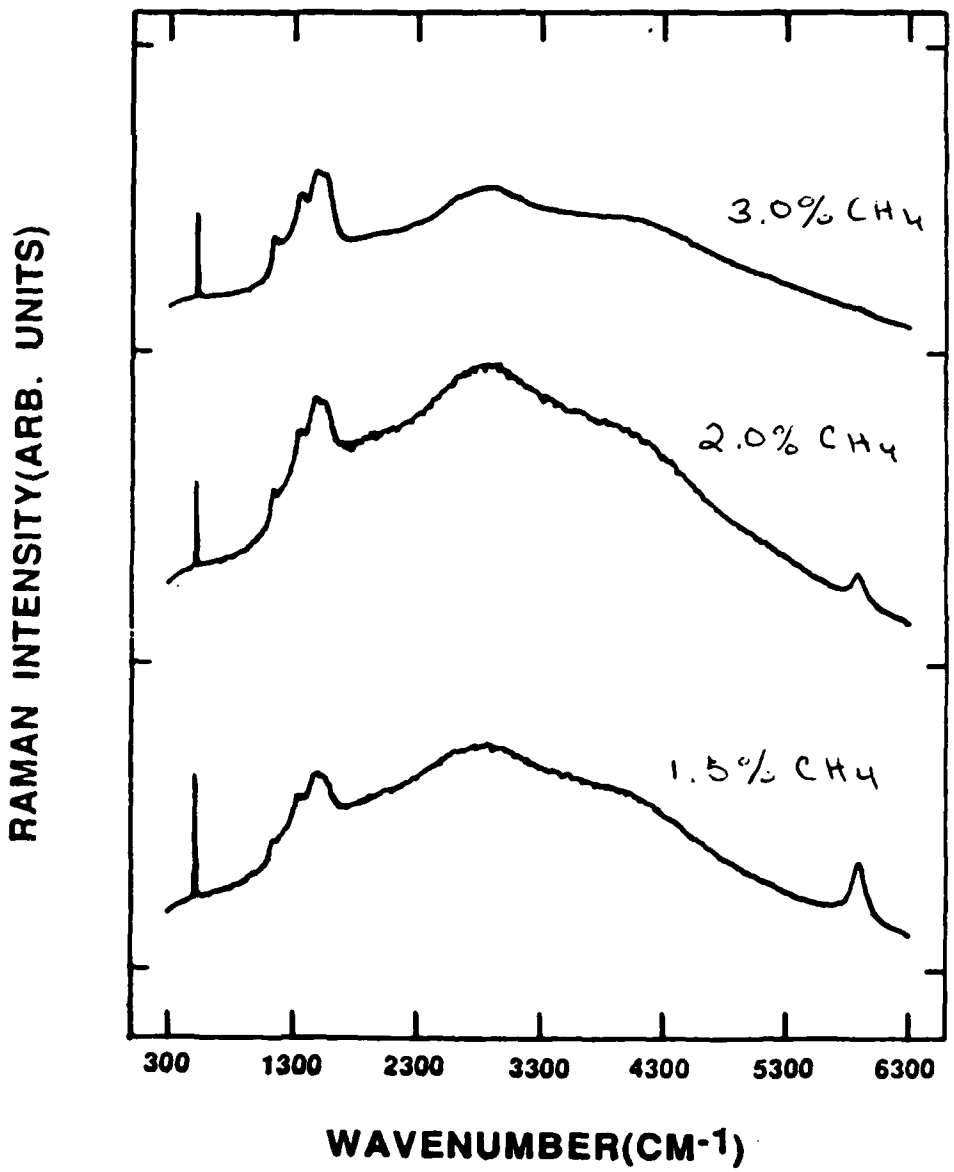
RAMAN INTENSITY(ARB. UNITS)
3.0% CH4
2.0% CH4
1.5% CH4
300
1300
2300
3300
4300
5300
6300
WAVENUMBER(CM-1)

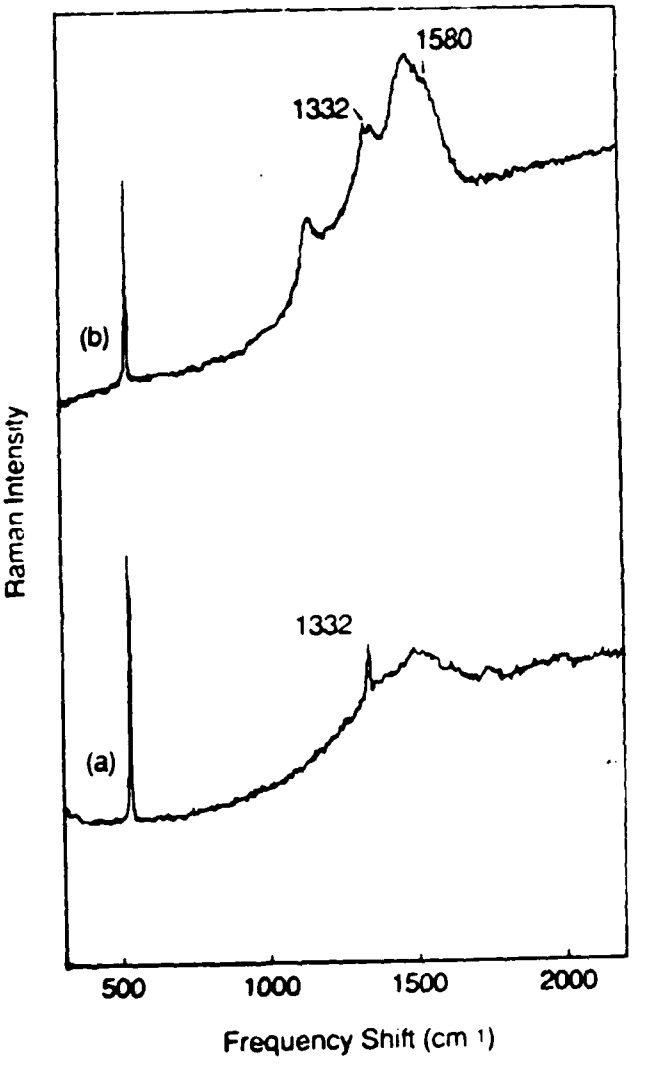
1580
1332
(b)
1332
(a)
Raman Intensity
500
1000
1500
2000
Frequency Shift (cm 1)

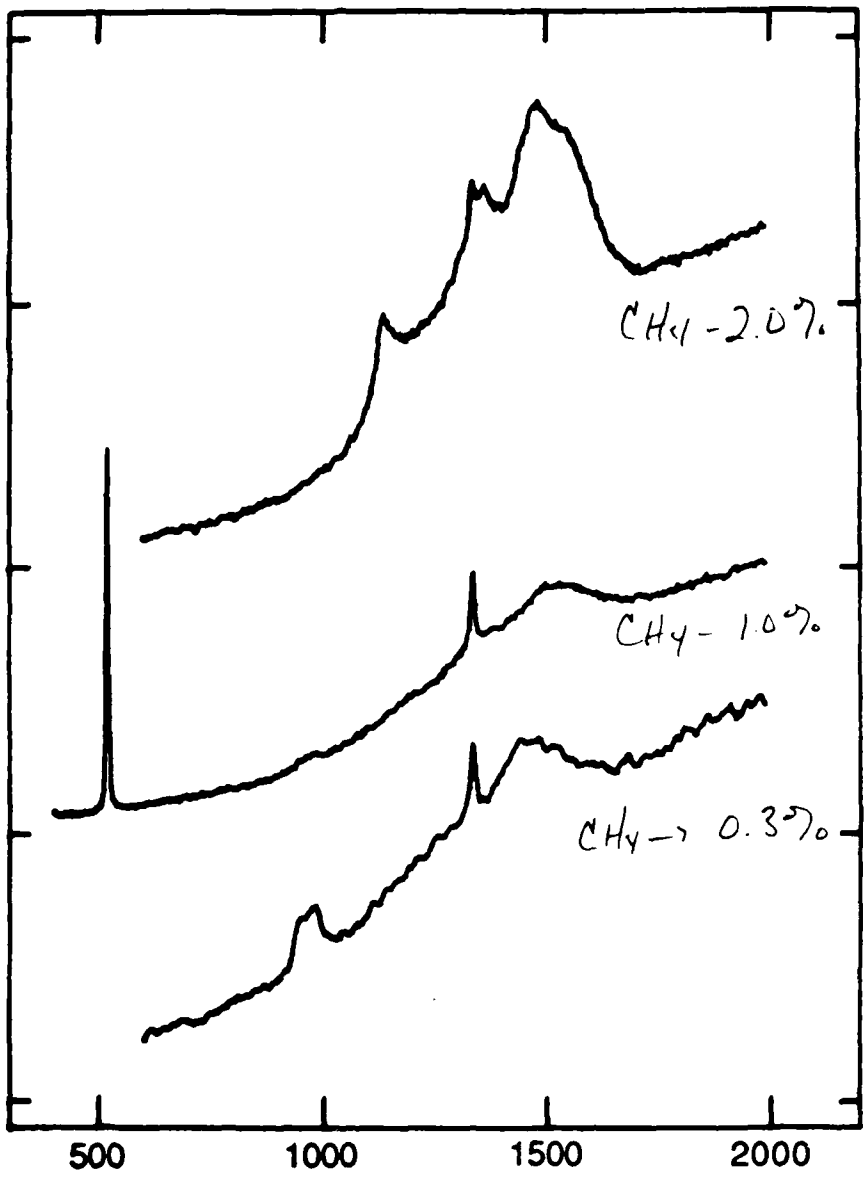
CH4 - 2.0%
CH4 - 1.0%
CH4 - 0.3%
500
1000
1500
2000
FREQUENCY SHIFT (cm -1)

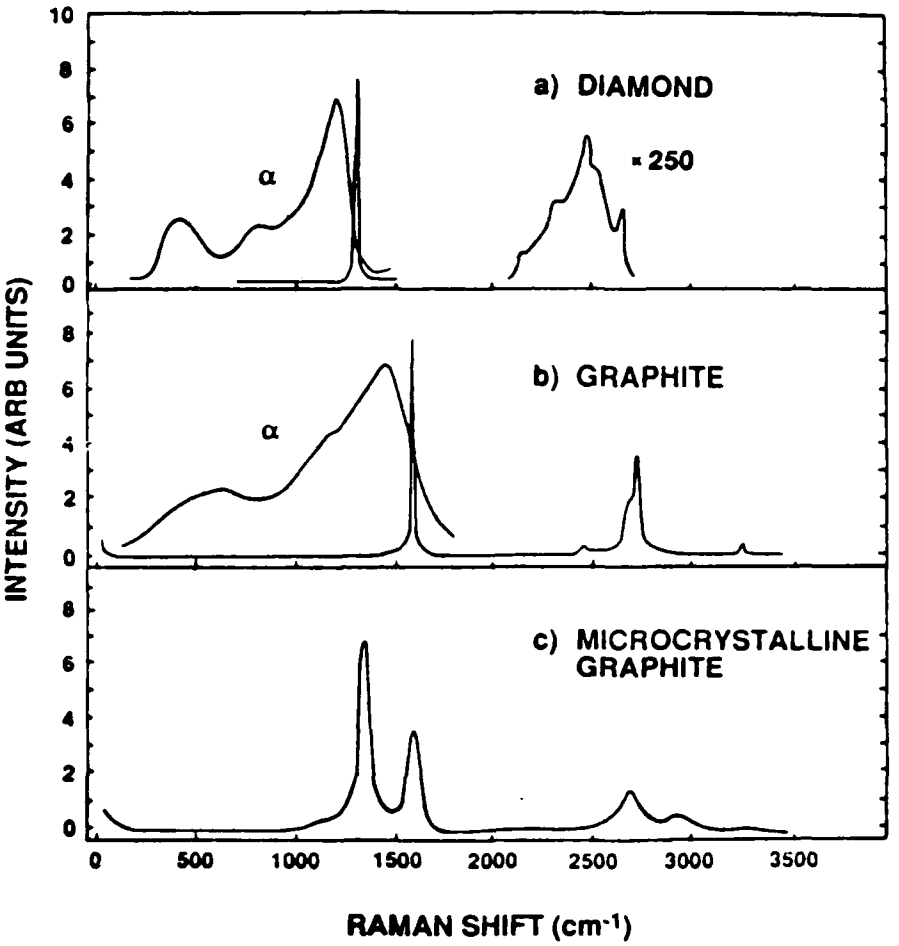
a) DIAMOND
× 250
α
b) GRAPHITE
α
c) MICROCRYSTALLINE GRAPHITE
INTENSITY (ARB UNITS)
RAMAN SHIFT (cm-1)
0
2
4
6
8
10
0
500
1000
1500
2000
2500
3000
3500

SUMMARY

1) CVD CARBON FILMS ARE COMPOSITES

2) RAMAN FEATURES GREATER THAN 1340 cm^{-1} ARE DUE TO 3-FOLD COORDINATED STRUCTURES

3) RAMAN FEATURES FOR 4-FOLD COORDINATED STRUCTURES WILL OCCUR AT LESS THAN 1340 cm^{-1}.

4) RAMAN FEATURE AT 1140 cm^{-1} :

   OCCURS AT ONSET OF DIAMOND FORMATION.

   CORRESPONDS TO "AMORPHOUS, TETRAHEDRAL C"

5) LUMINESCENCE AT 1.68 eV CORRELATES WITH 1332 cm^{-1} DIAMOND FEATURE.

6) GROWTH PROCESS APPEARS NON-LINEAR

The Growth and Characterization of Cu Single Crystals and the Hot Filament Assisted CVD of Diamond on Various Substrates

J. T. Glass, Y. H. Lee, P. D. Richard,
H. S. Kong and K. J. Bachmann

Department of Materials Science and Engineering
North Carolina State University
Raleigh, NC 27695-7907

Objective: Monocrystalline Diamond Films for Electronic Applications

Approach: Construct and characterize CVD system for diamond growth

Evaluate various single crystal substrates which have potential for growing 2-D, monocrystalline diamond films

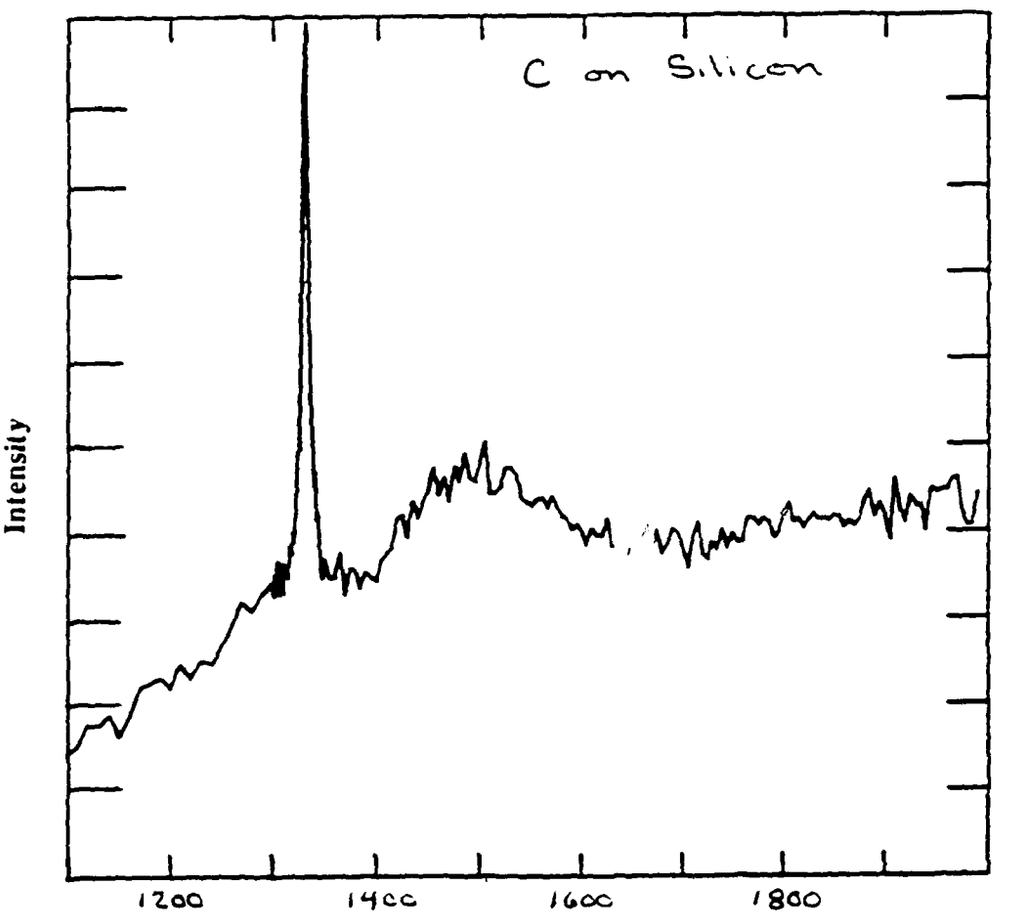
C on Silicon
Intensity
1200
1400
1600
1800
Frequency Shift (cm-1)

Substrates Investigated

I. Control and System Characterization

Si (100), on– and off–axis

II. High Bond Energy Substrates

β-SiC (100), on– and off–axis
α-SiC (0001)
NbC (large grain polycrystalline)

III. Lattice Matched Substrates

Cu (111)
Ni on Cu (111)
Ni on β-SiC (100)

Criterion for Two Dimensional Growth*

I. Surface Energies

- **Dupre Relation:** $\sigma^* = \sigma_A + \sigma_B - \beta$

σ^* = excess interfacial energy
β = adhesion energy
A $\Rightarrow$ film
B $\Rightarrow$ substrate

1)  $\beta = 0$ $(\sigma^* = \sigma_A + \sigma_B)$

2)  $\beta = \sigma_A$ $(\sigma^* = \sigma_B)$

3) 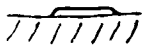 $\beta > \sigma_A$

II. Nucleation Energy Considerations

- $\beta > 2\sigma_A$ or $\sigma_A < \sigma_B - \sigma^* \Rightarrow$ 2-D

III. Atomic Model (Kossel's Model)

- $\Phi_{AB} > \Phi_{AA} \Rightarrow$ 2-D

(If $\Phi_{AA} > \Phi_{AB} \Rightarrow$ always get 3-D growth)

---

* From R. Kern, G. LeLay and J. J. Metois, Chapter 3 in Current Topics in Materials Science, Vol. 3, edited by E. Kaldis, North-Holland Pub. Co. (1979).

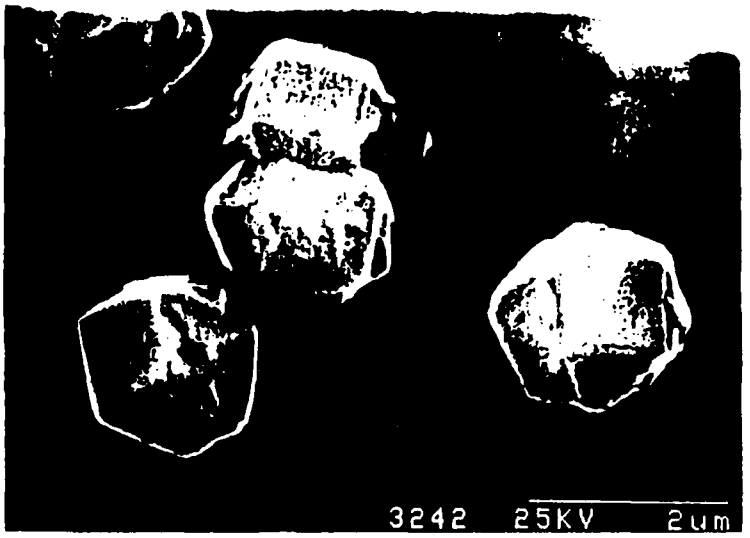

Si substrate

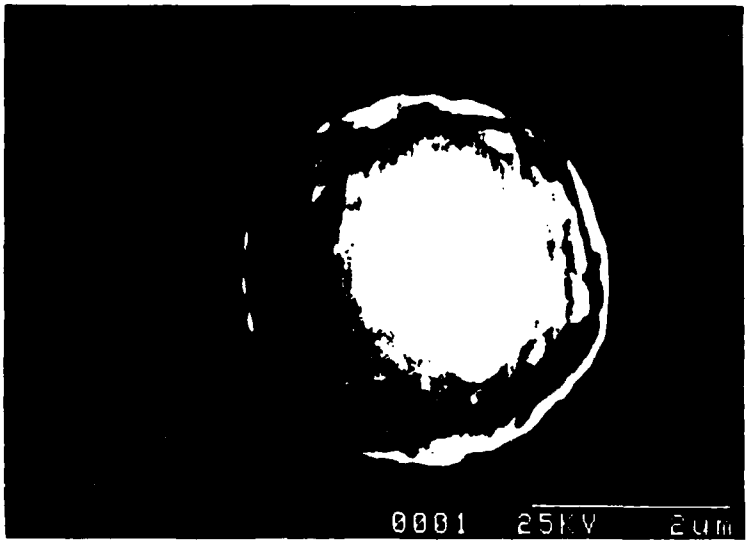

SiC substrate

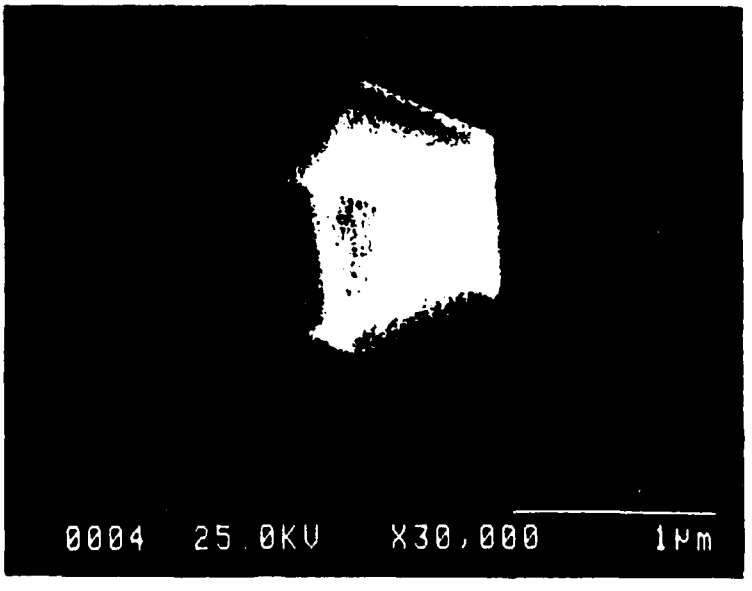

NbC substrate

BRIDGEMANN FURNACE

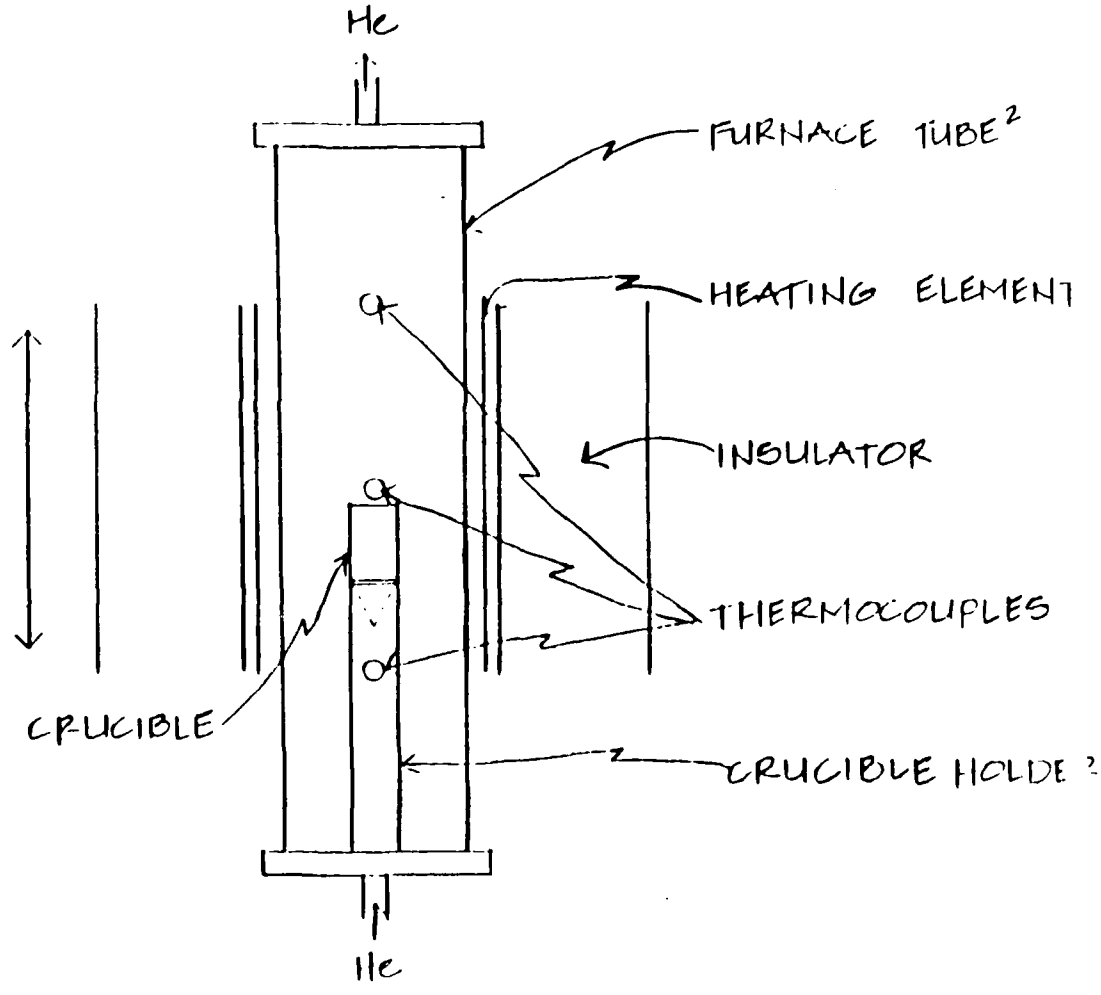

[1] GRAPHITE FOR Cu
ALUMINA FOR Ni

[2] QUARTZ FOR Cu
ALUMINA FOR Ni

(a)

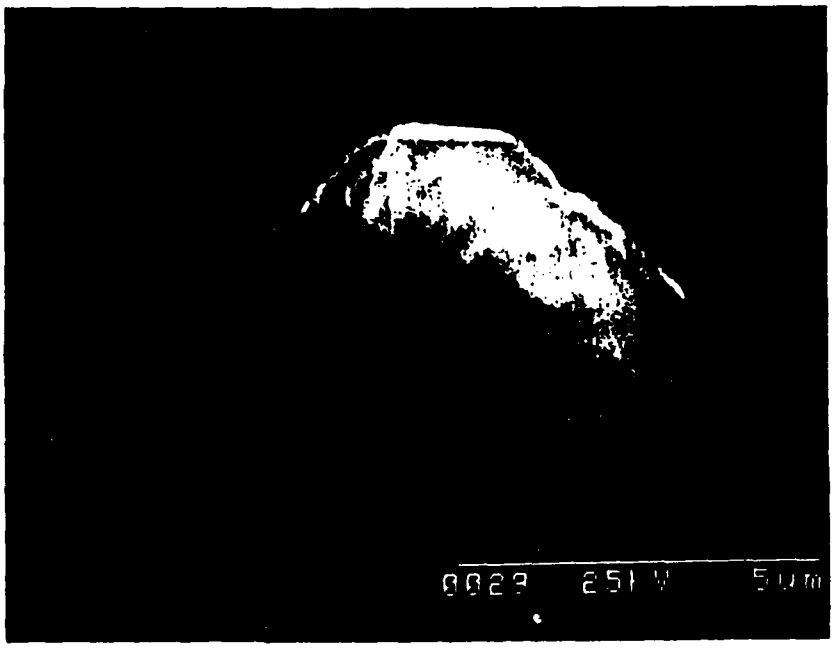

(b)

Diamond particles on (a) Cu (111)
and (b) Ni coated (200Å) Cu (111)

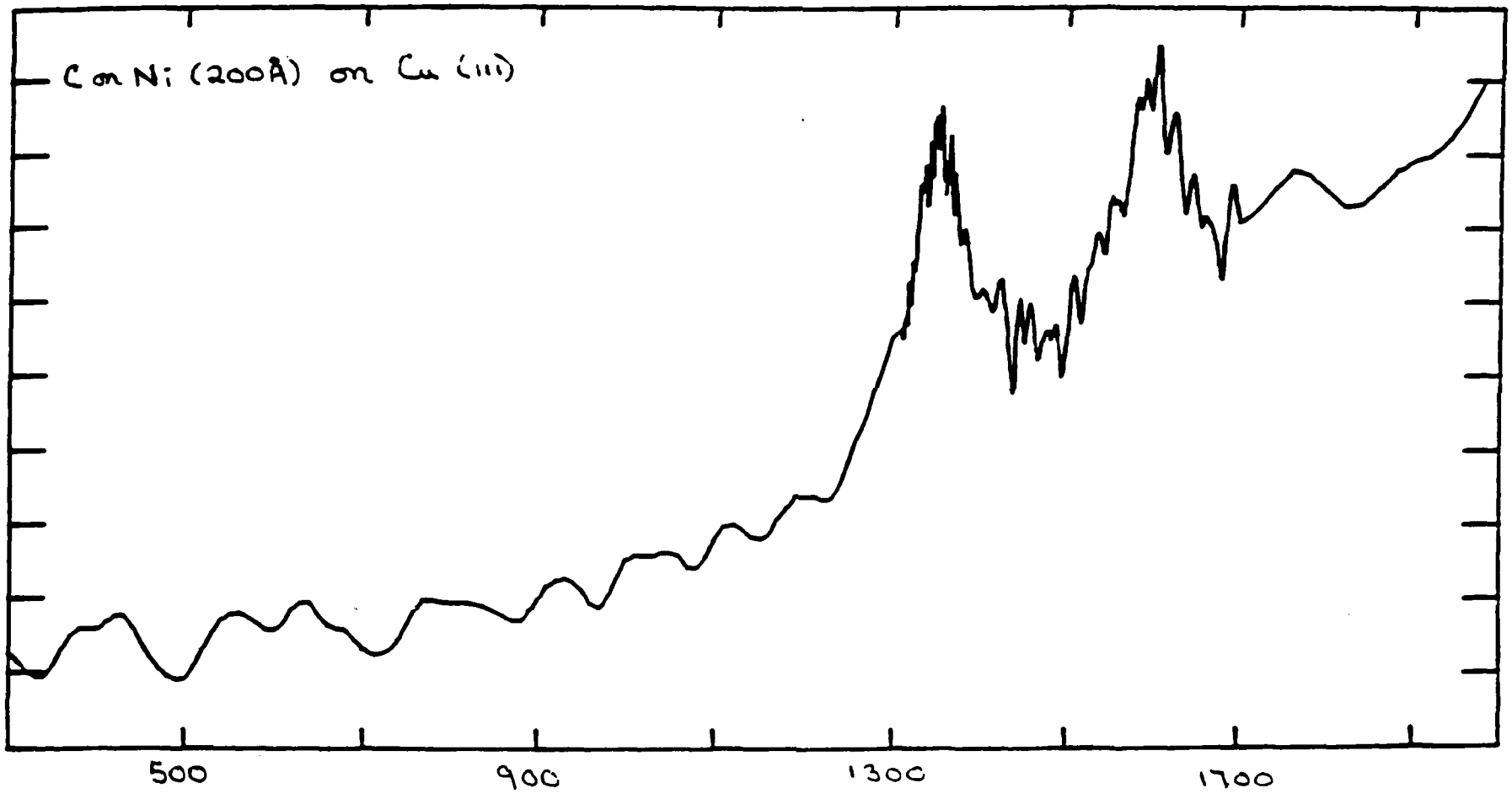

Frequency Shift (cm^{-1})

5

Carbon deposition onto Ni coated (50Å) β-SiC.

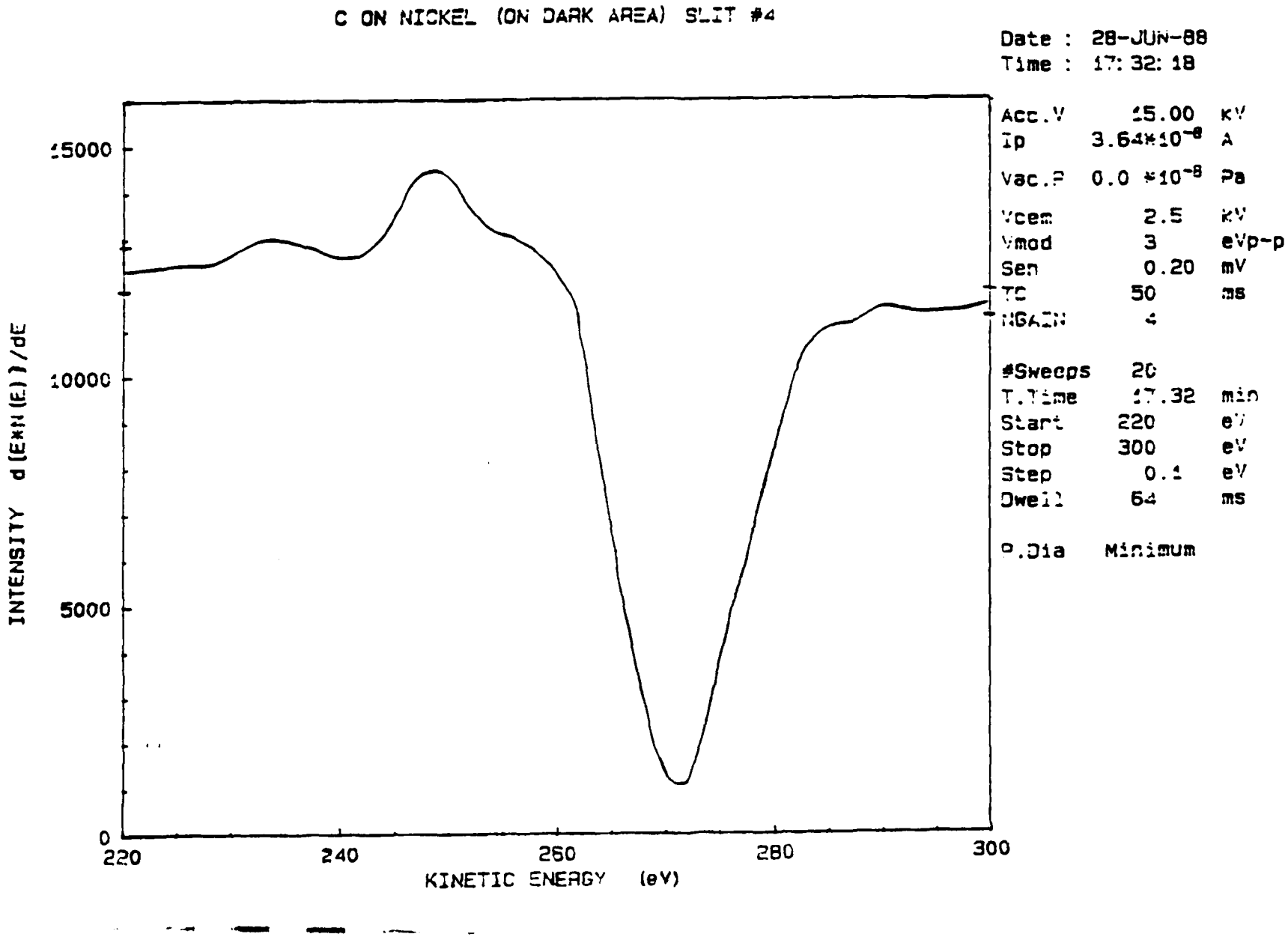
C ON NICKEL (ON DARK AREA) SLIT #4
Date : 28-JUN-88
Time : 17:32:18
Acc.V 15.00 kV
Ip 3.64*10-8 A
Vac.P 0.0 *10-8 Pa
Vcem 2.5 kV
Vmod 3 eVp-p
Sen 0.20 mV
TC 50 ms
NGAIN 4
#Sweeps 20
T.Time 17.32 min
Start 220 eV
Stop 300 eV
Step 0.1 eV
Dwell 64 ms
P.Dia Minimum
INTENSITY d(EXN(E))/dE
15000
10000
5000
0
220
240
260
280
300
KINETIC ENERGY (eV)

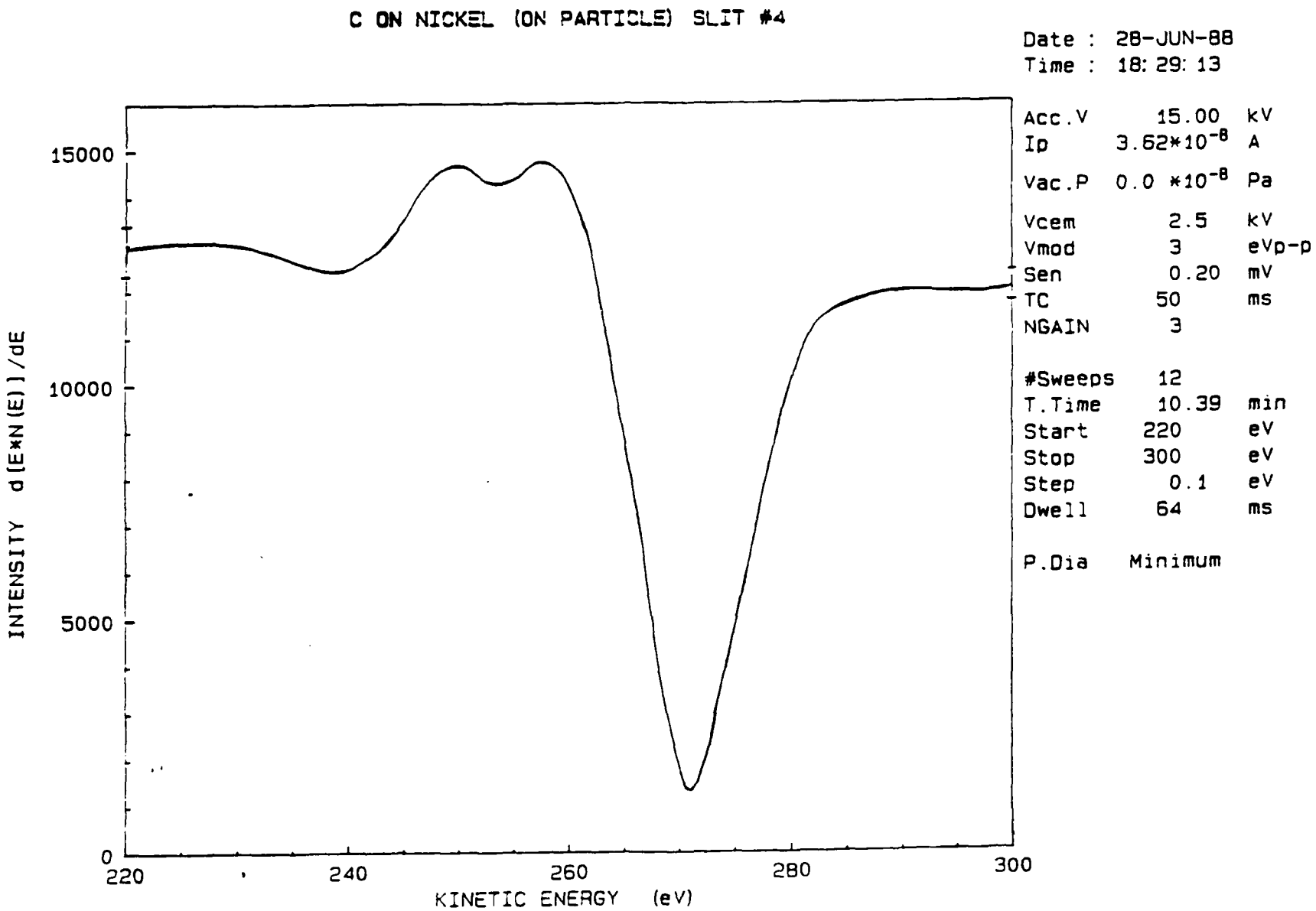
C ON NICKEL (ON PARTICLE) SLIT #4
Date : 28-JUN-88
Time : 18: 29: 13
Acc.V 15.00 kV
Ip 3.62*10^-8 A
Vac.P 0.0 *10^-8 Pa
Vcem 2.5 kV
Vmod 3 eVp-p
Sen 0.20 mV
TC 50 ms
NGAIN 3
#Sweeps 12
T.Time 10.39 min
Start 220 eV
Stop 300 eV
Step 0.1 eV
Dwell 64 ms
P.Dia Minimum
INTENSITY d[E*N(E)]/dE
15000
10000
5000
0
220
240
260
280
300
KINETIC ENERGY (eV)

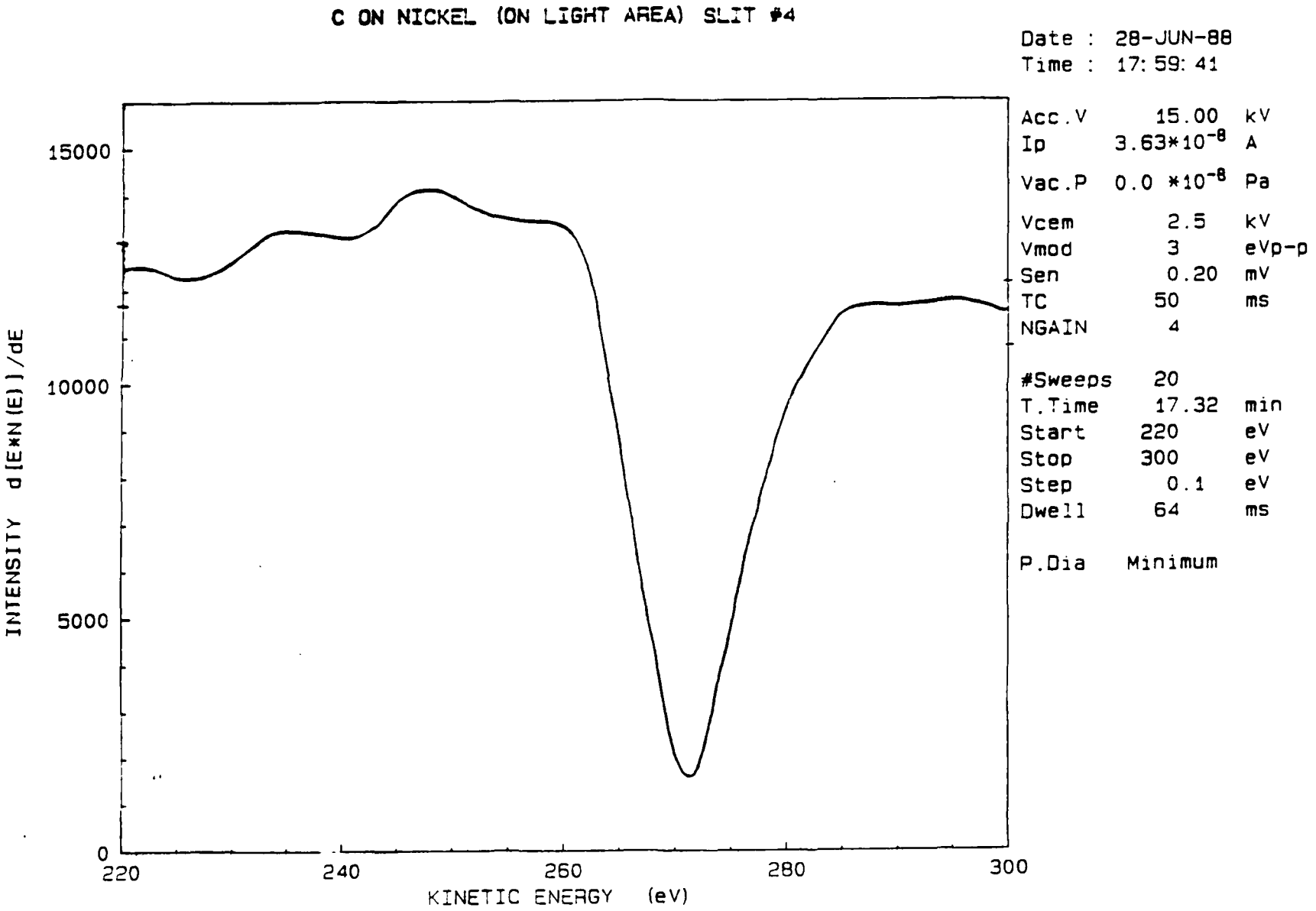
C ON NICKEL (ON LIGHT AREA) SLIT #4
Date : 28-JUN-88
Time : 17:59:41
Acc.V 15.00 kV
Ip 3.63*10-8 A
Vac.P 0.0 *10-8 Pa
Vcem 2.5 kV
Vmod 3 eVp-p
Sen 0.20 mV
TC 50 ms
NGAIN 4
#Sweeps 20
T.Time 17.32 min
Start 220 eV
Stop 300 eV
Step 0.1 eV
Dwell 64 ms
P.Dia Minimum
INTENSITY d[E*N(E)]/dE
15000
10000
5000
0
220
240
260
280
300
KINETIC ENERGY (eV)

Summary

	Nucleation	Faceting
Si (100)		
On-Axis		
Scratched	High	Medium
Polished		
10° off-axis		
19° off-axis	Low	Medium
25° off-axis		
β-SiC		
on-axis		
polished	High	Low
pol, ox, etch		
4° off-axis	Low	Low
10° off-axis		
α-SiC		
on-axis	Low	Low
Nb–C	Low	High
Cu		
(210)	Medium	Low
(111)		
S/C	Medium	Medium
D/C	Low	Low
Ni on		
Cu (111)	Low	Low
β-SiC		
graphite islands	High	—
diamond particles	Low	Low

Conclusions

- A UHV compatible Hot Filament CVD System has been designed, constructed and characterized.
- The use of large angle off-axis polished Si (lll) substrates yielded results similar to on-axis substrates.
- High bond energy single crystal substrates were examined (β-SiC, α-SiC and NbC) and found to affect particle morphology.
- Cu single crystal substrates resulted in particles and a thin background film.
- Ni sputtered onto β-SiC single crystals caused a mixture of diamond particles, graphitic islands and a background yielding both amorphous carbon and diamond characteristics.

DIAMOND CVD AND IN SITU ANALYSIS SYSTEMS AT NCSU

ANALYSIS SYSTEM

- **Initial Capabilities**

  RVLEED
  AES
  XPS
  ESD/ESDIED
  SIMS

- **Future Capabilities**

  UPS
  IPS
  STM

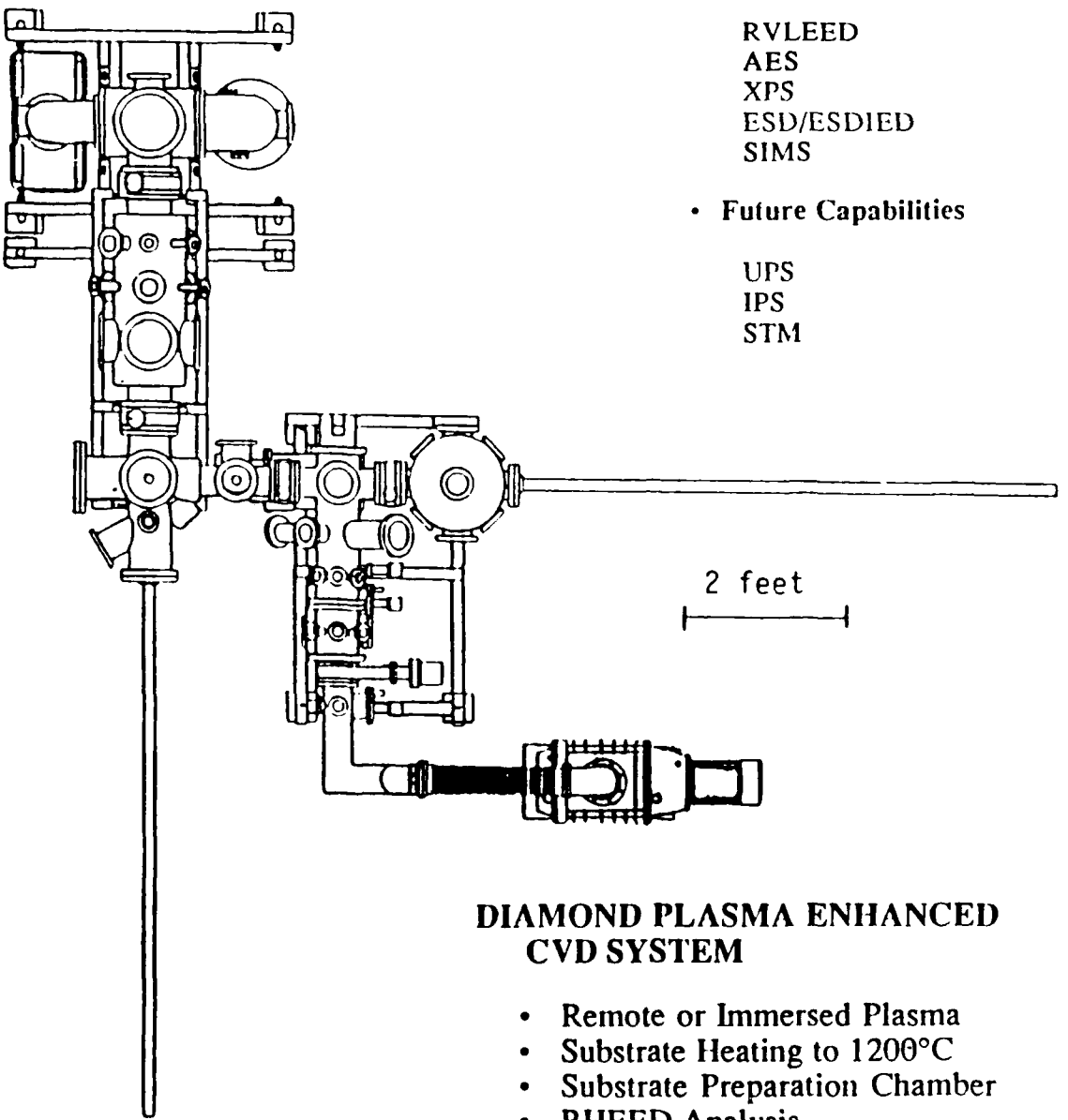

DIAMOND PLASMA ENHANCED CVD SYSTEM

- Remote or Immersed Plasma
- Substrate Heating to 1200°C
- Substrate Preparation Chamber
- RHEED Analysis

PROSPECTS FOR A DIAMOND POWER MESFET*

R. J. Trew and J. B. Yan

Electrical and Computer Engineering Department

North Carolina State University

Raleigh, North Carolina 27695-7911

*This work was supported by SDIO/IST through the Office of Naval Research

Objective: To investigate the suitability of semiconducting diamond as a material for fabrication of microwave power MESFETs.

Approach: Design a diamond power MESFET and study its RF operation by means of computer simulations using the NCSU large-signal MESFET model.

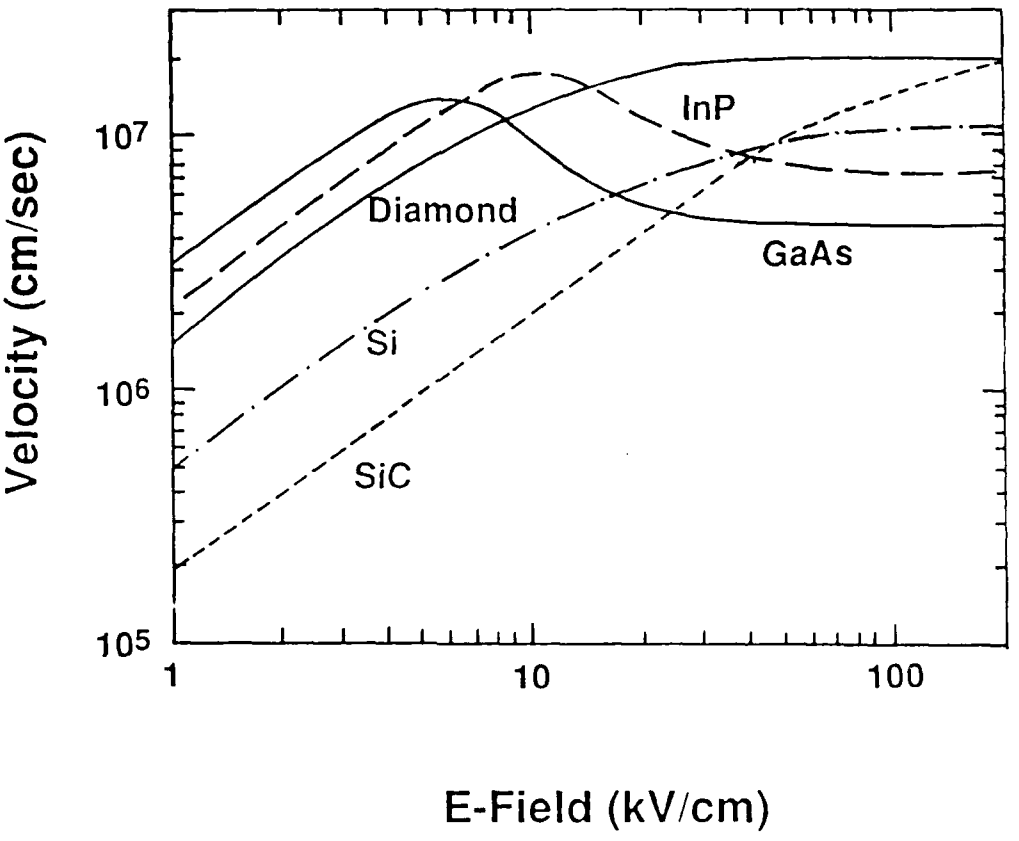

Electron Velocity vs Electric Field
for Several Semiconductors at $N_d = 10^{17}cm^{-3}$

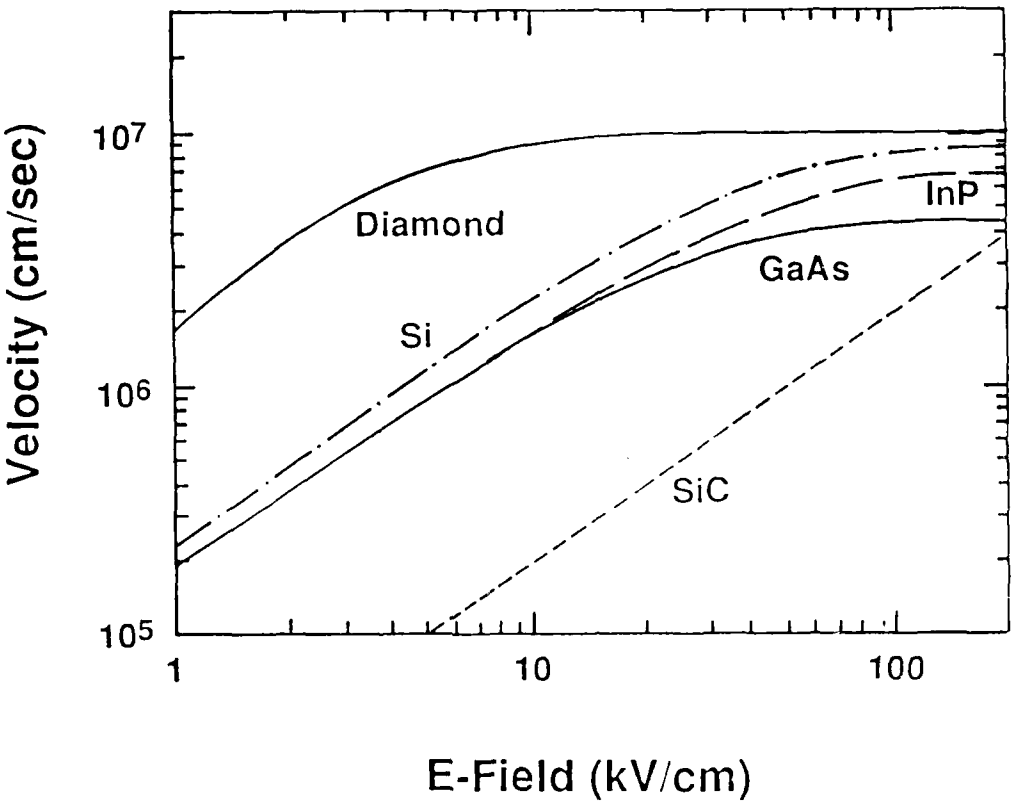

Hole Velocity vs Electric Field for
Several Semiconductors at $N_d = 10^{17}cm^{-3}$

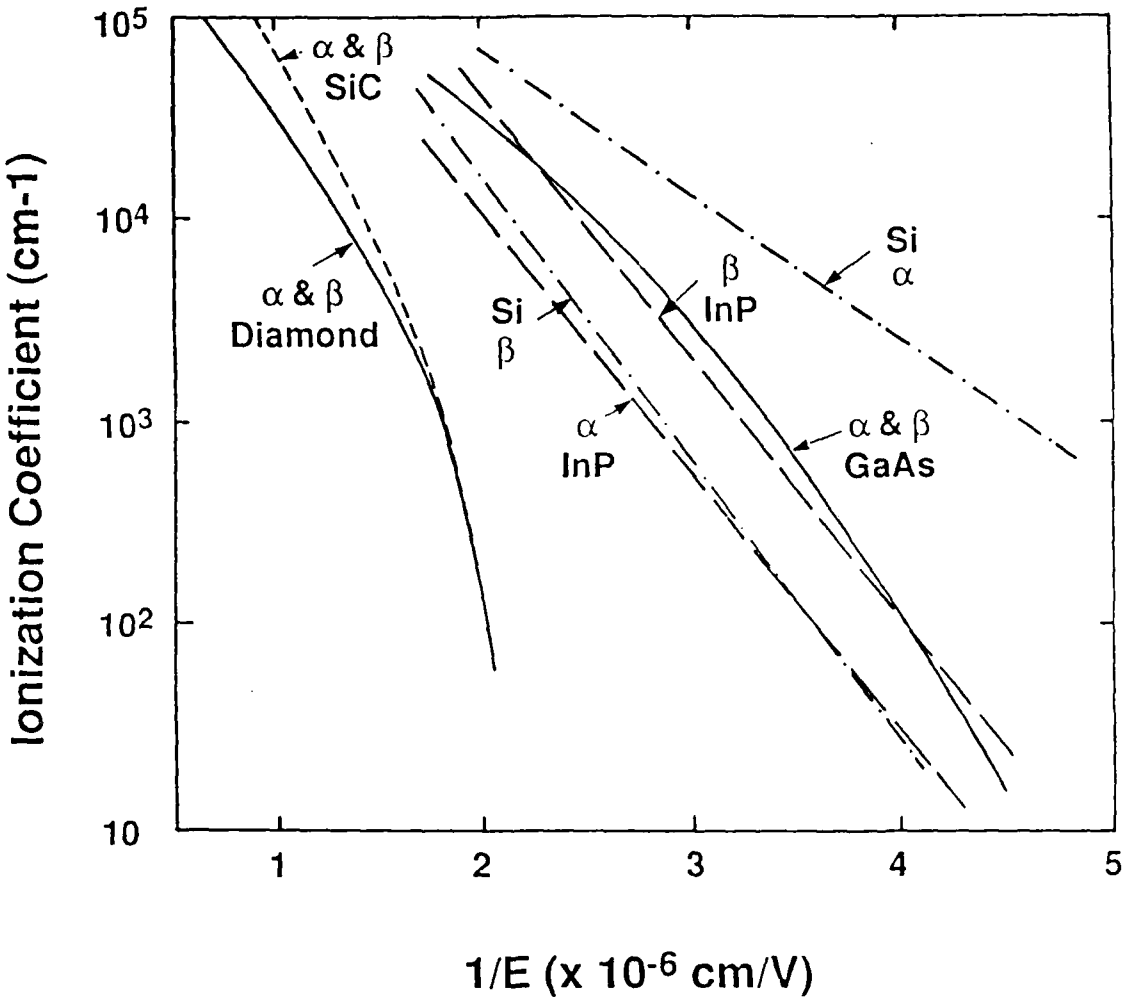

Ionization rates for Several Semiconductors

DIAMOND POWER MESFET

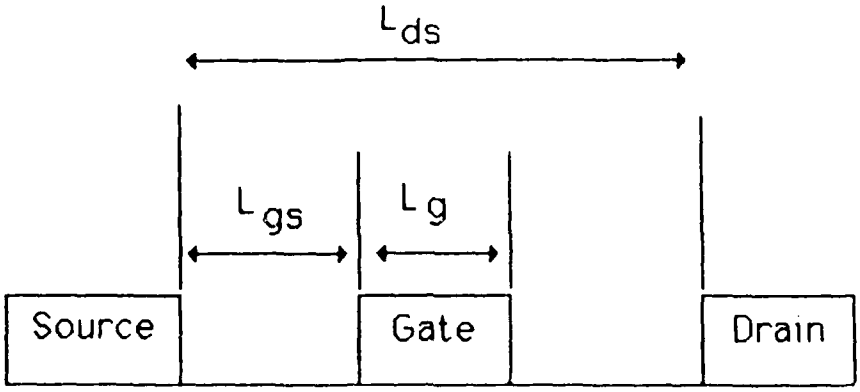

Channel

Substrate

Parameter	Value
L_g	1 μm
L_{ds}	4 μm
L_{gs}	1 μm
N_d	$2.7 \times 10^{17} cm^{-3}$
a	0.27 μm
W	1 mm
ϕ_{bi} (Au)	1.71 eV
R_c	$\sim 10^{-4}\ \Omega - cm^2$

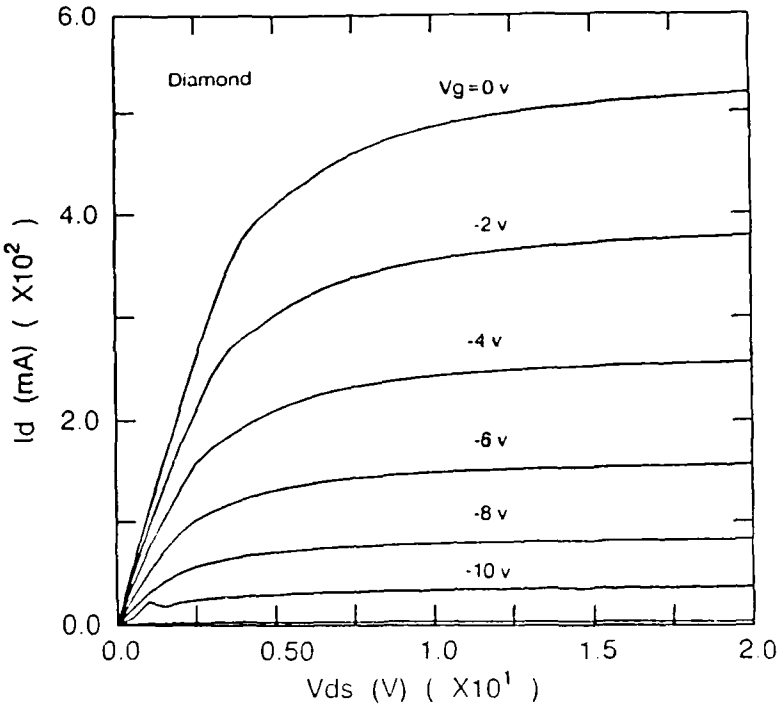
Diamond
Vg=0 v
-2 v
-4 v
-6 v
-8 v
-10 v
6.0
4.0
2.0
0.0
0.0
0.50
1.0
1.5
2.0
Id (mA) (X10^2)
Vds (V) (X10^1)

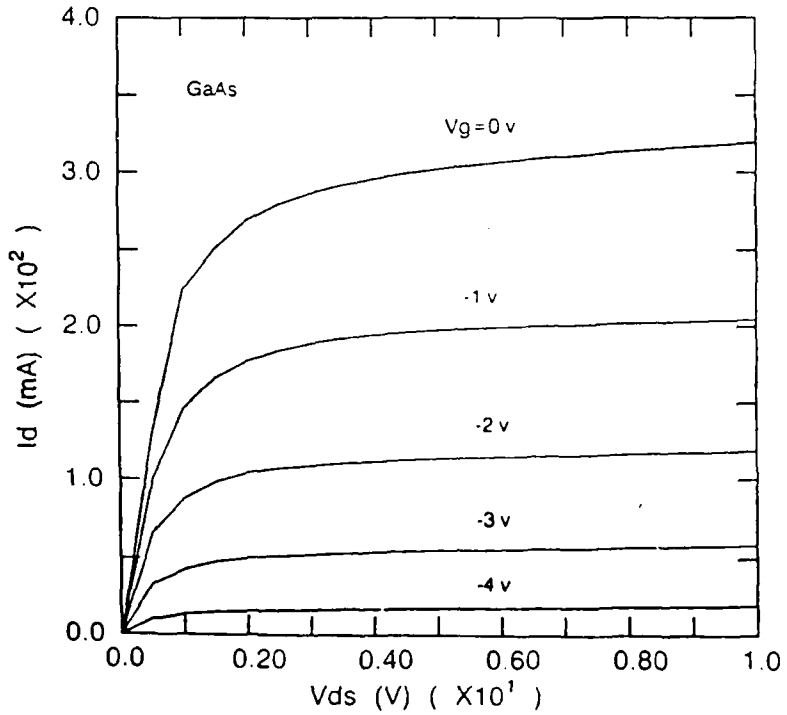
GaAs
Vg=0 v
-1 v
-2 v
-3 v
-4 v
4.0
3.0
2.0
1.0
0.0
0.0
0.20
0.40
0.60
0.80
1.0
Id (mA) (X10^2)
Vds (V) (X10^1)

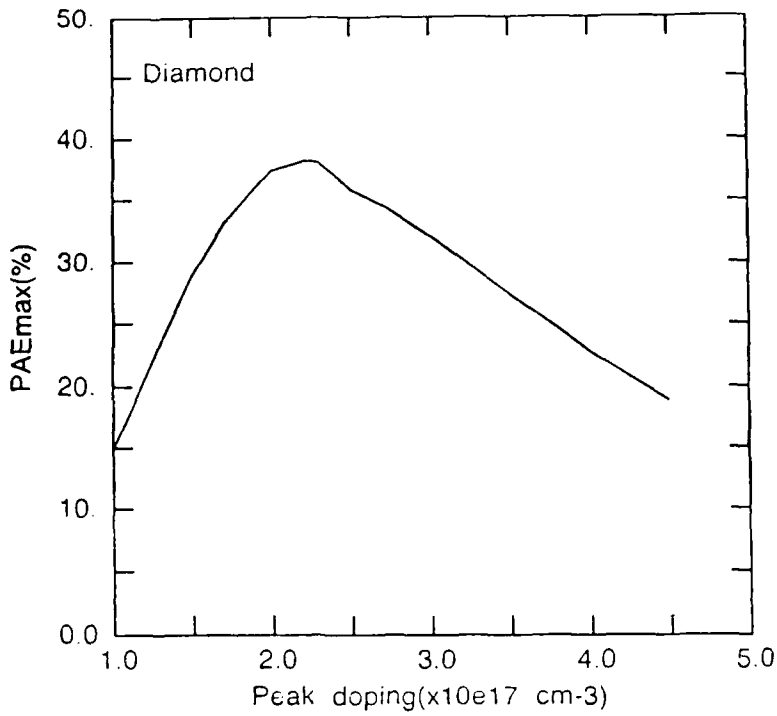
Diamond
PAEmax(%)
50.
40.
30.
20.
10.
0.0
1.0
2.0
3.0
4.0
5.0
Peak doping(x10e17 cm-3)

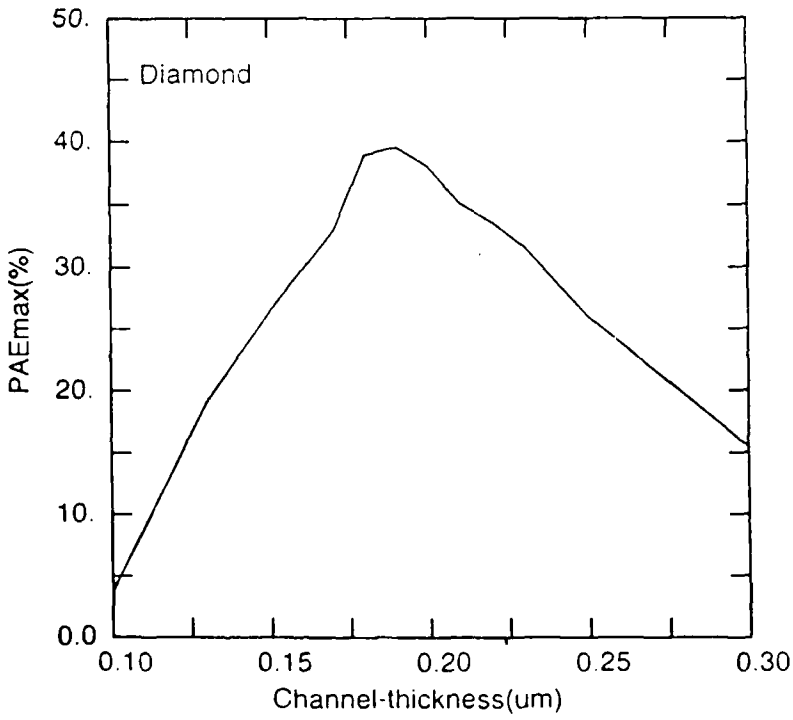
Diamond
PAEmax(%)
50.
40.
30.
20.
10.
0.0
0.10
0.15
0.20
0.25
0.30
Channel-thickness(um)

FACTORS LIMITING THE ATTAINABLE RF OUTPUT POWER OF A MESFET

- Charge Carrier Transport Characteristics
  Low-Field Mobility
  Saturation Velocity

- Gate-Drain Breakdown Voltage
  DC Bias
  RF Voltages

- Semiconductor Thermal Conductivity
  Heat Dissipation

- Maximum Allowed Channel (Junction) Temperature

- Input Circuit Impedance Matching Considerations
  Maximum Gate Width

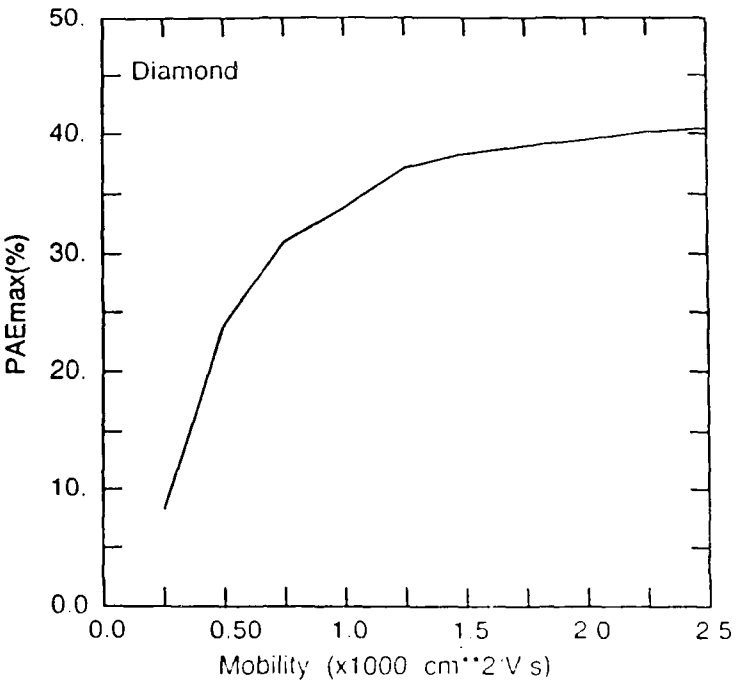
Diamond
PAEmax(%)
50.
40.
30.
20.
10.
0.0
0.0
0.50
1.0
1.5
2.0
2.5
Mobility (x1000 cm**2/V.s)

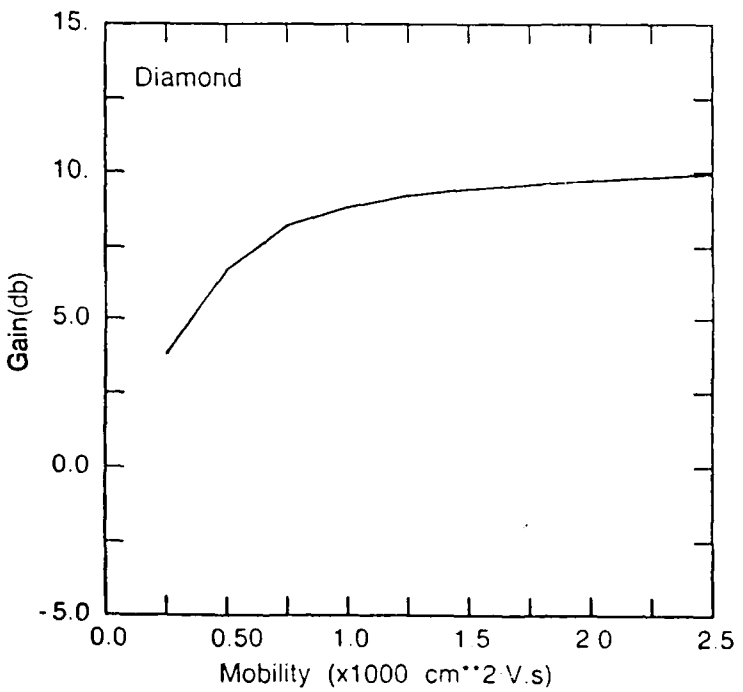
Diamond
Gain(db)
15.
10.
5.0
0.0
-5.0
0.0
0.50
1.0
1.5
2.0
2.5
Mobility (x1000 cm**2/V.s)

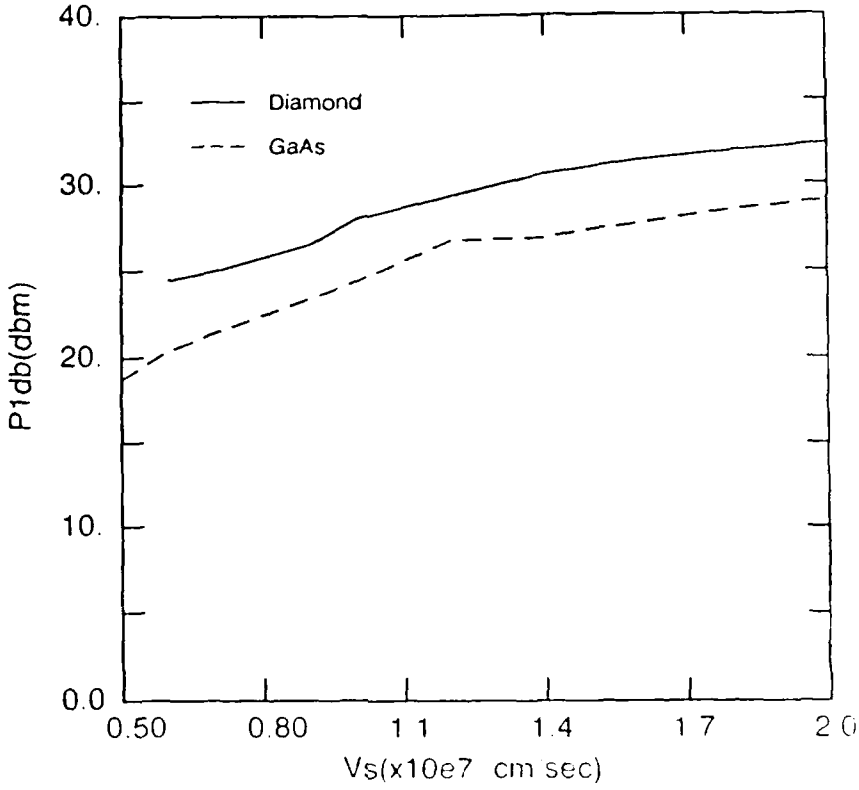
40.
30.
20.
10.
0.0
Diamond
GaAs
P1db(dbm)
0.50
0.80
1 1
1.4
1 7
2 0
Vs(x10e7 cm sec)

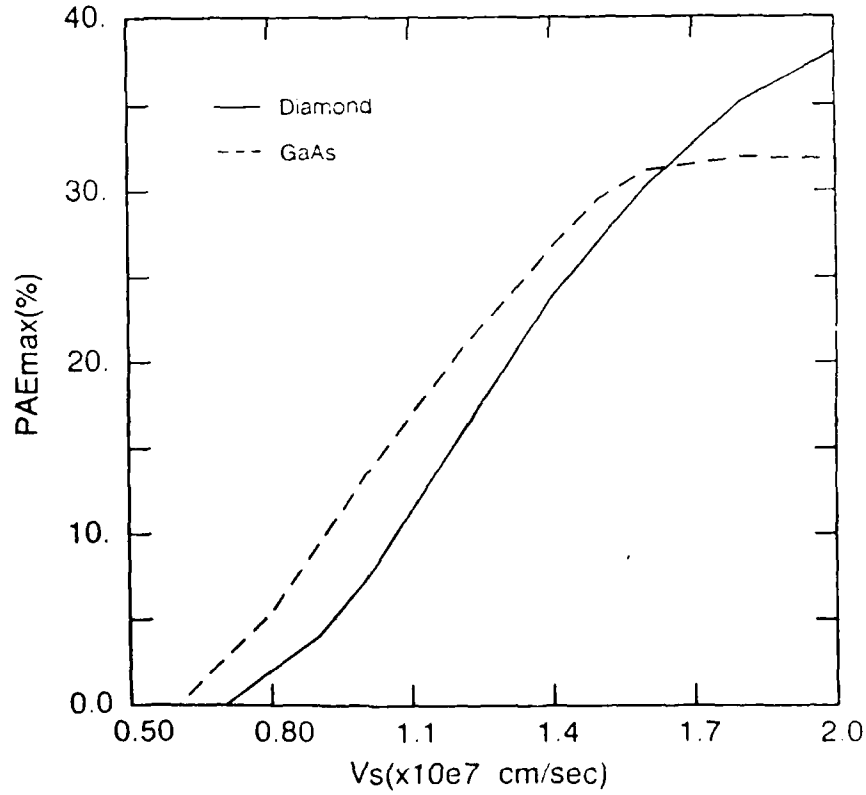
40.
30.
20.
10.
0.0
Diamond
GaAs
PAEmax(%)
0.50
0.80
1.1
1.4
1.7
2.0
Vs(x10e7 cm/sec)

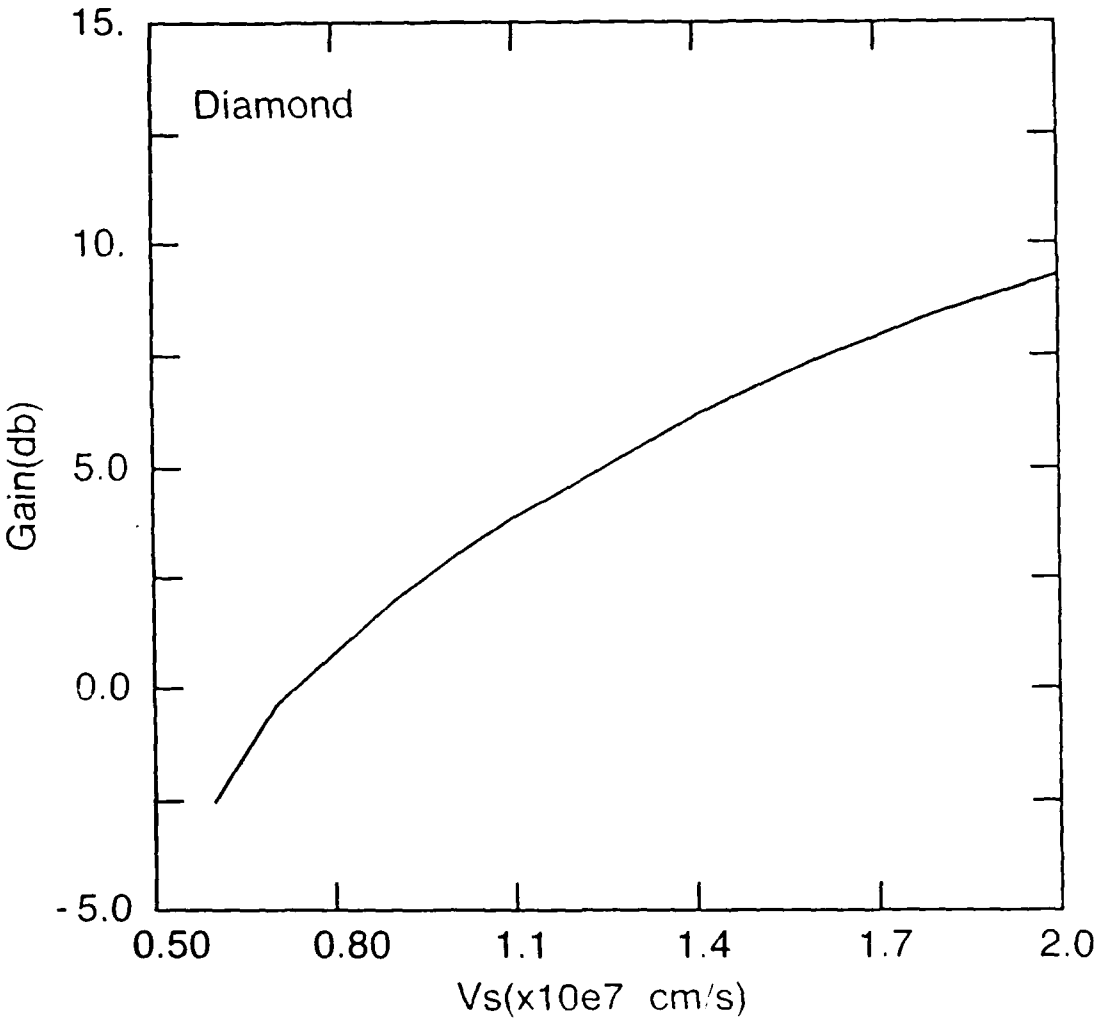
Diamond
15.
10.
5.0
0.0
-5.0
Gain(db)
0.50
0.80
1.1
1.4
1.7
2.0
Vs(x10e7 cm/s)

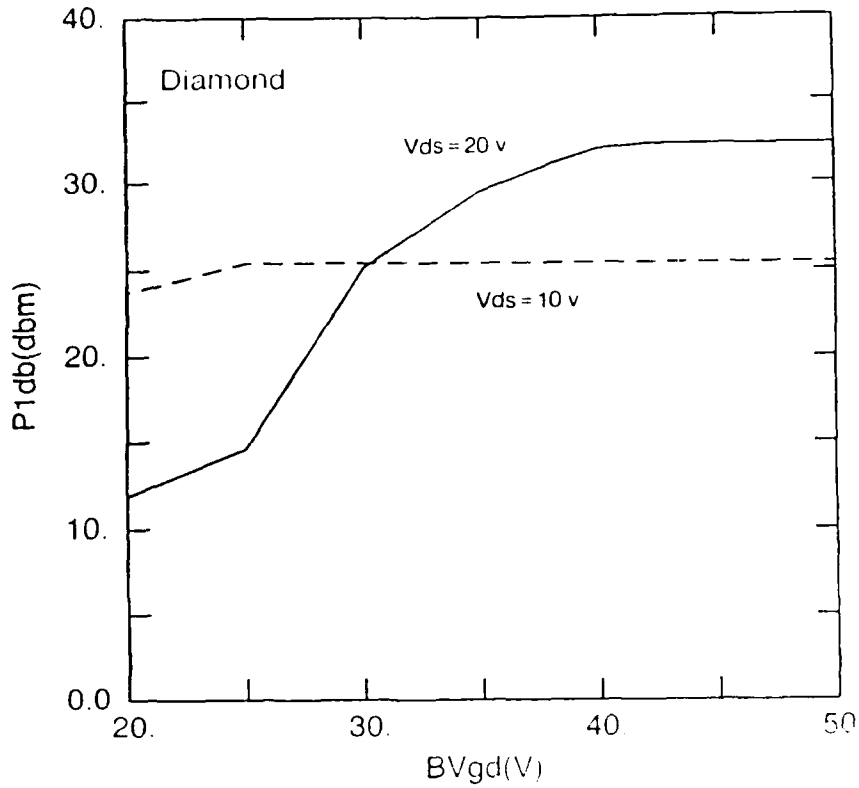
Diamond
Vds = 20 v
Vds = 10 v
P1db(dbm)
40.
30.
20.
10.
0.0
20.
30.
40
50
BVgd(V)

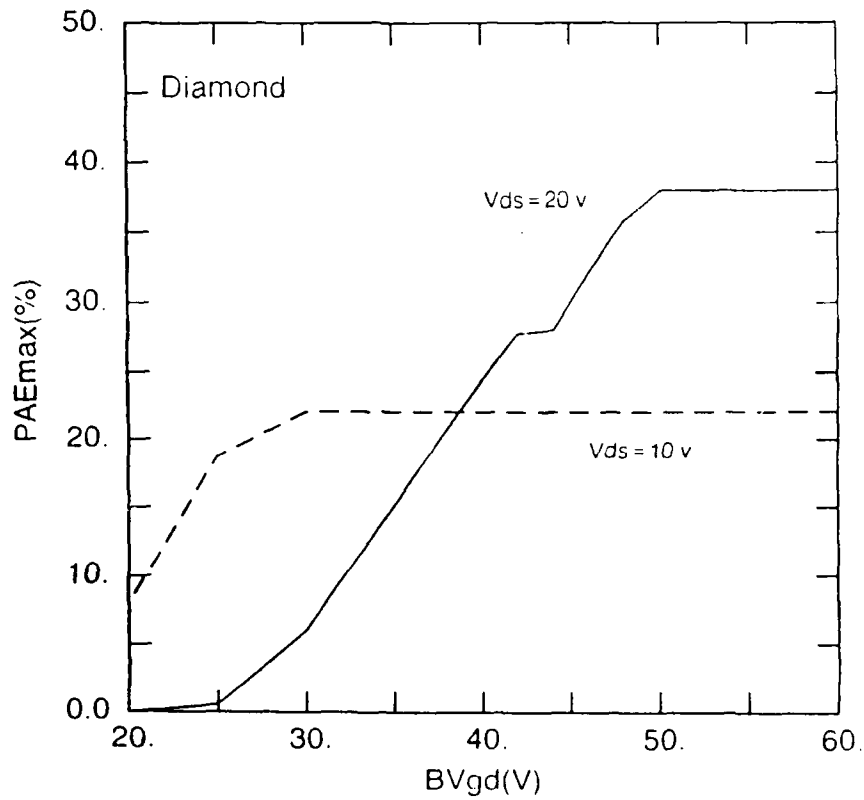
Diamond
Vds = 20 v
Vds = 10 v
PAEmax(%)
50.
40.
30.
20.
10.
0.0
20.
30.
40.
50.
60.
BVgd(V)

THERMAL RESISTANCE

Spreading resistance between device and heat sink

Thermal resistance of substrate

Thermal resistance of active layer

$$\Theta_{th} = \frac{2}{\pi \kappa_{hs} d} + R_{pkg} + \frac{4 l_1 T_1}{225 \kappa \pi d^2} + \frac{4 l_2 T_2}{560 \kappa \pi d^2} \ (^\circ K/W)$$

d = diameter (cm)
κ_{hs} = thermal conductivity of heat sink (W/°K-cm)
κ = thermal conductivity of semiconductor (W/°K-cm)
R_{pkg} = thermal resistance of package and bonding (°K/W)
l_1 = substrate thickness (cm)
T_1 = average temp. of substrate (°K)
l_2 = active layer thickness (cm)
T_2 = average temp. of active layer (°K)

JUNCTION TEMPERATURE

$$T_j = 300 + \Theta_{th}(1-\eta) V_{dc} J_{dc} A \ (^\circ K)$$

J_{dc} = Bias current density (A/cm^2)
A = Channel area (cm^2)
η = RF generation efficiency
V_{dc} = Bias voltage (V)

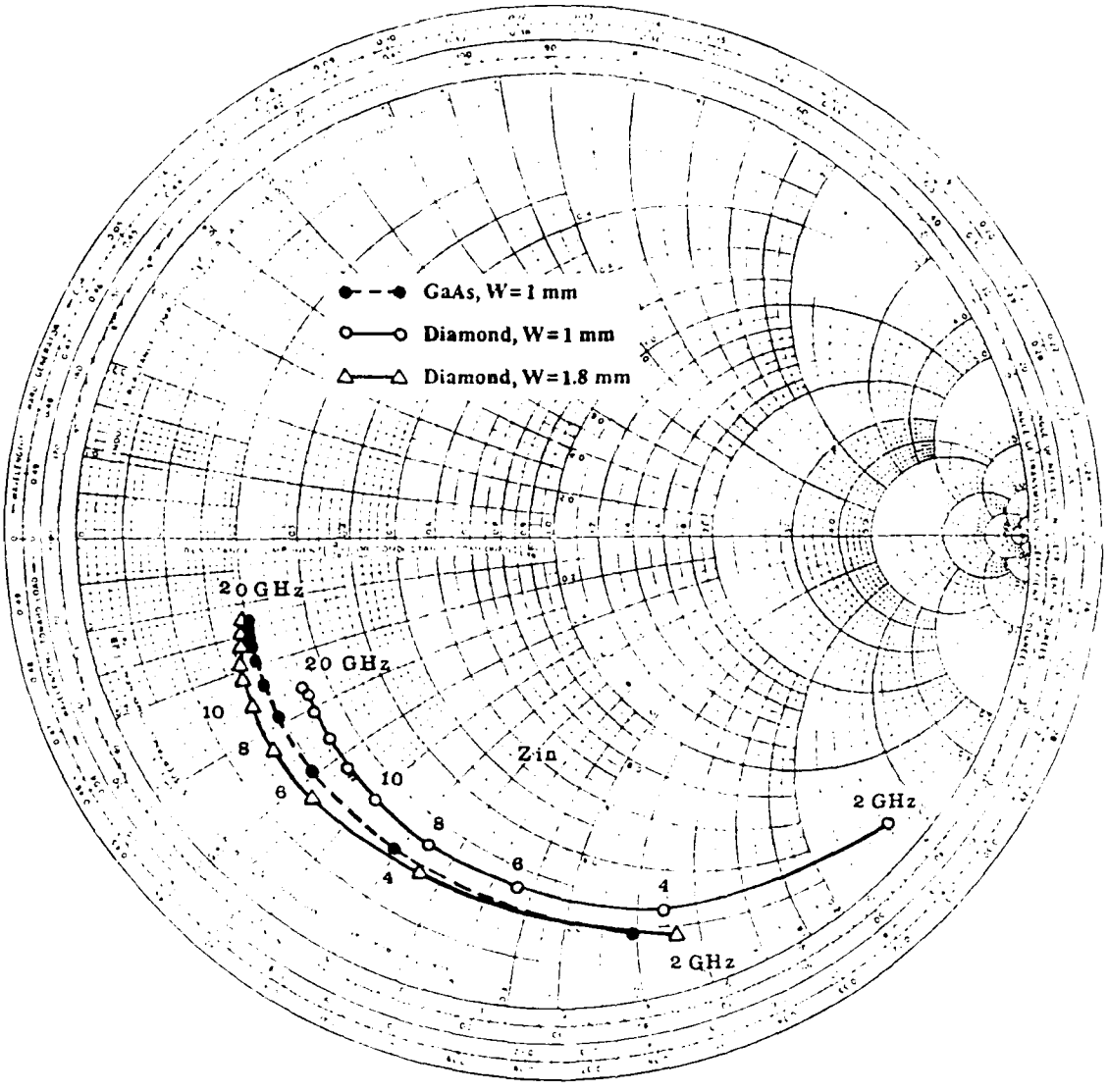
GaAs, W = 1 mm
Diamond, W = 1 mm
Diamond, W = 1.8 mm
20 GHz
20 GHz
10
8
6
4
Zin
10
8
6
4
2 GHz
2 GHz

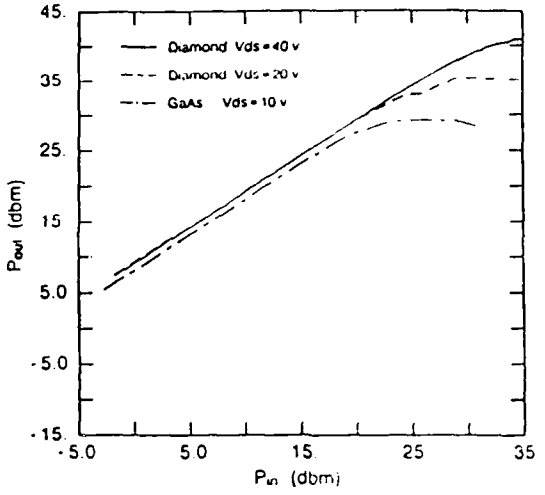
Diamond Vds = 40 v
Diamond Vds = 20 v
GaAs Vds = 10 v
45.
35
25.
15
5.0
-5.0
-15.
-5.0
5.0
15.
25
35
P_{out} (dbm)
P_{in} (dbm)

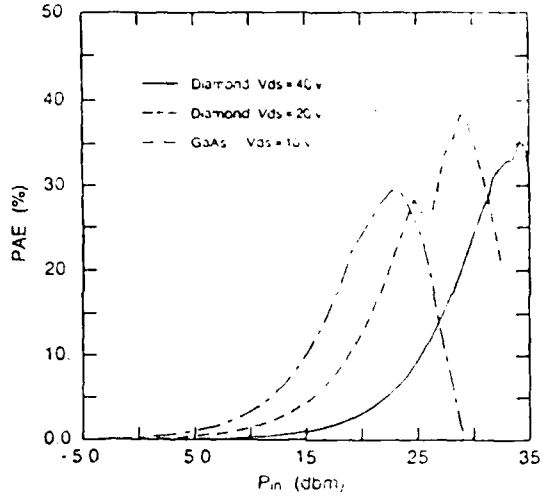
Diamond Vds = 40 v
Diamond Vds = 20 v
GaAs Vds = 10 v
50
40
30
20
10.
0.0
-5.0
5.0
15
25
35
PAE (%)
P_{in} (dbm)

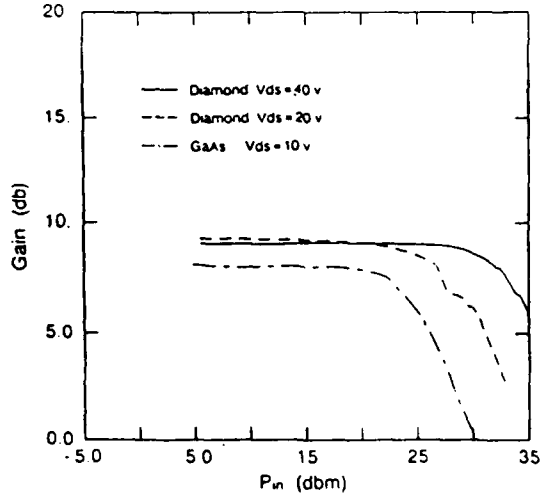
Diamond Vds = 40 v
Diamond Vds = 20 v
GaAs Vds = 10 v
20
15.
10.
5.0
0.0
-5.0
5.0
15
25
35
Gain (db)
P_{in} (dbm)

Maximum RF Output Power at 10 GHz

Device Input Impedance Matched to 1 Ohm

	GaAs	Diamond
Input Impedance (Ohm)		
Z_{in} for Z = 1 mm	10 -j11.5	12.5 -j25
Z_{in} for max. width	1 - j1.15 (10mm)	0.7 - j1.39 (18mm)
RF Power at Max. Width (W)	**8**	**225**
Thermal Resistance (^{O}C/W)	10.2	1.8
P_{diss} (W)	15.8	187
Power-Added Efficiency (%)	30	36
Channel Temp. Increase (^{O}C)	**113**	**215**

NORMALIZED MICROWAVE RF POWER ACHIEVABLE FROM TRANSISTORS

$$\bar{P} = \frac{P_{RF}}{\bar{Z}}$$

P_{RF} = Microwave Output Power (W)

$\bar{Z}$ = Gate (Base) periphery normalized to equivalent input impedance

Device	$\bar{P}$ (W/unit width)
GaAs MESFET	~ 1-1.5
HEMT	~ 1
Heterojunction Bipolar	~ 4.5-5
Diamond MESFET	~ 25
Diamond Bipolar	?
Diamond PBT	?

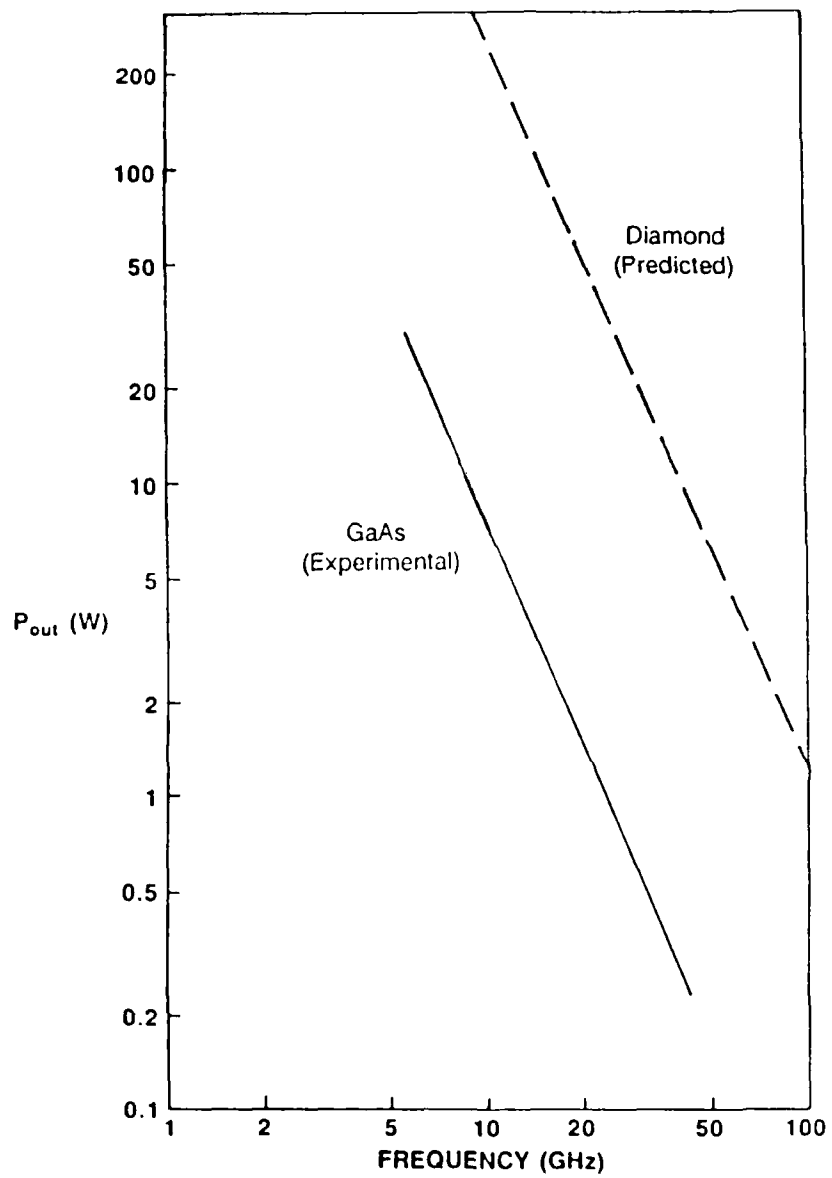

1 db Compressed RF Output Power for Microwave Power MESFETs

CONCLUSIONS

- The RF performance of a diamond power MESFET has been investigated theoretically using a large-signal device simulator.

- Diamond power MESFETs are capable of generating RF output power levels greater than existing or proposed compound semiconductor transistors ($P_{RF} \sim 25$ W/unit periphery).

- A diamond power MESFET can generate microwave power at X-band with an efficiency in excess of 40%.

- Diamond power MESFETs have more linear response and greater dynamic range than GaAs MESFETs.

Acknowledgements

The principle investigators listed on the cover page of this report wish to acknowledge a variety of students, post doctorates and other researchers for their efforts and/or useful discussions pertaining to this research: NCSU: B. Williams, R. Shroder, J. Yan, D. Asbury, P. Richard, Y. H. Lee, C. Harris, H. S. Kong, S. Hofmeister, D. Griffis and S. Corcoran; MCNC: S. Chevacharoenkul; RTI: R. Rudder, J. Posthill, M. Mantini and D. Vitkavage; ORAU: K. More; ORNL: J. Bentley, P. Angelini; KSL: K. Kobashi, Y. Kawate, and K. Nishimura.

Appendix

Distribution List – Annual Report

Contract Number N00014-86-K-0666

Address	Number of Copies
Mr. Max Yoder Office of Naval Research Electronics Program–Code 1114 800 North Quincy Street Arlington, VA 22217	8
Office of Naval Research Resident Representative Georgia Institute of Technology 206 O'Keefe Building Atlanta, GA 30332-0490	1
Director Naval Research Laboratory Attention: Code 2627 Washington, DC 20314	6
Defense Technical Information Center Building 5, Cameron Station Alexandria, VA 22314	12
Robert J. Markunas Research Triangle Institute Post Office Box 12194 Research Triangle Park, NC 27709	1
Michael Geiss Lincoln Laboratories 244 Wood Street Lexington, MA 02173	1
Professor W. K. Chu University of North Carolina at Chapel Hill Physics Department Chapel Hill, NC 27514	1

Professor Russell Messier 1
265 Materials Research Laboratory
Pennsylvania State University
University Park, PA 16802

Dr. James Butler 1
Naval Research Laboratory
Code 6115
Washington, DC 20375

James Mayer 1
Dept. Materials Science and Engineering
210 Bard Hall
Cornell University
Ithica, NY 14853

Dr. Bradford Pate 1
Stanford Synchotron Radiation Laboratory
Stanford, CA 94305

Professor Pancove 1
University of Colorado, ECE
Boulder, CO 80309-0455

Office of Naval Research 1
Attention: Code 1131M
Arlington, VA 22217

Naval Research Laboratory 1
Attention: Code 4683
Washington, DC 20375

Naval Research Laboratory 1
Attention: Code 6820
Washington, DC 20375

Naval Research Laboratory 1
Attention: Code 6211
Washington, DC 20375

Naval Research Laboratory 1
Attention: Code 6684
Washington, DC 20375

Naval Research Laboratory 1
Attention: Code 4684
Washington, DC 20375

Naval Ocean Systems Center
Attention: Code 1211
San Diego, CA 92152 — 1

Naval Ocean Systems Center
Attention: Code 911
San Diego, CA 95152 — 1

Naval Ocean Systems Center
Attention: Code 56
San Diego, CA 95152 — 1

SDIO/IST
Pentagon
Washington, DC 20301-7100 — 1

DARPA/D.S.O.
1400 Wilson Boulevard
Arlington, VA 22209 — 1

Professor R. F. Davis
Materials Science and Engineering
North Carolina State University
Raleigh, NC 27695-7907 — 1

Professor K. J. Bachmann
Materials Science and Engineering
North Carolina State University
Raleigh, NC 27695-7907 — 1

Professor R. J. Nemanich
Department of Physics
North Carolina State University
Raleigh, NC 27695-8202 — 1

Professor G. Lucovsky
Department of Physics
North Carolina State University
Raleigh, NC 27695-8202 — 1

Professor R. J. Trew
Dept. of Electrical and Computer Engineering
North Carolina State University
Raleigh, NC 27695-7911 — 1

Dr. S. Holly 1
Rocketdyne, Division of Rockwell International
Mailstop FAO3
6633 Canoga Avenue
Canoga Park, CA 91304

Professor G. Walrafen 1
Howard University
Chemistry Department
5325 Potomac Avenue, NW
Washington, DC 20016

Professor I. Lindau 1
Synchotron Radiation Laboratory
Stanford, CA 94305

A. J. Purdes 1
Texas Instruments
MS 147
P. O. Box 655936
Dallas, TX 75265

W. D. Partlow 1
Westinghouse Research and Development Center
1310 Beulah Road
Pittsburgh, PA 15235

R. L. Adams 1
21002 North 19th Avenue
Suite 5
Phoenix, AZ 85027

Professor J. Angus 1
Dept. of Chemical Engineering
Case Western Reserve University
Cleveland, OH 44106

T. R. Anthony 1
General Electric Corporation
Research and Development Center
Building K-1, Room 1CSO
Schnectady, NY 12345

Yehuda Arie 1
SRI Sarnoff Center
Princeton, NJ 08540

P. J. Boudreaux 1
Laboratory for Physical Science
4928 College Avenue
College Park, MD 20740

Professor R. F. Bunshaw 1
University of California at Los Angeles
6532 Buelter Hall
Los Angeles, CA 90024

Ray Calloway 1
Aerospace Corporation
Post Office Box 92957
Los Angeles, CA 90009

IBM 1
T. J. Watson Center
Attention: J. J. Cuomo
Yorktown Heights, NY 10598

Professor P. H. Fang 1
Department of Physics
Boston College
Chestnut Hill, MA 02167

Wen Hsu 1
Division 8347
Box 969
Sandia National Laboratories
Livermore, CA 94550

Professor W. Lanford 1
Physics Department
S.U.N.Y
Albany, NY 12222

Professor E. S. Machlin 1
44 Morningstar Drive
Croton-on-Hudson, NY 10520

Michael Pinneo 1
Crystallume
3180 Porter Drive, Suite 2
Palo Alto, CA 94304

Kenneth Russell 1
J. P. L. M. S. 122-123
4800 Oak Grove Drive
Pasadena, CA 91109

Professor T. D. Moustakas 1
Exxon Research
Ammandale, NJ 08801

Professor J. L. Davidson 1
200 Brown Hall
Auburn University
Auburn, AL 36849

IBM 1
T. J. Watson Center
Attn: B. Meyerson
Yorktown Heights, NY 10598

Paul Caldwell 1
DASIAS Field Office
256º Huntington Avenue
Suite 500
Alexandria, VA 22303

Defense Nuclear Agency 1
Attn: RAEE (CAPT Fore)
Washington, DC 20305-1000

Dr. Ian Brown 1
University of California
Lawrence Berkeley Laboratory
Bldg. 53
Berkeley, CA 94720

Dr. Andrez Badzian 1
Materials Research Laboratory
The Pennsylvania State University
University Park, PA 16802

Dr. Daniel L. Flamm 1
AT&T Bell Laboratories
Room 6E-216
600 Mountain Avenue
Murray Hill, NJ 07974